

The Sensitivity of Tropical Forests to Climate Variability and Change in Bolivia

Christian Seiler

Thesis committee

Promotor

Prof. Dr P. Kabat
Professor of Earth System Science
Wageningen University
Director General and Chief Executive Officer at the International Institute for Applied
Systems Analysis, Laxenburg, Austria

Co-promotors

Dr R.W.A. Hutjes
Associate professor, Earth System Science Group
Wageningen University

Dr B. Kruijt
Senior research scientist, ALTEERRA
Wageningen UR

Other members

Prof. Dr P.L. Ibisch, Eberswalde University, Germany
Prof. Dr G.M.J. Mohren, Wageningen University
Prof. Dr B. Smith, Lund University, Sweden
Dr P.A. Zuidema, Wageningen University

This research was conducted under the auspices of the SENSE Research School.

The Sensitivity of Tropical Forests to Climate Variability and Change in Bolivia

Christian Seiler

Thesis

submitted in fulfillment of the requirements for the degree of doctor
at Wageningen University

by the authority of the Rector Magnificus

Prof. Dr M.J. Kropff,

in the presence of the

Thesis Committee appointed by the Academic Board

to be defended in public

on Monday 19 May 2014

at 1:30 p.m. in the Aula.

Christian Seiler

The Sensitivity of Tropical Forests to Climate Variability and Change in Bolivia,
157 pages.

PhD thesis, Wageningen University, Wageningen, NL (2014)

With references, with summaries in English, Spanish and Dutch

ISBN 978-90-6173-923-0

Abstract

This thesis studies the sensitivity of wet and dry tropical forests to climate variability and change in Bolivia. The complexity of the problem was approached by integrating information from climate observations, climate projections, biomass measurements, remote sensing data, and a dynamic vegetation model (LPJ-GUESS). Meteorological observations (1960 to 2009) revealed a warming trend (0.1°C per decade), as well as a drying trend since 1985 (-4% during the wet, and -10% during the dry season). Anomalies were significantly affected by the two climate modes Pacific Decadal Oscillation (PDO), and El Niño Southern Oscillation (ENSO). A multi-model ensemble of 35 general circulation models from the CMIP3 and CMIP5 archive projected significant increases in temperature (2.5 to 5.9°C), but conflicting changes of annual rainfall for the end of this century. Climate observations were then used to drive LPJ-GUESS in order to simulate Bolivia's present-day potential vegetation as a baseline for assessing climate change impacts. Results were compared to biomass measurements from 819 plots, and to remote sensing data. Using regional parameter values for allometric relations, specific leaf area, wood density, and disturbance interval, a realistic spatial transition from the evergreen Amazon to the deciduous dry forest was simulated. The model reproduced reasonable values for seasonal leaf abscission, vegetation carbon (c_v), and forest fires. Modeled Gross Primary Productivity (GPP) and remotely sensed Normalized Difference Vegetation Index (NDVI) showed that dry forests were more sensitive to rainfall anomalies than wet forests. Modeled GPP was positively correlated to ENSO in the Amazon, and negatively correlated to consecutive dry days. Decreasing rainfall trends were simulated to decrease GPP in the Amazon. Using the same model configuration, the impacts of climate change were then assessed for two contrasting projections (wet and dry), revealing a large range of uncertainty. The loss of c_v simulated under a dry scenario was primarily driven by a reduction in GPP, and secondarily by enhanced emissions from fires. In the wet forest, less precipitation and higher temperatures equally reduced c_v , while in the dry forest, the impact of precipitation was dominating. The temperature-related reduction of c_v was mainly due to a decrease in photosynthesis, and only to lesser extent because of more autotrophic respiration and less stomatal conductance as a response to an increasing atmospheric demand. Tropical dry forests were simulated to virtually disappear, regardless of the potential fertilizing effect of rising concentrations of atmospheric carbon dioxide, suggesting a higher risk for forest loss along the drier southern fringe of the Amazon. The possibility of a forest dieback poses a serious threat to biodiversity, as well as rural livelihoods. Adaption measures for Bolivian forests should prioritize actions related to deforestation, fire management, grazing, and water resource management. Progress in climate change impact assessments for the Amazon will greatly depend on our ability to reduce uncertainties of future rainfall projections, possibly through physical reasoning rather than pure ensemble statistics. Otherwise, large uncertainties will remain for climate change impact assessments in the Amazon, despite extensive model improvements.

Contents

1. General Introduction	1
1.1. Context	1
1.2. Climate variability and change	3
1.3. Dynamic vegetation modeling	4
1.4. Research questions	6
1.5. Thesis outline	7
2. Climate Variability and Trends in Bolivia	9
2.1. Introduction	9
2.2. Study area	11
2.3. Methods	14
2.3.1. Data	14
2.3.2. Data homogenization	16
2.3.3. Climate means and extremes	18
2.3.4. Variability	18
2.3.5. Trends	19
2.4. Results	21
2.4.1. Climate means	21
2.4.2. Climate extremes	24
2.5. Discussion	24
3. Likely Ranges of Climate Change in Bolivia	35
3.1. Introduction	35
3.2. Study area	37
3.3. Methods	39
3.3.1. Data	39
3.3.2. Emission scenarios	40
3.3.3. Validation	41
3.3.4. Ensemble weighting	42
3.3.5. Multi-model agreement	43
3.4. Results	44
3.4.1. Validation and ensemble weighting	44
3.4.2. Temperature projections	46
3.4.3. Precipitation projections	47
3.4.4. Shortwave radiation projections	50
3.5. Discussion	51

4. Measuring and Modeling Carbon Stocks	57
4.1. Introduction	58
4.2. Study area	59
4.3. Methods	61
4.3.1. Model description	61
4.3.2. Data	64
4.3.3. Experimental design and analysis	67
4.4. Results	70
4.4.1. Plant Functional Types	70
4.4.2. Carbon stocks	74
4.4.3. Climate sensitivity	76
4.5. Discussion	80
5. The Sensitivity of Wet and Dry Tropical Forests to Climate Change	85
5.1. Introduction	86
5.2. Study area	89
5.3. Methods	89
5.3.1. Model description	89
5.3.2. Data	92
5.3.3. Experimental design	94
5.4. Results	94
5.4.1. Changes in carbon pools	94
5.4.2. Mechanisms of forest loss	97
5.5. Discussion	102
6. General Discussion	107
6.1. Research questions	107
6.2. Climate change adaptation and mitigation measures	112
6.3. Outlook	114
A. Appendix	117
A.1. Climate Indices	117
Bibliography	121
Summary	137
Resumen	141
Samenvatting	145
Acknowledgments	149
Curriculum Vitae	151

Publications	153
Education Certificate	154
Funding	156

1. General Introduction

1.1. Context

The Plurinational State of Bolivia is home to vast wilderness areas ranging from the Amazon rainforest to the glaciers of the Andes (Figure 1.1). Located at the southern fringe of the Amazon, Bolivia covers a transition zone of extraordinary biodiversity, with wet evergreen forests in the north, and dry deciduous forests towards the south (Ibisch and Mérida, 2003). Forests store about 6 Gt of carbon (Saatchi et al., 2011), and affect the water cycle of one of the main contributors of the Amazon river, the Madeira basin (Roche and Jauregui, 1988). Ecosystems are threatened by human pressures, including deforestation (Cuéllar et al., 2012), fires (Rodríguez, 2012a), livestock grazing (Jarvis et al., 2010), and open-pit mining (Tejada, 2013). Conservation efforts intend to preserve natural habitats at varying scales, ranging from local land-use planning, to protected area management of a large-scale bio-corridor (Ibisch, 2005). In 1997, the Noel Kempff Mercado National Park was extended by 642,500 ha of tropical forests, terminating logging rights, and avoiding future deforestation in the respective region (Virgilio, 2009). Methods for carbon quantification were certified in 2005, creating one of the world's first projects eligible under the REDD mechanism (reducing emissions from deforestation and forest degradation in developing countries; UNFCCC, 2010). A second sub-national REDD project was launched in 2010 in an indigenous territory of Bolivia's Amazon (FAN, 2010). Carbon stocks protected by REDD could be threatened by a climate change induced forest die-back, as suggested by modeling experiments (Cox et al., 2004; Gumpenberger et al., 2010). The possibility of such a forest loss triggered a discussion on the implications for biodiversity and long-term conservation strategies (Malhi et al., 2008). It must be noted that at the time of writing the Bolivian government opposes the carbon trading scheme of REDD projects, and is promoting an alternative mechanism including voluntary markets instead, namely the joint mitigation and adaptation mechanism for the comprehensive and sustainable management of forest and the mother earth (JMA; RREE, 2012). For simplicity, we continue referring to both projects as REDD, as they originally were designed as such.

Model experiments exploring the impacts of climate change on vegetation dynamics are typically based on coupling general circulation models (GCMs) with dynamic global vegetation models (DGVMs) under different emission scenarios. Results are subject to large uncertainties arising from conflicting climate change projections (Poulter et al., 2010), as well as different representations of the physiological responses

of plants to rising concentrations of atmospheric carbon dioxide ($[\text{CO}_2]$), increasing temperatures, and water stress (Galbraith et al., 2010). The focus of previous studies has been mainly on the Amazon basin as a whole, and less on the drier transition zones from evergreen to deciduous forests along the southern margin of the basin. The impacts of climate change however may actually be higher in these transition zones, as species are closer to the extreme limits of their ecological requirements (Killeen et al., 2006). Results from previous studies cannot easily be applied to the Bolivian case, due to coarse spatial resolutions and serious misrepresentations of vegetation types for historic climate conditions. A global application of the DGVM LPJ simulated grasslands instead of deciduous trees in Bolivia's semi-dry and dry forests (Sitch et al., 2003). Similarly, the potential vegetation model CPTec-PVM (Oyama and Nobre, 2004) simulated mainly savanna in Bolivia's Amazon forest under present day climate (Salazar et al., 2007), limiting the validity of any future projections for the region. Also, model results are based on empirical parameter values derived from studies not necessarily representative of the Amazon.

While the impacts of climate change are of great concern in the long-term, present-day climate variability is of immediate relevance. Bolivia is heavily affected by droughts and floods associated with the El Niño – Southern Oscillation (ENSO; Smith et al. 2000) (UNDP, 2011). During the La Niña related drought of 2010, Bolivia's Amazon was amongst the most affected regions within the entire Amazon basin (Lewis et al., 2011). The total area of forest and savanna fires was unusually high during this year, as well as during the previous severe, and El Niño related drought of 2005 (Rodriguez, 2012a). An assessment of the country's climate variability and its impacts is therefore of great interest, not only for Bolivia, but also in the context of the wider Amazon basin.

A better understanding of climate variability and climate change requires a systematic analysis of climate observations and climate projections from multiple climate models. Implications for vegetation dynamics and associated uncertainties have not been assessed at a scale suitable for climate change adaption and mitigation purposes. The increasing demand for such information was the primary motive for this research. The complexity of the problem was approached by integrating information from climate observations, climate projections, biomass measurements, remote sensing data, and dynamic vegetation modeling. The first part of the thesis (Chapter 2 and 3) assesses historic climate variability and future climate projections, while the second part (Chapter 4 and 5) explores vegetation dynamics for recent and possible future climates from a modeling perspective. Special attention was paid to mechanisms of forest loss, and uncertainties arising from climate change projections, as well as the physiological responses of plants to rising $[\text{CO}_2]$ and increasing temperatures. The following two sections highlight important aspects on climate variability and change (section 1.2), and dynamic vegetation modeling (section 1.3). We then formulate our overall research questions (section 1.4), followed by the outline of this thesis (section 1.5).

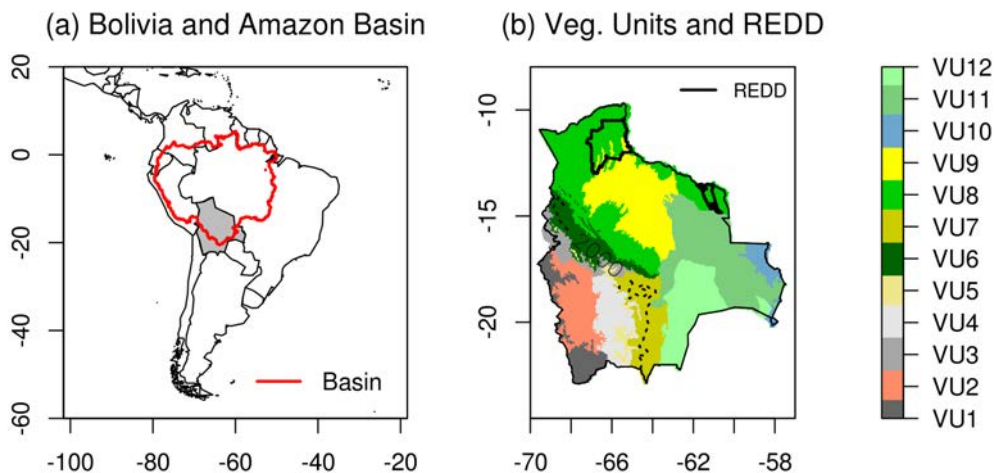


Figure 1.1: (a) Bolivia (gray shaded) and the Amazon basin water shed boundary; (b) vegetation units (VU1 = Western Cordillera, VU2 = Altiplano, VU3 = Eastern Cordillera and Northern Altiplano, VU4 = Eastern Cordillera and Central and Southern Altiplano, VU5 = Prepuna, VU6 = Yungas, VU7 = Tucumano Forest, VU8 = Amazon, VU9 = Beni savannas, VU10 = Pantanal, VU11 = Chiquitania, VU12 = Chaco (Navarro and Ferreira, 2004)), and the limits of two REDD projects. The dotted line denotes the altitude contour line at 2000 m MSL.

1.2. Climate variability and change

Climate variability impacts human and natural systems in Bolivia mainly through floods and droughts, with single El Niño and La Niña events affecting thousands of people and leading to economic losses of millions of U.S. dollars (UNDP, 2011). Bolivia is a developing country with one-third of the labor force working in the agricultural sector (www.ine.gov.bo), and is therefore considered to be extremely vulnerable to climate change (WorldBank, 2010). Important sources of climate variability in South America include the Pacific Decadal Oscillation (PDO; Mantua et al. 1997), El Niño – Southern Oscillation (ENSO; Smith et al. 2000), and the Antarctic Oscillation (AAO; Thompson and Wallace, 2000; Garreaud et al. 2009). Though correlations between observed climate variability and climate modes are reasonably well established on a continental scale, a regional analysis for Bolivia is still missing. Also, the underlying physics behind these correlations are still subject of ongoing research, but are beyond the scope of this study. Along climate variability, long-term climate trends have been detected in South America (e.g. Vuille et al., 2003; Marengo, 2004; Espinoza Villar et al., 2009). However, previous research on observed climate variability

and trends is of varying spatial scale, and usually included only very few Bolivian stations. The lack of spatial and temporal detail makes it difficult to apply this information to Bolivia, given the country's heterogenic topography. Proper knowledge and data of the present climate and its variability is not only valuable in itself, but is also an important input for evaluating the skills of climate models.

The Fourth and Fifth Assessment Report of the Intergovernmental Panel on Climate Change (AR4 and AR5, respectively) document climate change projections from multiple GCMs belonging to the 3rd and 5th Coupled Model Intercomparison Project (CMIP3 and CMIP5, respectively) (IPCC, 2007, 2013). Changes from CMIP3 to CMIP5 GCMs include changes in emission scenarios, improved model physics, finer spatial resolution and additional processes related to the oceanic and terrestrial carbon cycle, aerosols, atmospheric chemistry and ice sheets. Given the coarse spatial resolution of GCMs, regional climate impact studies require data with higher spatial resolutions. Numerous attempts have therefore been made to dynamically downscale global climate change scenarios for tropical South America (e.g. Soares and Marengo, 2009; Urrutia and Vuille, 2009; Marengo et al., 2009), with more projections to be expected in the context of the CORDEX project (Elguindi et al., 2013). However, at the time of writing regional climate change projections have been driven by only very few lateral boundary conditions, limiting their robustness in a region with little agreement among GCMs on the directional change of rainfall. Previous analyses of climate change scenarios are of mainly sub continental scale and include only very few Bolivian stations for model evaluation, making it difficult to apply this information to Bolivia. Given the potential disagreement among models on the directional change of precipitation, a comprehensive evaluation of multiple GCMs is a necessary precursor to any downscaling effort, assuming a good model skill for present day climate can be extended to future climates.

1.3. Dynamic vegetation modeling

Dynamic Global Vegetation Models (DGVMs) simulate the exchange of water and carbon between soils, plants and atmosphere, as well as the resulting terrestrial ecosystem composition and structure. Models include processes related to plant geography, plant physiology and biogeochemistry, vegetation dynamics, and biophysics (Prentice et al., 2007). Predictive modeling in plant geography started with the world climate zones from Köppen (1931). However, it was not until Woodward (1987) that the distribution of biomes was modeled according to physiological processes controlling the survival and performance of plants. Further developments led to the equilibrium biogeography model BIOME of Prentice et al. (1992), an important basis for the model used in this thesis. While these models were able to reproduce the spatial distributions of biomes, they did not yet include any biogeochemistry. Melillo et al. (1993) was the first who simulated net primary productivity at a global scale using a terrestrial biogeochemistry model (TBM). More recent TBMs adapted the biochem-

ical model for photosynthesis from Farquhar et al. (1980), another key component of the model used in this thesis. Haxeltine and Prentice (1996) then integrated the equilibrium biogeography and TBM approaches, allowing biomes to compete for resources. Vegetation dynamics such as tree establishment, growth, and mortality have been incorporated at different levels of complexity, ranging from processes averaged over a grid cell, to the representation of individual trees (Smith et al., 2001). Newer developments allow individual plants to adopt a unique combination of trait values, and to change these values through evolutionary processes (Scheiter et al., 2013). DGVMs have now been incorporated into GCMs, allowing for a full physical coupling between the terrestrial biosphere and the other components of the earth system (e.g. Collins et al., 2011).

Model experiments presented in this thesis were conducted with the dynamic vegetation model LPJ-GUESS (Lund Potsdam Jena General Ecosystem Simulator) (Smith et al., 2001; Ahlström et al., 2013). Model inputs consist of temperature, precipitation, solar radiation, $[\text{CO}_2]$, and soil texture. Plants are grouped into plant function types (PFTs) according to structural and phenological differences. The structure of a tree is simplified to a cylinder with fine roots, sap- and heartwood, a crown area and a leaf area index (LAI). Grasses lack a structure and consist of roots and LAI only. Soils consist of an upper (0-0.5 m) and a lower layer (0.5-1.5 m) of identical soil texture. One grid cell represents the average of several replicate patches, typically of 0.1 ha in size each. A patch may contain several PFT cohorts, each represented by an average individual. Replicate patches are driven by the same input data, however, vegetation dynamics differ due to stochastics in establishment, mortality and disturbance processes. Photosynthesis is calculated according to the coupled photosynthesis and water balance scheme of BIOME 3 (Haxeltine and Prentice, 1996). A detailed model description can be found in Sitch et al. (2003) and Gerten et al. (2007), as well as in Chapter 4 and 5 of this thesis.

LPJ-GUESS is a state-of-the-art DGVM, sharing many features with other vegetation models. Some processes relevant in the context of this study however are not incorporated in LPJ-GUESS, but can be found in other models. This includes processes related to the physiological responses of plants to rising $[\text{CO}_2]$, increasing temperatures, and water stress. Free-Air CO_2 Enrichment (FACE) experiments showed that plant growth under elevated $[\text{CO}_2]$ is constrained by a decreasing availability of nitrogen as carbon and nitrogen are sequestered in long-lived plant biomass and soil organic matter (Reich et al., 2006; Norby et al., 2010). While comparable field experiments for the Amazon are still in preparation (Tollefson, 2013), it can be expected that the sensitivity of DGVMs to rising $[\text{CO}_2]$ is most likely exaggerated due to missing nutrient cycles (Oren et al., 2001; Körner, 2006; Hickler et al., 2008). An interactive nitrogen cycle has only recently been incorporated into LPJ-GUESS (Fleischer et al., 2013), but was not available at the time of writing. The further incorporation of phosphorus is still missing, but has already been included into the land surface model JSBACH (Raddatz et al., 2007).

The response of photosynthesis to rising leaf temperatures can be described with

a bell-shaped curve (Hickler et al., 2008). The associated uncertainty arises from the exact shape and plasticity of this curve, as plants are known to adapt their temperature optimum to changes in their environment (Berry and Bjorkman, 1980; Medlyn et al., 2002; Atkin and Tjoelker, 2003). This is of great relevance, as model experiments for the Amazon show that the projected rise in temperature can cause the same amount of biomass loss as the projected reductions in precipitation (Galbraith et al., 2010). Thermal acclimation of photosynthesis is currently not implemented in LPJ-GUESS, but is part of the models JSBACH, Hybrid (Friend, 2010), Orchidee (Krinner et al., 2005), and BETHY (Ziehn et al., 2011) (Smith and Dukes, 2013).

A variety of approaches have been applied to estimate the resilience of the Amazon to water stress. The Amazon appears to be well adapted to seasonal drought due to the existence of deep roots accessing soil water at more than eight meters of depth (Nepstad et al., 1994). Also, soil water was found to rise upwards from wetter to drier regions during the dry season (Romero-Saltos et al., 2005). Both processes are usually not incorporated in DGVMs, but were tested in the land surface model SiB3 (Baker et al., 2008). The incorporation of these processes were found to be essential for reproducing seasonal fluxes of net ecosystem exchange in the Tapajos site (Brazil). Deep roots however don't seem to fully compensate for water stress related to inter-annual climate variability. Biometric measurements revealed a reduction in biomass in monitoring plots after the drought of 2005 (Phillips et al., 2009). Remote sensing data first suggested a greening of the Amazon during the same year (Saleska et al., 2007), but such findings were questioned by Samanta et al. (2010), as results were not reproducible. The contrary was then found for the drought of 2010, with severe declines in vegetation greenness across large areas of the Amazon (Xu et al., 2011). Multiple-year throughfall exclusion experiments reveal an enhanced mortality of large trees (Nepstad et al., 2007), as well as a decline in net primary productivity with an increase in autotrophic respiration (da Costa et al., 2013). Long-term responses of forest growth to precipitation anomalies can be studied from tree ring widths. Significant correlations between tree ring widths and annual rainfall anomalies were found for trees in the Bolivian Amazon, indicating the sensitivity of these forests to rainfall (Brienen and Zuidema, 2005).

1.4. Research questions

Based on the review above, four guiding research questions were posed to assess the sensitivity of vegetation dynamics to climate variability and change in Bolivia. The first two questions focus on Bolivia's present and possible future climates, while the last two questions explore vegetation dynamics under present and future climates.

1. Are there any trends in observed climate means and extremes, and how do they relate to global climate modes? (Chapter 2)
2. How well do GCMs reproduce the current climate, and what are the projections for the future? (Chapter 3)

3. Can we reproduce historic vegetation dynamics realistically, and how do forests respond to climate variability? (Chapter 4)
4. How sensitive are forests to climate change, and what are the main drivers of change? (Chapter 5)

The answers to these questions will help us to better understand the impacts of climate variability and change on vegetation dynamics across different forest types, and to identify the driving processes and associated uncertainties relevant in this part of the Amazon. Results are expected to provide important inputs for the discussion on climate change adaptation and mitigation options for Bolivian forests.

1.5. Thesis outline

The following four chapters address each one of the four research questions posed above. Chapter 2 detects historic climate variability and trends for Bolivia from newly consolidated daily temperature and precipitation observations with unprecedented station density from 1960 to 2009. Variability and trends of climate means and extremes were put into context of climate modes (PDO, ENSO, AAO), and compared to the atmospheric moisture transport reproduced by reanalysis data.

Chapter 3 analyzes projections from 35 different GCMs, including model results not only from CMIP3, but also from the only very recently available CMIP5 collection, as well as 5 emission scenarios. GCMs were evaluated against climate observations from 1961 to 1990, and were ranked and weighted according to their performance to reproduce the historic climate. Projected changes in climate means and annual climate variability were assessed.

Chapter 4 implements, adapts, and evaluates the dynamic vegetation model LPJ-GUESS for the Bolivian case. Adaptations were required in order to reproduce a realistic transition from evergreen to deciduous forests. For this purpose, default model parameter values were replaced by regional values of allometric relations, specific leaf area, wood density, and disturbance interval. Results were evaluated against remote sensing data, as well as biomass measurements from 21 new plots, and 798 plots from previous field experiments. Measured carbon pools were documented for different vegetation zones.

Chapter 5 explores the range of uncertainty associated with the potential impacts of climate change on vegetation dynamics. For this purpose, LPJ-GUESS was forced with two contrasting climate change projections which were statistically downscaled and bias-corrected. Drivers of change were evaluated by quantifying carbon fluxes, as well as the individual contributions of atmospheric carbon dioxide, temperature and precipitation. Special attention was paid to the effect of rising temperatures on photosynthesis, respiration, and stomatal conductance related to an increasing atmospheric demand. Implications for the two Bolivian REDD projects are discussed.

Chapter 6 elaborates on the principal findings in the context of current literature. Methodological limitations are highlighted, and recommendations for future research are provided. Finally, we discuss implications for climate change mitigation and adaptation measures for Bolivian forests.

2. Climate Variability and Trends in Bolivia

Abstract

Climate-related disasters in Bolivia are frequent, severe, and manifold and affect large parts of the population, economy, and ecosystems. Potentially amplified through climate change, natural hazards are of growing concern. To better understand these events, homogenized daily observations of temperature (29 stations) and precipitation (68 stations) from 1960 to 2009 were analyzed in this study. The impact of the positive (+) and negative (-) phases of the three climate modes (i) Pacific Decadal Oscillation (PDO), (ii) El Niño – Southern Oscillation (ENSO) with El Niño (EN) and La Niña (LN) events, and (iii) Antarctic Oscillation (AAO) were assessed. Temperatures were found to be higher during PDO(+), EN, and AAO(+) in the Andes. Total amounts of rainfall, as well as the number of extreme events, were higher during PDO(+), EN, and LN in the lowlands. During austral summer [December–February (DJF)], EN led to drier conditions in the Andes with more variable precipitation. Temperatures increased at a rate of 0.1°C per decade, with stronger increases in the Andes and in the dry season. Rainfall totals increased from 1965 to 1984 [12% in DJF and 18% in June–August (JJA)] and decreased afterward (-4% in DJF and -10% in JJA), following roughly the pattern of PDO. Trends of climate extremes generally corresponded to trends of climate means. Findings suggest that Bolivia’s climate will be warmer and drier than average in the near-term future. Having entered PDO(-) in 2007, droughts and LN-related floods can be expected in the lowlands, while increasing temperatures suggest higher risks of drought in the Andes.

2.1. Introduction

Climate variability impacts human and natural systems in Bolivia mainly through floods and droughts, with single El Niño (EN) and La Niña (LN) events affecting thousands of people and leading to economic losses of millions of U.S. dollars (USD).

This chapter has been published as:

Seiler, C., R.W.A. Hutjes, and P. Kabat, 2013: Climate Variability and Trends in Bolivia. *Journal of Applied Meteorology and Climatology*, **52** (1), 130–146.

The EN events of 1982/83 and 1997/98 and LN events of 2007/08 affected about 1.6 million, 135 000, and 619 000 people with economic losses of about 837, 515, and 758 million USD, respectively (UNDP, 2011). Climate change may alter the frequency and intensity of such natural hazards (Field et al., 2012). The Plurinational State of Bolivia, a developing country with one-third of the labor force working in the agricultural sector (www.ine.gob.bo), is considered to be extremely vulnerable to climate change (WorldBank, 2010). Bolivia's disaster deficit index (DDI) (the ratio of the potential economic loss caused by a natural disaster to the country's economic resilience) is estimated at 1.47, expressing the country's inability to cope with extreme disasters (Cardona and Carreño, 2011). Understanding the country's climate variability is therefore of great national interest.

Important sources of climate variability in South America include the Pacific Decadal Oscillation (PDO; Mantua et al. 1997), El Niño – Southern Oscillation (ENSO; Smith et al. 2000), and the Antarctic Oscillation (AAO; Thompson and Wallace, 2000; Garreaud et al. 2009). PDO is the leading principal component of monthly sea surface temperature anomalies in the Pacific Ocean north of 20°N and exhibits a decadal oscillation between warm [PDO(+)] and cold [PDO(-)] phases. ENSO is a coupled oceanic and atmospheric oscillation of the equatorial Pacific switching between warm (EN) and cold phases (LN) with an irregular oscillation ranging from 2 to 7 years. An AAO is defined as the leading principal component of 850-hPa geopotential height anomalies south of 20°S. PDO, ENSO, and AAO are associated with the following temperature and precipitation anomalies in South America. Garreaud et al. (2009) found positive correlations between surface air temperature and PDO and ENSO in many parts of South America, including Bolivia, with highest correlations in the Andes. Regarding rainfall, the same study shows negative (positive) correlations of rainfall anomalies and PDO in some parts of South America, mainly north (south) of about 10°S. Negative correlations between ENSO and rainfall exist in December–February (DJF) in the Bolivian Andes and positive correlations in June–August (JJA) in the Bolivian lowlands. Ronchail and Gallaire (2006) found negative (positive) precipitation anomalies during EN (LN) events in the Altiplano, confirming previous studies (e.g., Vuille, 1999). ENSO-related anomalies are associated with the strength and position of the Bolivian high (see also section 2.2) (Vuille et al. 2003; SENAMHI 2009). Regarding the AAO, the associated precipitation anomalies are strongest in southern Chile and along South America's subtropical east coast (Garreaud et al., 2009).

Along climate variability, long-term climate trends have been detected in South America. In the tropical Andes, mean surface air temperatures have increased from 1950 to 1994 by 0.15°C per decade (Vuille et al., 2003). The same study found no clear pattern on trends in annually accumulated rainfall. Espinoza Villar et al. (2009) found a negative trend in rainfall in the Amazon basin (756 stations) with an annual rate of -0.32% during 1975–2003. Break tests showed that this decrease has been particularly important since 1982. Ronchail (1995) found a positive precipitation trend throughout Bolivia (29 stations) from the mid-1960s until the end of the series in 1984. A similar trend was found in the southern Amazon of Brazil (86 stations) by Marengo

(2004) with a positive trend from the mid-1960s until about 1990. Marengo (2004) associates the shift from negative to positive anomalies in the 1970s with the switch from the cold to the warm PDO phase in 1976/77. Toledo (2010) found a negative precipitation trend from 1982 to 2007 in Bolivia’s northern lowlands (20 stations). In the Bolivian Altiplano, Seth et al. (2010) detected a negative precipitation trend for the months September to November and a positive trend for January to March from 1960 to 2008 (3 stations); however, neither trend was statistically significant. Regarding climate extremes, numerous studies have detected significant increases in extreme temperature events, consistent with a warmer climate in South America (e.g., Vincent et al. 2005; Alexander et al. 2006; Seth et al. 2010; Thiabeault et al. 2010; Marengo et al. 2010). The overall confidence in these trends however is estimated to range from low to medium, due to insufficient evidence or spatial variations in many regions (Field et al. 2012, Table 2.3).

Previous research on observed climate variability and trends listed above is of varying spatial scale and usually included only very few Bolivian stations. The lack of spatial and temporal detail makes it difficult to apply this information to Bolivia, given the country’s heterogenic topography. This motivated us to analyze climate variability and trends of temperature and precipitation means and extremes from a large number of Bolivian stations, distinguishing among seasons and climatologically contrasting regions. Our analysis aims for a better understanding of historic climate variability and trends, knowledge that in turn can be used for disaster risk reduction, as well as to aid adaptation to, and further research on regional climate change in Bolivia.

The following sections describe our study area, methods, results, and discussion. The method section outlines the data and theory of our approach, describing data homogenization, analysis of variance, and trends. The results section quantifies climate variability and trends of means and extremes. Our discussion interprets the results in the context of existing literature and elaborates on the principal findings.

2.2. Study area

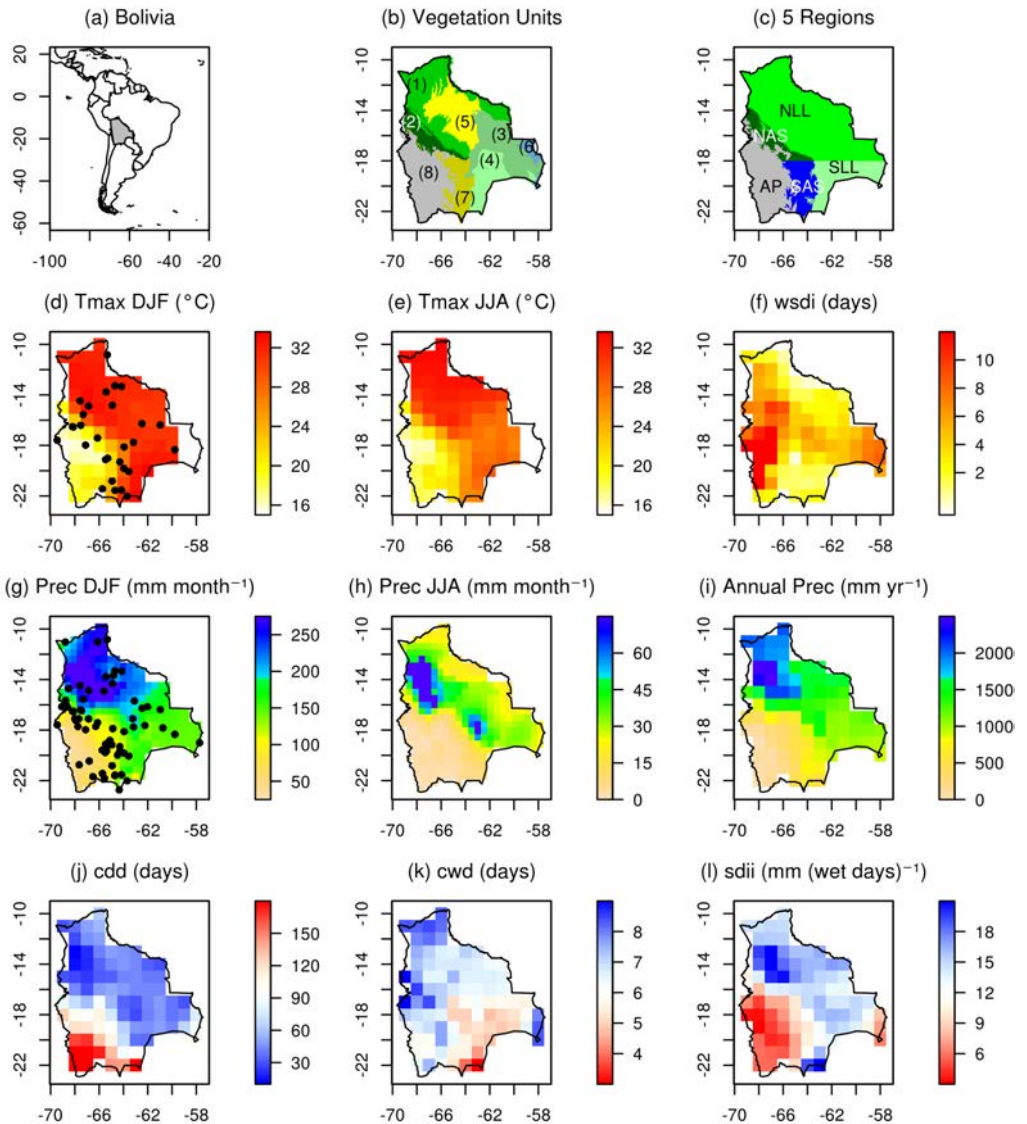
Bolivia is a tropical country measuring more than one million km² (Figure 2.1a). Its main altitudinal divisions are lowlands (<800 m MSL), Andean slopes (800–3200 m MSL), and highlands (Altiplano; 3200–6500 m MSL). Temperature and precipitation gradients lead to the formation of contrasting vegetation units, including Amazonian rain forest in the northern lowlands, dry deciduous forest (Chiquitania and Chaco) in the southern lowlands, and alpine grasslands in the Altiplano (Figure 2.1b). Temperatures decrease with altitude, with annual mean maximum temperatures ranging from 32°C in the lowlands to 16°C in the highlands (Altiplano) (Figure 2.1d,e). The number of warm days (see Table A.1 Table A.2 for definition of all indices) ranges from 5 to 25 days yr⁻¹(not shown) and the duration of warm spells ranges from 2 to 10 days (Figure 2.1f), both with higher numbers in the Altiplano. The warmer

austral summer (DJF) and colder winter (JJA) coincide with the wet and dry season, respectively. Rainfall varies from high to low from the northern Andean slopes, northern lowlands, southern lowlands, southern Andean slopes to the Altiplano and ranges from <250 to >2000 mm yr⁻¹ (Figure 2.1i). Much higher values (>5000 mm yr⁻¹) along the northern Andean slopes are documented by Bolivia's National Service of Meteorology and Hydrology (SENAMHI, 2009) from stations not included in this research. Seasonal rainfall ranges from 50 to 250 mm month⁻¹ and from 0 to 60 mm month⁻¹ in DJF and JJA, respectively (Figure 2.1g,h). Consecutive dry days increase from the lowlands to the Altiplano, ranging from less than 1 month in the northwest lowlands to 5 months in the southwest Altiplano (Figure 2.1j). Consecutive wet days range from 5 to 8 days with higher values in the northern lowlands and lower values in the southern lowlands and Altiplano (Figure 2.1k). Rainfall intensity ranges from 6 to 18 mm (wet days)⁻¹ (Figure 2.1l) and rainfall during very wet days ranges from 50 to 400 mm yr⁻¹ (not shown), both with spatial patterns corresponding to patterns of yearly rainfall. The pronounced wet season leads to regular floods from January to March in the lowland savannas with an average extension of about 100,000–150,000 km² (Bourrel et al., 2009). However, floods in the Andes are also possible, especially in the catchment areas of Lake Titicaca and Poopó (UNDP, 2011). Droughts take place mainly from June to August in the southern lowlands and in the southwestern part of the Altiplano (CONARADE, 2010).

These climate patterns are shaped by the following synoptic-scale systems. In austral summer (DJF) a low pressure system called Chaco low intensifies at 25°S, enhancing the easterly trade winds to transport moisture from the northern tropical Atlantic into the continent. Deflected by the Andes, moisture is transported southward from the Amazon to subtropical plains by a lowlevel jet (LLJ) located at about 925–850 hPa (~1 km MSL) and <100 km east of the Andean slopes (Marengo et al., 2004). This leads to enhanced precipitation with a southeastward extension toward the Atlantic Ocean, referred to as the South Atlantic Convergence Zone (SACZ). Simultaneously, the release of condensational heat over the Amazon and Andean slopes leads to the formation of the upper-level Bolivian high at 200 hPa (~12 km MSL) (Lenters and Cook, 1997), which further enhances moisture advection from the Amazon to the

Figure 2.1: (a) Location of Bolivia; (b) vegetation units with 1) Amazonian rainforest, 2) cloud forest (Yungas), 3) dry forest (Chiquitania), 4) Chaco, 5) savannas, 6) Pantanal, 7) Andean valleys with Tucumano forest and 8) Altiplano with mountain ranges (Navarro and Ferreira, 2004); (c) location of regions NLL, SLL, NAS, SAS and AP; monthly mean maximum temperature (°C) in (d) DJF with locations of 29 meteorological stations and (e) JJA; (f) warm-spell duration (days); monthly mean precipitation (mm month⁻¹) in (g) DJF with locations of 68 meteorological stations and (h) JJA; (i) annual precipitation (mm yr⁻¹); (j) consecutive dry days (days); (k) consecutive wet days (days); (l) rainfall intensity [mm (wet days)⁻¹]. Climate indices are defined in Table A.1 and Table A.2.

2.2 Study area



Bolivian low- and highlands (Vuille, 1999). The Chaco low, Bolivian high, LLJ, and SACZ together form the main components of the South American Monsoon System (SAMS) (Zhou and Lau, 1998), affecting rainfall in DJF. In austral winter (JJA), the Chaco low and the SACZ weaken, leading to less moisture transport from the north. Cold fronts from the south (Argentina) penetrate into the Bolivian lowlands, leading to low temperatures and to limited precipitation when colliding with warm tropical air masses (Ronchail and Gallaire, 2006; SENAMHI, 2009). The Bolivian high is displaced to the northwest of the continent and westerly winds prevail in Bolivia, preventing moisture transport from the lowlands to the Andes in JJA (Vuille, 1999).

2.3. Methods

2.3.1. Data

Our data consisted of meteorological observations, reanalysis data, and indices from various climate modes (PDO, ENSO, AAO, and others). From a total of 108 meteorological stations provided by SENAMHI we selected all stations that covered at least 30 years with less than 25% of missing data. We made one exception to the rule for a station with 29 years of data in a region with low station density. We tested all stations for homogeneity and excluded all stations with more than five change points within 30 years (see also subsection 2.3.2 on data homogenization). This left us with 29 and 68 stations of daily temperature (minimum and maximum) and precipitation measurements, respectively (Figure 2.1d,g). Temperature (precipitation) was measured by 11 (20) stations in the northern lowlands, 2 (4) in the southern lowlands, 2 (9) in the northern Andean slopes, 10 (15) in the southern Andean slopes, and 4 (20) in the Altiplano. Observation periods varied among stations, ranging from 29 to 94 years. On average, observations lasted from 1960 to 2009, covering 50 years with less than 8% missing data. Vertically integrated moisture flux convergence (VIMFC) ($\text{kg m}^{-1}\text{s}^{-1}$) was calculated from surface pressure and 3D fields of specific humidity and zonal and meridional components of wind speed from the National Centers for Environmental Prediction–National Center for Atmospheric Research (NCEP–NCAR) reanalysis dataset ($2.5^\circ \times 2.5^\circ$) (Kalnay et al., 1996):

$$VIMFC = -\frac{1}{g} \int_{300hPa}^{1000hPa} \frac{\partial uq}{\partial x} + \frac{\partial vq}{\partial y} dp, \quad (2.1)$$

where q is the specific humidity ($\text{kg}_{\text{H}_2\text{O}} \text{kg}^{-1}$), p is the pressure (Pa), u and v are the zonal and meridional component of wind speed (m s^{-1}), and g is the gravitational acceleration (m s^{-2}) (Van Zomeren and Van Delden, 2007). From the numerous PDO indices available, we used the index from Zhang et al. (1997) with an updated version available at (<http://jisao.washington.edu/pdo/>) (Figure 2.2). The ENSO index was obtained from Smith et al. (2000) with an updated version available at

(www.esrl.noaa.gov/psd/enso). This ENSO index identified EN and LN events for months when both the SST and Southern Oscillation index (SOI) exceeded the 20th percentile. Most EN events occurred during PDO(+), whereas all LN events during PDO(-). From 1960 to 2009, there were a total of 7 EN events and 5 LN events. The AAO index was obtained from Thompson and Wallace (2000) with an updated version available at www.jisao.washington.edu/aao/. In addition to PDO, ENSO and AAO we also looked at numerous other climate modes, including the Atlantic Multidecadal Oscillation (AMO; Enfield et al. 2001), as well as the Atlantic and Pacific Meridional Mode (AMM and PMM, respectively; Chiang and Vimont 2004), all available at (www.esrl.noaa.gov/psd/data/climateindices/list/). However, AMO, AMM, and PMM had no significant impact on climate variability in Bolivia and are therefore not presented in the results section.

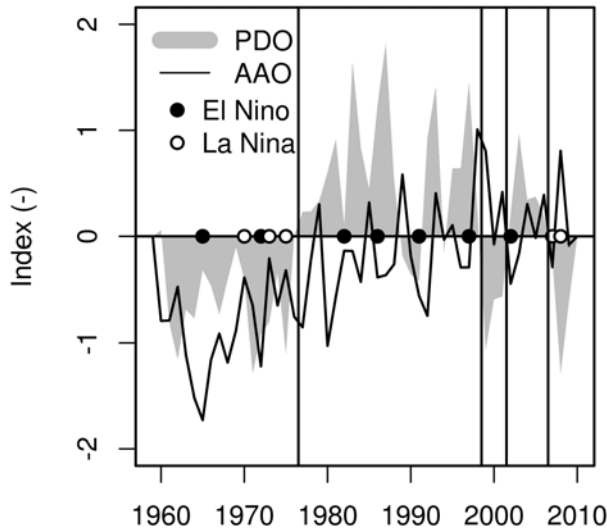


Figure 2.2: PDO, EN, and LN events and AAO (annual averages). Vertical lines mark warm (+) and cold (-) phases of PDO.

2.3.2. Data homogenization

Prior to data homogenization, all values were converted to missing values if precipitation was negative, and if daily minimum temperature exceeded daily maximum temperature. In case of the latter, both minimum and maximum values were set to missing values. The data were then homogenized by detecting and adjusting for multiple changepoints, using the software RHtestV3 (www.clivar.org/organization/etccdi/etccdi.php). Changepoints not related to climate processes can be introduced by changes in measurement instruments, measurement location, or measurement procedures. Adjusting for changepoints homogenizes the data such that temporal variations are assumed to be caused by climate processes only. There are three fundamental differences between the nature of temperature and precipitation series. Temperature series have a more Gaussian-like distribution, may contain negative and positive values, and are continuous. Precipitation series do not have a Gaussian distribution, only contain nonnegative values, and are not continuous. Given these differences, methods for changepoint detection and adjustment slightly differ for temperature and precipitation series. However, in both cases, changepoint detection is based on the two-phase regression model (Wang, 2003). Here, a time series is divided into segments, and a linear regression is fitted to each segment:

$$X_t = \begin{cases} \mu_1 + \beta_1 t + \epsilon_t & 1 \leq t \leq c \\ \mu_2 + \beta_2 t + \epsilon_t & c < t \leq n \end{cases}, \quad (2.2)$$

where $\{X_i, i=1, \dots, N\}$ is a data series observed at times $t_1 < \dots < t_i \dots < t_N$, and $\{\epsilon_t\}$ is the zero-mean independent random error with a constant variance. Changepoints occur when the mean (step type) and/or the slope (trend type) among segments changes. Thus, the time c is a changepoint if $\mu_1 \neq \mu_2$ (step type) and/or if $\beta_1 \neq \beta_2$ (trend type). In the case of temperature, a penalized maximal t and F test identify c and test for its statistical significance (Wang, 2008). In the case of precipitation, c is identified and tested for statistical significance with two maximal F tests (Wang et al., 2010). Changepoints were adjusted with the quantilematching (QM) adjustment (Wang et al., 2010). This approach homogenizes the data by adjusting the series in such a way that the empirical distributions of all segments of the detrended series match each other. Series are detrended by subtracting the estimated linear trend component from the series. This detrended series is then used to develop empirical cumulative distribution functions (ECDF) for each segment of the base series, and to define the adjustments needed to make the base series homogeneous. Regarding precipitation, it is necessary to model the event occurrence and the nonzero amounts separately. Days without precipitation are not altered. To promote a high quality level, we excluded all stations with more than five changepoints within 30 years. The impact of homogenization was assessed by comparing trends from 2 datasets, one where homogenization was applied to all stations with changepoints, and the other

where homogenization was not applied. In theory, homogenization should eliminate all artificial trends. In practice however, homogenization may (i) not change a trend, (ii) eliminate a trend, (iii) introduce a trend, or (iv) change the direction of a trend. We considered homogenization to be successful for cases (i) and (ii) and not successful for cases (iii) and (iv). Since trend detection varied among indices, we chose two indices that indicated whether homogenization was successful or not. We chose the two basic and straight forward indices of total annual precipitation (prcptot) and monthly maximum temperature (txx). We then built a final database that consisted of stations with homogenized time series for which homogenization was successful and stations with nonhomogenized time series for which changepoints were absent or homogenization was unsuccessful. This conservative approach avoided many questionable impacts of homogenization, without having to reduce the number of stations.

The RHtest revealed that the majority of time series did contain changepoints. According to this test, only 11 maximum and 4 minimum temperature time series (38% and 14% of stations) and 21 precipitation time series (31% of stations) were assessed to be homogeneous (Fig. 2.3). About half of the temperature and 93% of the precipitation time series exhibited no more than two changepoints per 30 years. In most cases, homogenization did not introduce or change the sign of a trend of the time series. This did occur though for 6 temperature and 21 precipitation time series (21% and 31% of stations) (Tab. 2.1). The homogenization from these stations was rejected and the not-homogenized time series were used for further analysis instead. Some temperature time series included more than five changepoints per 30 years. These stations were retained for further analysis if their corresponding minimum or maximum temperature series did not exceed five changepoints per 30 years.

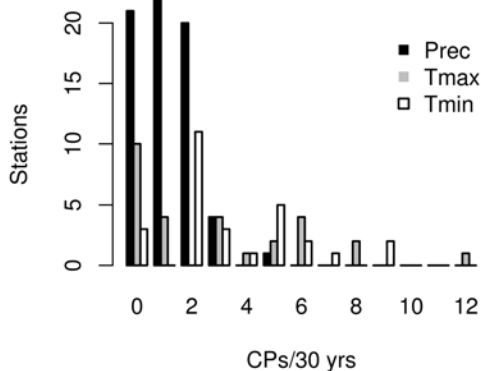


Figure 2.3: Number of stations with the number of detected change points per 30 years for precipitation (black), maximum temperature (gray), and minimum temperature (white).

Table 2.1: Number of all stations (Total), stations without changepoints, not homogenized (NH) stations despite the existence of changepoints, and homogenized stations for maximum temperature (Tmax), minimum temperature (Tmin), and precipitation (Prec).

	Number of stations			
	Total	No changepoints	NH despite changepoints	Homogenized
Tmax	29	11	6	12
Tmin	29	4	6	19
Prec	68	21	21	26

2.3.3. Climate means and extremes

Monthly and annual values of climate means and extremes were calculated from daily data applying the following decision rules. Monthly values were calculated if no more than 3 days were missing in a month, while annual values were calculated if no more than 15 days were missing in a year. No annual value was calculated if any one month's data was missing. Regarding climate extremes, we calculated 27 indices defined by the Expert Team on Climate Change Detection and Indices (www.clivar.org/organization/etccdi/etccdi.php). Indices can be grouped into five categories: absolute indices, threshold indices, percentile-based indices, duration indices and others. There were 17 indices related to temperature and 10 to precipitation. (Names, definitions and example values of indices are provided in Tab. A.1 and Tab. A.2 in the appendix.) Some threshold indices (e.g., summer days) were initially designed for temperate climates. Such indices were nevertheless useful in higher (colder) and in drier regions of Bolivia. We included one user-defined threshold index more suitable for the tropics, namely the annual count of days with maximum temperatures exceeding 30°C (su30). Climate indices were computed with the software RCLimDex (www.clivar.org/organization/etccdi/etccdi.php).

2.3.4. Variability

We quantified the impacts of the PDO, ENSO, and AAO on anomalies of climate means and extremes for five climatologically contrasting regions, namely the northern lowlands (NLL) and southern lowlands (SLL) (<800 m MSL), northern Andean slopes (NAS) and southern Andean slopes (SAS) (800–3200 m MSL) and Altiplano (AP) (3200–6500 m MSL). The north–south division was defined at 18°S, roughly distinguishing between a wet northern and a dry southern part. We applied an analysis of variance (ANOVA) to the station data, declaring PDO phases, ENSO phases, AAO phases, regions, and seasons as treatments. Impacts were expressed as differences in the mean and the corresponding confidence interval. The statistical significance of

changes in the mean was verified using a t -test and a significance level of 5%. Following the approach from Silva et al. (2011), we accounted for the impacts of the warm and cold phases of PDO on ENSO as follows. If the EN year occurred during PDO(+) [PDO(-)], the anomalies were calculated by subtracting the mean value of neutral years during the PDO(+) [PDO(-)] from the value of the particular EN month. In case of LN, all events occurred during PDO(-). Thus, LN anomalies were calculated by subtracting the mean value of neutral years during the PDO(-) from the value of the particular LN month. We classified a year as an EN or LN year if the EN or LN event occurred either during December, January, or February.

2.3.5. Trends

First we determined appropriate periods for trends in climate means. For this purpose we calculated the standardized anomalies (i.e., anomalies divided by the standard deviation) of monthly temperature and precipitation from all stations from 1960 until 2009. We computed the monthly mean of these anomalies across all stations, checked that the data were normally distributed, and detected the optimal positioning and number of changepoints that marked a shift in the mean, using the Segment Neighborhood method (Auger and Lawrence, 1989). We then smoothed the data applying a locally weighted polynomial regression (LOESS; Cleveland and Devlin 1988) and tested the robustness of the changepoints and of the shape of smoothed curve by excluding stations. Appropriate periods for calculating trends were then identified from minima and maxima of the smoothed curve and from the changepoints of the standardized anomalies. Periods contained one changepoint and started and ended with a minimum and maximum (or vice versa) of the smoothed curve. In addition, we calculated standardized anomalies from 1944 to 2010 for a subset of 10 rainfall time series that were assessed to be homogeneous using the RHTest and that exceeded 60 years of data. These stations were distributed throughout Bolivia and included Cochabamba, Concepción, La Paz, Magdalena, Potosi, Roboré, San Borja, San Calixto, Sucre, and Trinidad.

Trends were calculated for each station separately (confidence intervals in Fig. 2.4 and Fig. 2.7) and for spatially interpolated values (maps in Fig. 2.6 and Fig. 2.11), applying a linear regression analysis with the least squares approach and tested for significance using the Mann–Kendall trend test (Mann, 1945). The spatial interpolation was achieved with the Cressman function (Cressman, 1959) and accounted for the orographic effects on temperature by bringing actual temperatures down to sea level before, and back to real height after the interpolation. For this we used a local lapse rate of $-3.4^{\circ}\text{C km}^{-1}$ ($R^2 = 0.9$) derived from our data of monthly mean maximum temperature, as well as station heights and a digital elevation model

Regarding climate extremes, trends of all indices were computed for the whole time series of each individual station, as well as for two contrasting precipitation subperiods for selected indices [very wet days (r95p), rainfall intensity (sdii), consecutive dry

days (cdd), and consecutive wet days (cwd)]. As for climate means, trends were calculated with a linear regression analysis using the least squares approach and tested for significance using the Mann–Kendall trend test (Mann, 1945). The more the stations agreed on a trend, the more likely this trend was due to a general trend and not due to any site specific disturbance. We considered an index to show a clear signal if more than one-third of all stations detected either significant increasing or decreasing values and if more than 75% agreed on the direction of change. We applied this rule to Bolivia as a whole and to the three regions of lowlands, Andean slopes, and Altiplano.

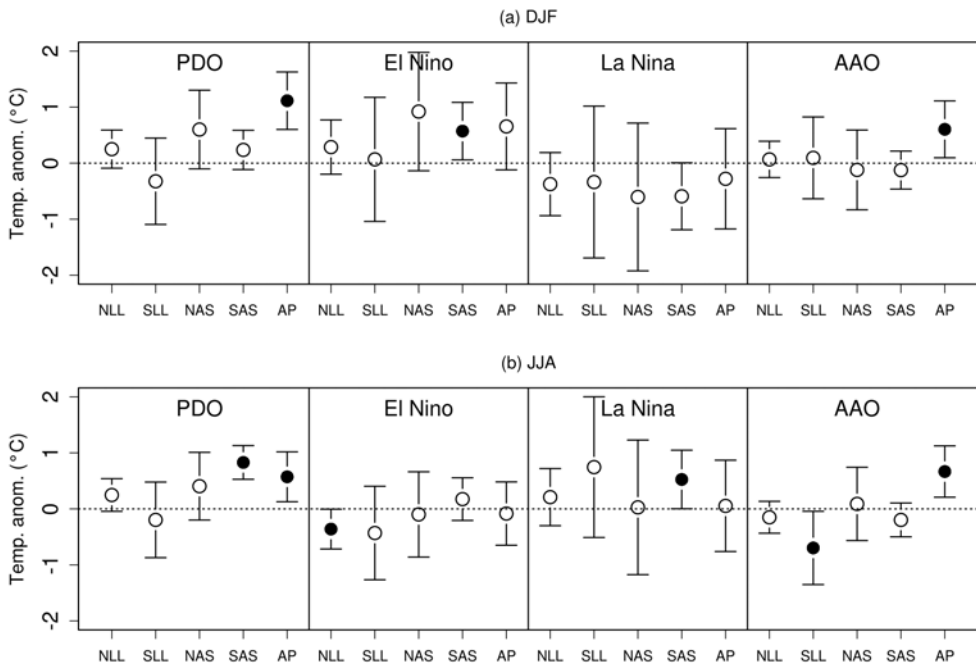


Figure 2.4: Differences in monthly mean maximum temperature anomalies ($^{\circ}\text{C}$) comparing PDO(+) to PDO(-), El Niño events to neutral years, La Niña events to neutral years, AAO(+) to AAO(-) in (a) DJF and (b) JJA for NLL, SLL, NAS, SAS, and AP. Dots present the difference of the means, while the bars show the respective confidence intervals with a probability of 95%. Black dots denote statistically significant changes with a significance level of 5% (t -test).

2.4. Results

2.4.1. Climate means

Temperature

Impacts of climate modes were assessed by comparing positive against negative phases of PDO and AAO, as well as ENSO events against neutral years. In DJF, temperatures were generally warmer in the Andes during PDO(+), EN, and AAO(+) with significant changes as big as 1.1°C (Fig. 2.4). In JJA, temperatures were higher in the Andes during PDO(+), LN, and AAO(+) and lower in the northern lowlands during EN and southern lowlands during AAO(+).

Standardized temperature anomalies showed an overall increasing trend with a change-point located in 1986/87, coinciding with an EN event (Fig. 2.5). A smoothed curve revealed a steady increase of temperature between 1965 and 2004 and short-term negative trends during 5 years before and after this period. The increase of standardized temperature anomalies from 1965 to 2004 was statistically significant (Mann–Kendall trend test with $p < 0.05$), with most stations having detected a temperature increase of 0.1°C per decade, corresponding to an overall increase of 0.4°C from 1965 to 2004 (Tab. 2.2). About half of the stations detected significant increases in temperature (17 stations in DJF and 14 stations in JJA). No significant changes were detected by 10 and 13 stations during DJF and JJA, respectively. Highest trends were detected during JJA in the Andes (Fig. 2.6). Some cooling has also occurred in this season close to the Titicaca Lake.

Precipitation

Annual rainfall was higher in the lowlands during PDO(+) (196 mm yr⁻¹), EN (105 mm yr⁻¹), and LN (143 mm yr⁻¹) (Fig. 2.7). In DJF, rainfall was higher in the lowlands during PDO(+) (35 mm month⁻¹) and LN (36 mm month⁻¹) and lower during EN in the Andes (-26 mm month⁻¹). In JJA, rainfall in the northern lowlands was higher during EN (15 mm month⁻¹) and lower during AAO(+) (-10 mm month⁻¹). PDO- and ENSO- related rainfall anomalies in DJF were accompanied by corresponding changes in moisture convergence (Fig. 2.8). In the southern lowlands, moisture convergence anomalies during PDO(+) opposed observations, but were not statistically significant.

Monthly standardized precipitation anomalies showed oscillating trends with change-points located in 1972 and 1988, the first one just before and the second just after an EN event (Fig. 2.9a). The smoothed curve revealed an increasing trend from about 1965 until 1984 and a decreasing trend from about 1985 until 2004. The increase and decrease of standardized precipitation anomalies from these two periods were

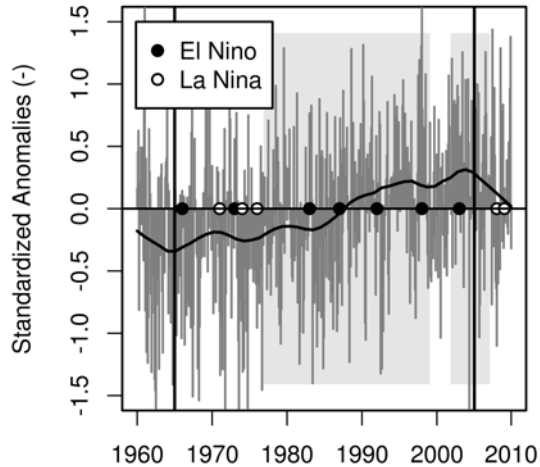


Figure 2.5: Monthly mean standardized temperature anomalies (-) (gray bars) from 29 stations with a fitted LOESS curve (black curve). Black dots denote El Niño and white dots La Niña events. Periods shaded in gray correspond to PDO(+) and not shaded periods to PDO(-). Vertical black lines mark the period 1965-2004.

both statistically significant (Mann–Kendall trend test with $p < 0.05$). Standardized anomalies from 10 homogeneous (RHtest) stations and >60 years of data revealed a similar pattern. Here, however, the negative trend that started around 1985, continued until the end of the time series in 2010 (Fig. 2.9b). The LOESS curve remained below 0 throughout 1944 until 1972 with a minimum located around 1965. Annual standardized precipitation anomalies revealed a very similar pattern, following the basic structure of the PDO index (Fig. 2.10).

Most stations detected an increase in precipitation from 1965 to 1984 by 12% in DJF and 18% in JJA and from 1984 to 2004 by -4% in DJF and -10% in JJA (Tab. 2.2). Most stations with significant trends agreed on the sign of the trend. Statistically significant positive (negative) trends were detected by 17 (0) stations in DJF and 9 (1) stations in JJA from 1965 to 1984 and by 1 (11) stations in DJF and 3 (1) stations in JJA from 1985 to 2004 (Tab. 2.2). Positive trends during 1965–84 and negative trends during 1985–2004 were most evident in DJF in the lowlands (Fig. 2.11). In JJA and in the Andes, trends were less uniform. Trends during March to May (MAM) and September to November (SON) were generally increasing from 1965 to 1984 and decreasing from 1985 to 2009 (not shown).

2.4 Results

Table 2.2: Number of stations throughout Bolivia with significantly increasing (1), decreasing (2), and no significant (o) linear trends (p value 0.05, Mann–Kendall) of seasonal (DJF, JJA) temperature (T) and precipitation (P) for the period 1965–2004 for temperature and 1965–84 and 1985–2004 for precipitation. The bottom line gives the most frequently detected changes in temperature ($^{\circ}\text{C}$) and precipitation (%).

	DJF			JJA		
	T1965-04	P1965-84	P1985-04	T1965-04	P1965-84	P1985-04
+	17	17	1	14	9	3
-	2	0	11	2	1	1
o	10	51	56	13	58	64
	0.5 $^{\circ}\text{C}$	12%	-4%	0.4 $^{\circ}\text{C}$	18%	-10%

(a) T trend DJF 1965-04 ($^{\circ}\text{C}$ 10yrs $^{-1}$)



(b) T trend JJA 1965-04 ($^{\circ}\text{C}$ 10yrs $^{-1}$)

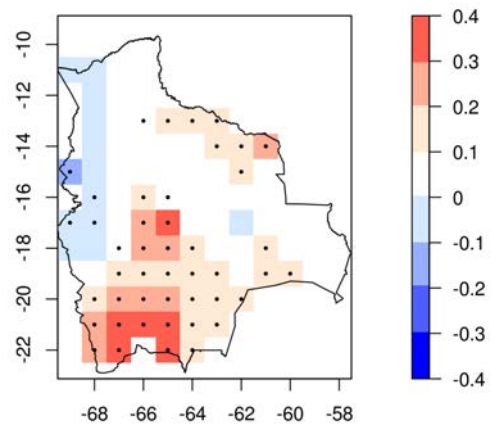


Figure 2.6: Trends of monthly mean maximum temperatures [$^{\circ}\text{C}$ (10 yrs) $^{-1}$] from 1965 to 2004 during (a) DJF and (b) JJA. Black lines encircle areas of statistical significance with a p value < 0.05 applying a Mann–Kendall significance test for linear trends.

2.4.2. Climate extremes

Temperature-related climate indices revealed a warming trend throughout Bolivia with significantly more warm nights and days (tn90p, tx90p), fewer cool nights and days (tn10p, tx10p), fewer frost days (fd0), longer warm spells (wsdi), more summer days (su25), and higher monthly minimum of daily minimum temperatures (tnn) (Fig. 2.12). Other significant trends included more tropical nights (tr20) and more days when maximum monthly temperatures were above 30°C (su30) in the lowlands. Furthermore, we detected a longer growing season (gsl), higher monthly maximum and minimum temperatures (txx, tnn), and a shorter duration of cold spells (csdi) in the Altiplano. Given the oscillating trend in rainfall, only two indices showed a coherent pattern, with an increase in cwd and a decrease in sdii in the lowlands.

Extreme precipitation events differed significantly among PDO, ENSO, and AAO phases. PDO(+) led to more intense or more frequent r95p in the northern and southern lowlands, more frequent cwd in the northern lowlands, and higher sdii in the southern lowlands (Tab. 2.3). EN led to less cdd and cwd in the Altiplano, while LN led to more intense or frequent r95p in the northern lowlands. During AAO(+), consecutive wet days were more frequent in the Altiplano.

Standardized anomalies of selected extreme precipitation events revealed the following trends for 1965–84 and 1985–2009. The r95p and sdii followed the basic pattern of annual precipitation (Fig. 2.13a). In the case of very wet days, 9 stations detected significant increases from 1965 to 1984 and 6 stations significant decreases from 1985 to 2004, whereas in the case of rainfall intensity, a fairly equal amount of stations detected increases and decreases from 1965 to 1984 and 11 stations detected significant decreases from 1985 to 2004 (Tab. 2.4). The number of cdd and cwd also followed the basic pattern of annual precipitation, with generally more (less) cdd (cwd) in years with less rainfall. Consecutive dry days decreased from 1960 until the 1980s and remained relatively constant afterward (Fig. 2.13b), with 5 stations detecting significantly decreasing trends from 1965 to 1984 (Tab. 2.4). The number of cwd, on the other hand, increased from 1965 to 1984 but also remained relatively constant afterward, with 10 stations detecting significantly increasing trends from 1965 to 1984.

2.5. Discussion

We quantified the impacts of PDO, ENSO, and AAO on temperature and precipitation means and extremes and detected trends from 1960 to 2009 in Bolivia, distinguishing among climatologically contrasting regions and seasons. Temperatures were found to be higher during PDO(+), EN, and AAO(+) in the Andes. Total amounts of rainfall, as well as the number of extreme events, were higher during PDO(+), EN, and LN in the lowlands. During austral summer (DJF), EN led to drier conditions in the Andes with more variable precipitation. Temperatures increased at a rate of 0.1°C per decade, with stronger increases in the Andes and in the dry season.

Other climate modes (AMO, AMM, and PMM) revealed no significant impacts on climate variability in Bolivia. Rainfall totals increased from 1965 to 1984 (12% in DJF and 18% in JJA) and decreased afterward (-4% in DJF and -10% in JJA), following roughly the pattern of PDO. Trends of climate extremes generally corresponded to trends of climate means.

These findings are subject to some remaining uncertainties, beyond those quantified, because of the following methodological issues. (i) Stations were not evenly distributed among regions, with low station densities in the southern lowlands and Altiplano. We encourage the installation of additional meteorological stations to better monitor climate variability and trends in these remote areas. (ii) Data homogenization was

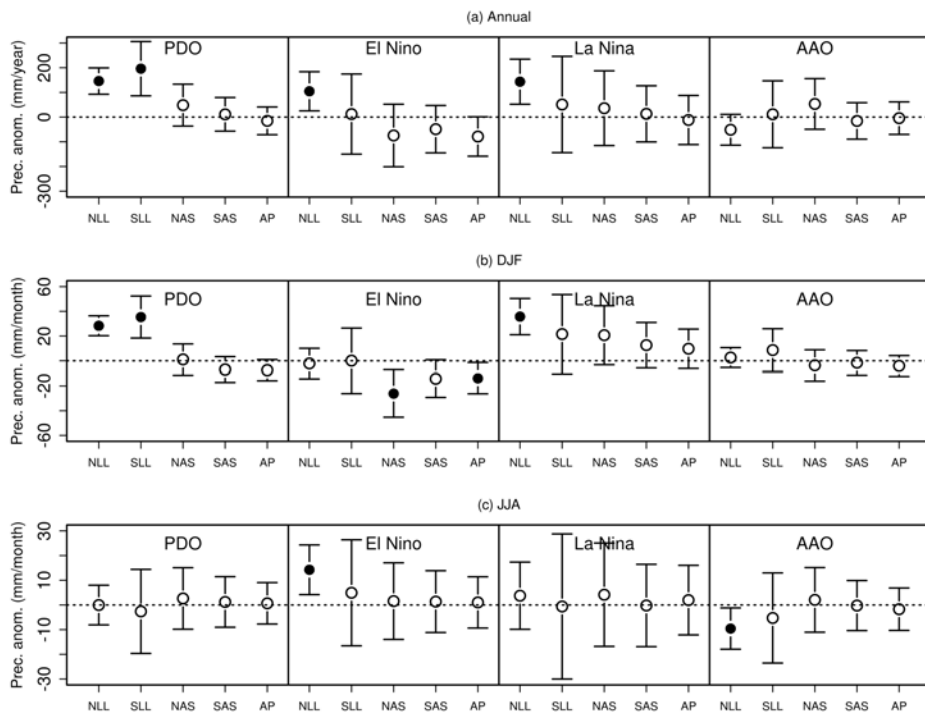


Figure 2.7: Differences in (a) annual precipitation anomalies (mm yr^{-1}) and monthly precipitation anomalies (mm month^{-1}) of (b) DJF and (c) JJA, comparing PDO(+) to PDO(-), El Niño events to neutral years, La Niña events to neutral years, and AAO(+) to AAO(-) for NLL, SLL, NAS, SAS, and AP. Dots present the difference of the means, while the bars show the respective confidence intervals with a probability of 95%. Black dots denote statistically significant changes with a significance level of 5% (t -test).

challenging given that changepoints were not previously documented. Our approach, rejecting data homogenization when it introduced or changed the sign of the direction of a trend, was of a rather practical nature. However, given the strong agreement among stations on the direction of significant trends of temperature and precipitation means, and given that 10 homogeneous (RHtest) stations reproduced the same basic patterns in rainfall trends as all stations combined, we are confident in our results. Nevertheless, it would be very beneficial for future research to start documenting any changes in measurement instruments, sites, and procedures. (iii) Our analysis of variance was not able to distinguish between impacts from the PDO, ENSO, AAO, and other sources, including climate change. Thus, part of the temperature differences among PDO and AAO phases was likely due to enhanced greenhouse gases rather than to the climate modes, given that most PDO(-) and AAO(-) years occurred earlier, while most PDO(+) and AAO(+) years later. Thus, the recent switch to PDO(-) in 2007 does not imply that temperatures will return to the values of the previous PDO(-) phase.

(iv) Finally, the increasing length of the growing season (gsl) detected in the Altiplano must be interpreted with care. The index assumes that the growing season is limited by temperature only. In the Altiplano however, the growing season is limited by both temperature and rainfall. Given that rainfall decreased since 1985 and that higher temperatures were likely to have increased evapotranspiration, the growing season may not have increased after all. We therefore recommend developing an index for which growing-season length is limited by both temperature and precipitation.

Despite limitations and differences in methods, data, and scale, our results confirmed and complemented numerous findings from the literature, including warmer conditions during PDO(+) and EN in DJF in the Andes, more rainfall during PDO(+)

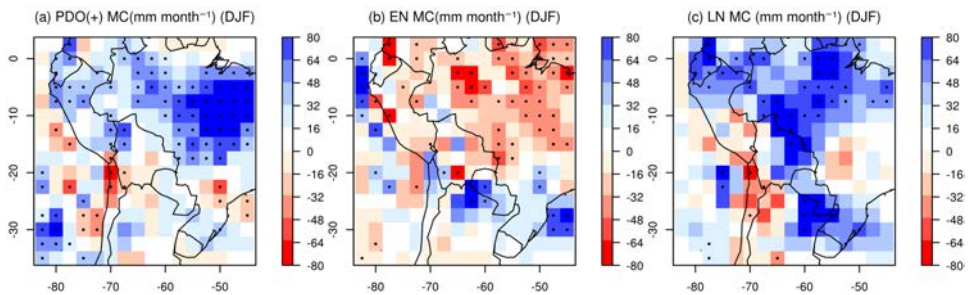


Figure 2.8: Differences in monthly mean vertically integrated moisture flux convergence (VIMFC) (mm month^{-1}) comparing (a) PDO(+) to PDO(-), (b) El Niño events to neutral years and (c) La Niña events to neutral years in DJF. Black dots denote areas of statistical significance with a p value < 0.1 , applying a t -test.

in the lowlands and less rainfall during EN in DJF in the Bolivian Andes (Garreaud et al., 2009). Rainfall anomalies during the wet season can be explained by changes in moisture convergence. However, this did not apply for rainfall anomalies during PDO(+) in the southern lowlands. A possible alternative cause of enhanced rainfall here may be a stronger low-level jet. Magnitudes of positive anomalies of mean and extreme rainfall related to PDO(+) and ENSO in the northern lowlands were comparable, making PDO(+) appear as a period with constant EN-like or LN-like conditions. Possible reasons for this counterintuitive similarity are differences in sample size and the fact that PDO anomalies included ENSO years as well as years with extreme weather from non-ENSO events. We also note that ENSO anomalies were not always extreme. This made a separation of the contribution of PDO(+), EN, and LN challenging.

Our estimated temperature trend of 0.1°C per decade is comparable but lower than the trend of 0.15°C per decade detected by Vuille et al. (2003). Differences may be due to the larger number of lowland stations used in our study. The fact that temperature trends were higher in the Andes compared to the lowlands (Fig. 2.6) may explain why our overall trend was slightly lower.

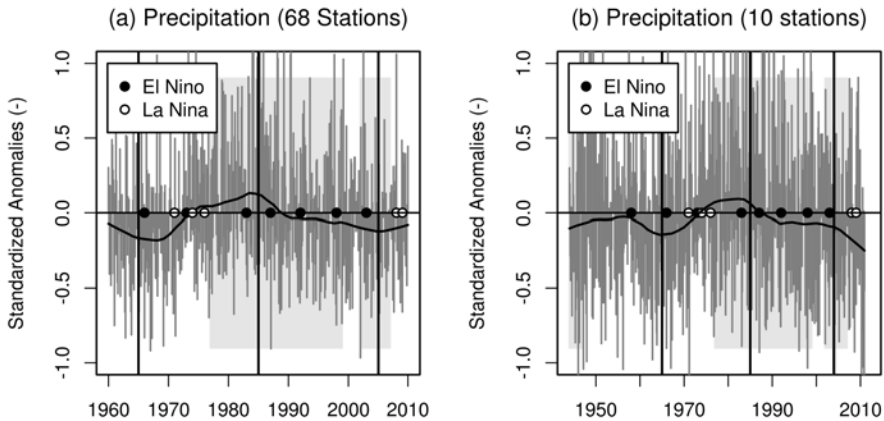


Figure 2.9: Monthly mean standardized precipitation anomalies (-) (gray bars) from (a) 68 stations with time series lasting from 1960 to 2009 and (b) 10 stations which were assessed to be homogeneous using the RHTest with time series lasting from 1944 to 2010, fitted with a LOESS curve (black curve). Black dots denote El Niño and white dots La Niña events. Periods shaded in gray correspond to PDO(+) and unshaded periods to PDO(-). Vertical black lines mark the periods 1965-1984/85-2004.

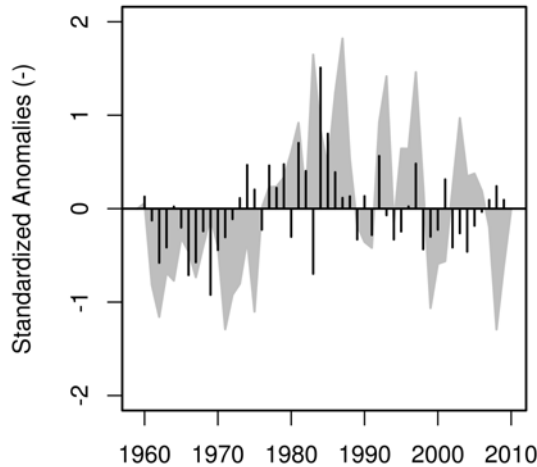


Figure 2.10: Annual mean standardized precipitation anomalies (-) (black bars) from 68 stations and the PDO index (gray polygon).

Our positive precipitation trend from 1960 to 1984 confirmed results from Ronchail (1995) and Marengo (2004). The shift from mainly negative to mainly positive anomalies in the 1970s may be associated with the shift from the cold to the warm PDO phase in 1976/77, as also suggested in Marengo (2004). The negative trend from 1985 to 2004 confirmed the decrease of rainfall after 1982 documented in Espinoza Villar et al. (2009) as well as Toledo (2010), and may be related to decreasing values of the PDO index. Observed decadal trends in annual rainfall anomalies showed considerable similarities with the PDO index, and no similarities with numerous other climate modes, including AAO, AMO, AMM, and PMM, suggesting that the PDO is a principal driver of decadal rainfall variability in Bolivia.

We conclude that Bolivia's climate is likely to continue to be warmer and drier than average in the near-term future. Since the PDO switched to a cold phase in 2007, not only the total rainfall but also the frequency and intensity of wet days, as well as the number of consecutive wet days and rainfall intensity, are likely to continue to be below average in the lowlands, increasing the risks of drought and partly associated wild fires. ENSO-related floods, however, can occur nevertheless. An increasing risk of drought can also be expected in the Andes, given the above-average temperature rise there. The current dry conditions in the lowlands may reverse back to wetter

conditions, while rainfall in the Andes may become even less, once the PDO reverses from its cold to its warm phase.

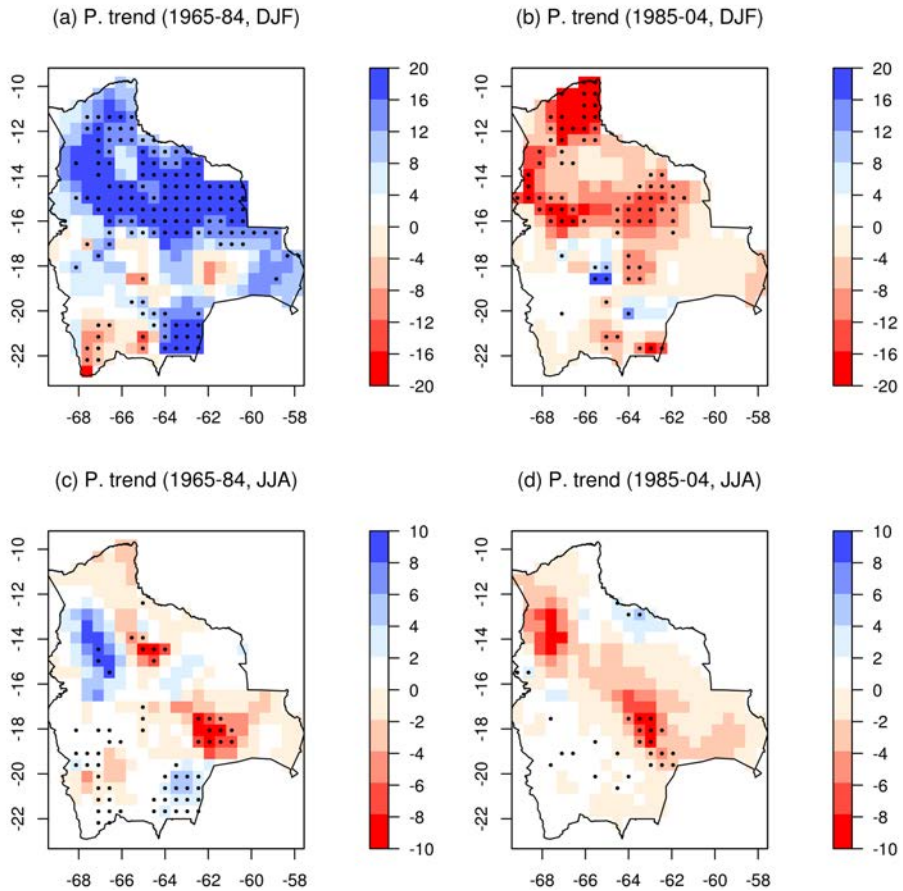


Figure 2.11: Trends of monthly precipitation [mm (10 yrs)^{-1}] from (a) 1965 to 1984 and (b) 1985 to 2004 in DJF. (c), (d) As in (a) and (b), but for JJA. Black dots denote areas of statistical significance with a p value < 0.05 , applying a Mann-Kendall significance test for linear trends.

Table 2.3: Differences of r95p (mm yr⁻¹), cdd (days), cwd (days), and sdii (mm day⁻¹) anomalies comparing PDO(+) with PDO(-), EN and LN events with neutral years, and AAO(+) with AAO(-) in the regions NLL, SLL, NAS, SAS, and AP. Boldface numbers denote statistically significant changes with a significance level of 5% (*t*-test).

Variable	Treatment	NLL	SLL	NAS	SAS	AP
r95p (mm/yr)	PDO	71.2	91.1	7.2	-11.0	-3.5
	El Niño	39.0	-17.7	-13.8	4.9	-9.9
	La Niña	63.3	5.6	-17.7	-4.8	-3.4
cdd (days)	AAO	-29.1	3.8	-0.5	-10.8	-6.4
	PDO	-2.1	-2.0	-2.3	-8.4	-4.0
	El Niño	-5.4	-10.3	-2.7	-2.7	-11.4
cwd (days)	La Niña	-5.3	0.9	-4.4	-0.4	0.3
	AAO	0.9	-1.6	-3.8	-3.3	-7.5
	PDO	0.8	0.7	-0.1	0.1	-0.5
sdii (mm/yr)	El Niño	-0.2	-0.8	-0.7	-0.7	-1.1
	La Niña	1.1	-0.7	1.7	0.5	0.6
	AAO	0.1	0.4	0.5	0.2	1.0
sdii (mm/yr)	PDO	0.2	2.0	-0.2	-0.6	-0.2
	El Niño	0.0	-0.5	-0.2	-0.2	-0.3
	La Niña	0.2	0.3	-0.3	-0.4	-0.1
	AAO	-0.6	-0.5	-0.1	-0.7	-0.4

Table 2.4: Number of stations throughout Bolivia with significantly increasing (+), decreasing (-), and no significant (o) linear trends (*p* value < 0.05, Mann–Kendall) of r95p, cdd, cwd, and sdii for the periods 1965–84 and 1985–2004.

		r95p	cdd	cwd	sdii
1965-84	+	9	1	10	7
	-	1	5	0	6
	o	58	62	58	55
1985-04	+	3	0	3	0
	-	6	1	1	11
	o	59	67	64	57

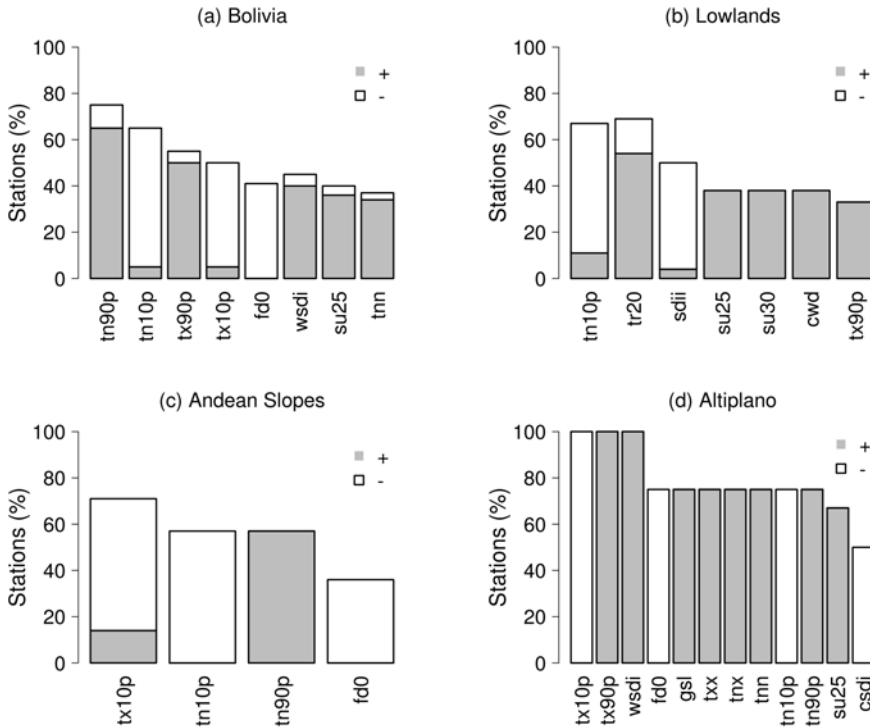


Figure 2.12: Percentage of stations with significantly increasing (gray) and decreasing (white) values of selected climate indices in (a) all of Bolivia, (b) Lowlands, (c) Andean slopes, and (d) Altiplano. Significance was tested with a Mann-Kendall trend test ($p < 0.05$).

The impact of climate change on the PDO and ENSO are highly uncertain. Most global circulation models (GCMs) used in the Intergovernmental Panel on Climate Change (IPCC) Fourth Assessment Report (AR4) do not properly represent the PDO for historic runs and show no significant changes under climate change scenario A1B (Furtado et al., 2011). The same models also do not agree on whether enhanced greenhouse gas emissions change the frequency and/or intensity of ENSO significantly (Collins et al., 2010). Projections from the most recent generation of climate models for the Fifth IPCC Assessment Report (AR5) are still to be assessed.

For future research we recommend analyzing the physical mechanism behind the rainfall trends in more depth, especially focusing on the role of the PDO. Furthermore,

we encourage developing threshold values that can be associated with historical disasters. Such values can be incorporated in an early warning system, which should also include the PDO index in addition to the ENSO index.

To conclude, we hope this research will contribute to a better understanding of historic climate variability and trends, and provide a basis for discussion on climate related disasters and research on regional climate change in Bolivia. Our findings may encourage further developing early warning systems for natural hazards and strategies for adaptation to climate change.

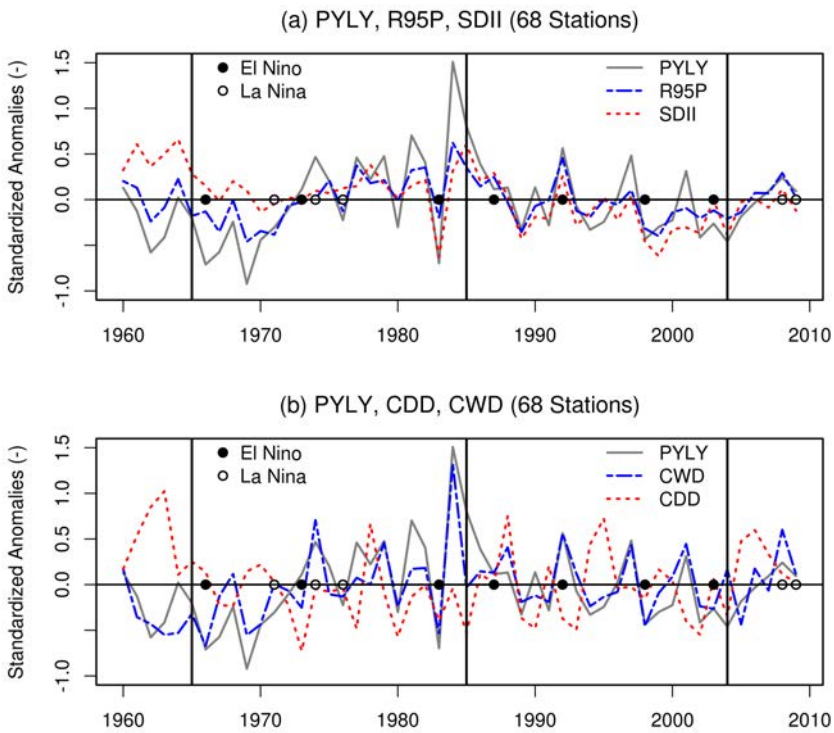


Figure 2.13: Standardized anomalies (-) of (a) annual precipitation (PYLY), r95p, and sdii; and (b) PYLY, cdd, and cwd from 68 stations with time series lasting from 1960 to 2009. Black dots denote El Niño and white dots La Niña events. Vertical black lines mark the periods 1965-1984/85-2004.

Acknowledgments

This research was supported by the Departmental Pilot Program of Adaptation to Climate Change (PDACC) as well as the project Raising the Alert about Critical Feedbacks between Climate and Land Use Change in Amazonia (AMAZALERT). PDACC is carried out by the Fundación Amigos de la Naturaleza (FAN) as well as the departmental government of Santa Cruz and funded by the embassy of the Netherlands. AMAZALERT is jointly funded by the European 7th Framework Programme and national organizations. We thank the Bolivian National Service of Meteorology and Hydrology (SENAMHI) for the provision of the meteorological data. We are thankful for the remarks from Prof. Dr. Wilco Hazeleger and Dr. Sarah Kew. We are grateful for the constructive comments from three anonymous reviewers who have helped to improve the quality of this paper.

3. Likely Ranges of Climate Change in Bolivia

Abstract

Bolivia is facing numerous climate related threats, ranging from water scarcity due to rapidly retreating glaciers in the Andes, to a partial loss of the Amazon forest in the lowlands. To assess what changes in climate may be expected in the future, 35 global circulation models (GCMs) from the 3rd and 5th Coupled Model Intercomparison Project (CMIP3/5) were analyzed for the Bolivian case. GCMs were validated against observed surface air temperature, precipitation and incoming shortwave (SW) radiation for the period 1961-1990. Weighted ensembles were developed and climate change projections for 5 emission scenarios were assessed for 2070-2099. GCMs revealed an overall cold, wet and positive SW radiation bias and showed no substantial improvement from the CMIP3 to the CMIP5 ensemble for the Bolivian case. Models projected an increase in temperature (2.5 to 5.9°C) and SW radiation (1 to 5%) with seasonal and regional differences. In the lowlands, changes in annual rainfall remained uncertain for CMIP3, while CMIP5 GCMs were more inclined to project decreases (-9%). This also applied to most of the Amazon basin, suggesting a higher risk of partial biomass loss for the CMIP5 ensemble. Both ensembles agreed on less rainfall (-19%) during drier months (JJA, SON), with significant changes in interannual rainfall variability, but disagreed on changes during wetter months (JFM). In the Andes, CMIP3 GCMs tended to less (-9%), while CMIP5 to more (+20%) rainfall during parts of the wet season. Our findings may provide inputs for climate change impact studies, assessing how resilient human and natural systems are under different climate change scenarios.

3.1. Introduction

The Plurinational state of Bolivia is facing numerous climate related threats. In the Andes, rapidly retreating glaciers affect the supply of drinking water, agricultural

This chapter has been published as:

Seiler, C., R.W.A. Hutjes, and P. Kabat, 2013: Likely Ranges of Climate Change in Bolivia. *Journal of Applied Meteorology and Climatology*, **52** (6), 1303–1317.

production and the provision of energy from hydropower (Bradley et al., 2006). In the lowlands, a reduction of rainfall as projected by some Global Circulation Models (GCMs) may lead to the partial loss of the Amazon forest (Rammig et al., 2010). Droughts and floods associated with the El Niño Southern Oscillation (ENSO) events affect thousands of people and lead to economic losses of millions of \$US (UNDP, 2011). Being a developing country with one third of the labor force working in the agricultural sector (www.ine.gob.bo), Bolivia is considered to be extremely vulnerable to climate change (WorldBank, 2010).

Given this exposure to climate related threats, a regional analysis of climate change projections is of great interest. The Fourth Assessment Report of the Intergovernmental Panel on Climate Change (AR4) documented climate change projections from multiple GCMs belonging to the 3rd Coupled Model Intercomparison Project (CMIP3) for the South American continent (Christensen et al., 2007). AR4 found that GCMs had a cold bias in the Andes and a slightly warm bias in the tropical lowlands. Averaged over tropical South America (12°N-20°S and 82°W-34°W, referred to as AMZ), this bias was estimated with an annual median of 0.6°C. Climate change projections in the same region showed a median increase of annual temperatures of 3.3°C and an interquartile range of 2.6 to 3.7°C under the intermediate emission scenario A1B. Regarding precipitation, the same report found a wet bias in the Andes and a dry bias in the tropical lowlands, estimated with an annual median of -8% for the AMZ region (Christensen et al. 2007, Figure S11.26 and Table S11.1). This dry bias was likely due to an underestimation, as well as a too far southward extension of the Intertropical Convergence Zone (ITCZ). In most of tropical South America, GCMs did not agree on the directional change of annual rainfall, resulting in a median change of 0% and an interquartile range of -3 to +6% in the AMZ region. This lack of agreement was confirmed by numerous other studies focusing on the Amazon region (e.g. Li et al., 2006; Jupp et al., 2010). Seasonal changes were more certain with more rainfall from January till March and less rainfall from July till September in major parts of the Amazon, including Bolivia's northern lowlands (Vera et al., 2006). In the Bolivian Altiplano, multiple GCMs revealed a warm and wet bias (Seth et al., 2010). Temperature projections under the high emission scenario A2 ranged from +5 to +6°C (monthly medians), while rainfall projections tended to less annual rainfall with decreases from May to September and increases from March and April.

Numerous attempts have been made to dynamically downscale global climate change scenarios for tropical South America (e.g. Soares and Marengo, 2009; Urrutia and Vuille, 2009; Marengo et al., 2010). Projections include temperature increases from 6-8°C with higher values during JJA, enhanced moisture transport from the Amazon to the La Plata Basin, leading to rainfall deficiency in the first and rainfall excess in the latter, and a more intense hydrological cycle with more rainfall in DJF and less rainfall in JJA in the Bolivian lowlands. However, projections are based on very few lateral boundary conditions (mainly HadAM3), limiting their robustness in a region with little agreement among GCMs on the directional change of rainfall. Other efforts include the CLARIS LPB project (www.claris-eu.org), which aims at predicting

regional climate change impacts on the La Plata Basin using several regional climate models in conjunction with 3 lateral boundary conditions (Boulanger et al., 2010). To our knowledge though, climate change scenarios related to CLARIS have so far only been published for southern South America (Nunez et al., 2009).

Previous analysis of climate change scenarios mentioned above are of mainly sub continental scale and include only very few Bolivian stations for model evaluation, making it difficult to apply this information to Bolivia. Also, an evaluation of the most recent generation of GCMs (CMIP5, see sec. 3.3.1) is still missing. The coarse spatial resolution of GCMs limits the validity of model results in the Andes. However, given the potential disagreement among models on directional changes of precipitation, a comprehensive evaluation of GCMs is a necessary precursor to any downscaling effort. We therefore analyzed projections from 35 different GCMs, including models from CMIP3 and CMIP5, as well as 5 emission scenarios. Doing this we assessed for the Bolivian case (i) how well GCMs reproduce historic climate patterns, (ii) what changes in climate means and variability may be expected and (iii) to what extent there are differences between the CMIP3 and CMIP5 ensemble. Our results may provide an input for climate change impact assessments, exploring the probability of climate related threats such as water scarcity or Amazon dieback in Bolivia.

The following sections describe our study area, methods, results and discussion. The method section outlines the data and emission scenarios, as well as approaches related to model validation, ensemble weighting and multi-model agreement. Model skills in reproducing historic climate patterns and future projections of temperature, precipitation and short wave (SW) radiation are presented in the results section. Our discussion interprets the results in the context of existing literature and elaborates on the principal findings.

3.2. Study area

Bolivia is a tropical country measuring more than one million km². With its main altitudinal divisions being lowlands (<800 m MSL), Andean slopes (800-3,200 m MSL) and highlands (Altiplano) (>3,200-6,500 m MSL), Bolivia's climate varies with increasing altitude from tropical to cold desert climate, with annual mean surface air temperatures ranging from 0 to 30°C (Fig. 3.1). Rainfall ranges from <300 to >3000 mm yr⁻¹ and varies from high to low from the northern Andean slopes, northern lowlands, southern lowlands and southern Andean slopes to the Altiplano, with a north-south division roughly at 18°S. Much higher values (>5000 mm yr⁻¹) along the northern Andean slopes are documented by SENAMHI (2009) from stations not included in this research. The austral summer (DJF) and winter (JJA) coincide with the wet and dry season respectively. Incoming SW radiation ranges from 160 to 260 W m⁻², with higher values in the Altiplano and southern lowlands. Seasonal differences in temperature, precipitation and SW radiation vary among regions, with largest seasonal differences being 8°C in the Andes, 180 mm month⁻¹ in the northern

lowlands and 112 W m^{-2} in the southern lowlands. To account for the spatial gradients in climate, we stratified Bolivia into the 3 regions northern lowlands (NLL), southern lowlands (SLL) and Andes (AND), roughly characterizing a warm humid, warm dry and cold dry climate respectively. Given the coarse spatial resolution of GCMs, Andean slopes were merged partly with lowlands and partly with Andes.

Climate patterns in Bolivia are shaped by the following synoptic scale systems. In austral summer (DJF) a low pressure system called the thermal Chaco low intensifies at 25°S , enhancing the easterly trade winds to transport moisture from the northern tropical Atlantic into the continent. Deflected by the Andes, moisture is transported southward from the Amazon to subtropical plains of Southeastern South America by a low level jet (LLJ) located at about 925-850 hPa ($\sim 1\text{km}$ MSL) and <100 km east of the Andean slopes (Marengo et al., 2004). This leads to enhanced precipitation with a southeastward extension towards the Atlantic Ocean, referred to as the South Atlantic Convergence Zone (SACZ). Simultaneously, the release of condensational heat over the Amazon and Andean slopes leads to the formation of the upper-level Bolivian high at 200 hPa (~ 12 km MSL) (Lenters and Cook, 1997), which further enhances moisture advection from the Amazon to the Bolivian low- and highlands (Vuille, 1999). An upper-tropospheric trough near the coast of Northeast Brazil forms as a response to the rising air motion over the continent (Silva and Kousky, 2012). The Chaco Low, Bolivian high, LLJ, SACZ and upper-tropospheric trough form the main components of the South American Monsoon System (SAMS) (Zhou and Lau, 1998), affecting rainfall in DJF. In austral winter (JJA), the Chaco low and the SACZ dissipate, leading to less moisture transport from the north. Cold fronts from the southern polar regions penetrate into the Bolivian lowlands, leading to low temperatures and to limited precipitation when colliding with warm tropical air masses (Garreaud, 2000; Ronchail and Gallaire, 2006; SENAMHI, 2009). The Bolivian high dissipates and westerly winds prevail in Bolivia, preventing moisture transport from the lowlands to the Andes in JJA (Vuille, 1999).

Sources of climate variability in Bolivia include the (i) Pacific Decadal Oscillation (PDO), (ii) El Niño Southern Oscillation (ENSO) and (iii) Antarctic Oscillation (AAO) (Garreaud et al., 2009; Seiler et al., 2013a). Climate variability may lead to extreme events including droughts and floods. Droughts mainly occur in the southern lowlands and in many regions in the Altiplano from June to August (CONARADE, 2010), while floods happen from January to March mainly in the savannas of the northern lowlands (Bourrel et al., 2009), but also in the catchment areas of the Lake Titicaca and Poopó (UNDP, 2011) in the Andes.

Meteorological observations reveal that Bolivia's climate is currently warming at a rate of 0.1°C per decade, with larger increases in the Andes and during the dry season (Seiler et al., 2013a). Rainfall increased from 1965-1984 (12% in DJF and 18% in JJA) and decreased from 1985-2004 (-4% in DJF and -10% in JJA), following roughly the pattern of the PDO.

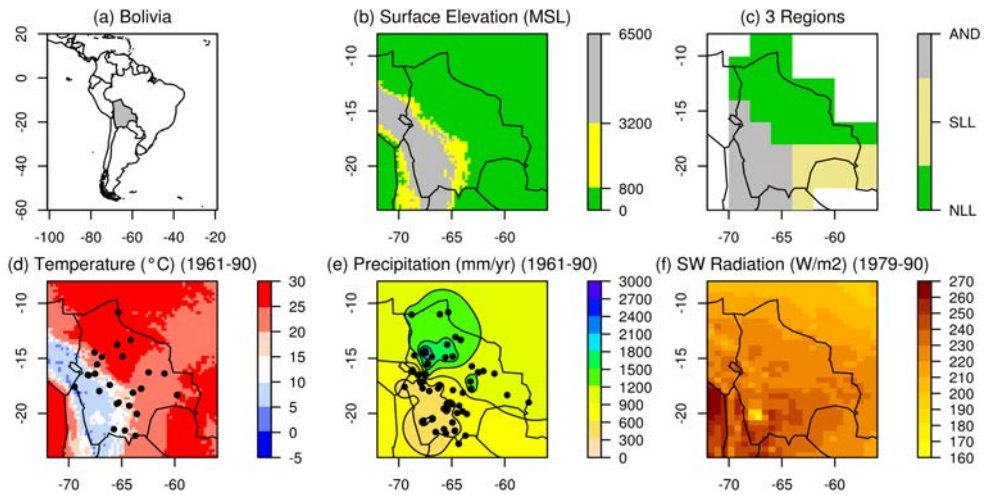


Figure 3.1: (a) Location of Bolivia, (b) surface elevation (m MSL), (c) 3 regions NLL (northern lowlands), SLL (southern lowlands) and AND (Andes), (d) annual mean air temperature ($^{\circ}\text{C}$) from 1961-1990, (e) annually accumulated precipitation (mm year^{-1}) from 1961-1990 and (f) mean SW radiation (W m^{-2}) from 1979-1990. Black dots denote locations of meteorological stations.

3.3. Methods

3.3.1. Data

Observations

Meteorological observations consisted of surface air temperature, precipitation and incoming shortwave radiation at the surface. Temperature and precipitation measurements were provided by the National Service of Meteorology and Hydrology (SENAMHI) and homogenized by Seiler et al. (2013a). Meteorological stations with sufficient data for the period 1961-1990 were selected from this homogenized data set, resulting in 25 stations with temperature and 59 stations with precipitation measurements (Fig. 3.1d, e). Stations contained at least 50% and on average 77% of daily temperature and 83% of daily precipitation measurements. There were 4 stations with slightly less than 50% of data in regions with low station density. Daily data were converted to monthly data if no more than 3 days were missing in a month.

Monthly mean SW radiation was obtained for the period 1979-1990 from the Modern-Era Retrospective Analysis for Research and Applications (MERRA), a NASA reanalysis for the satellite era using the Goddard Earth Observing System Data Assimilation System Version 5 (GEOS-5) (Rienecker et al., 2011). The data belong to a collection

of datasets (Obs4MIPs) that have been organized according to the CMIP5 model output requirements and made available on the earth system grid (ESG) gateway (<http://pcmdi3.llnl.gov>).

Global Circulation Models

We used a total of 35 different GCMs, with 23 GCMs corresponding to CMIP3 and 12 GCMs to CMIP5. CMIP3 GCMs contributed to the IPCC's Fourth Assessment Report (AR4, IPCC, 2007), while CMIP5 data will contribute to the IPCC's Fifth Assessment Report (AR5), expected for publication by 2014. Changes from CMIP3 to CMIP5 GCMs include changes in emission scenarios (see sec. 3.3.2), improved model physics, finer spatial resolution and additional processes related to the oceanic and terrestrial carbon cycle, aerosols, atmospheric chemistry and ice sheets. All GCMs were validated against observational data for the period 1961-1990, while future climates were evaluated for the period 2070-2099. The amount of GCMs for future climates depended on their availability at the time of writing and therefore varied among scenarios, with 21, 22, 18, 12 and 11 GCMs for the emission scenarios SRES B1, A1B, A2, RCP4.5 and RCP8.5 respectively (Tab. 3.1 and Tab. 3.2). To make a more valid comparison between CMIP3 and CMIP5 projections, we also used a sub-sample consisting of 12 CMIP3 GCMs, including only predecessors of the 12 CMIP5 GCMs (namely B, D, G, J, M, N, O, P, R, S, V and W, see Tab. 3.1).

3.3.2. Emission scenarios

Our analysis covered 3 SRES emission scenarios for the CMIP3 GCMs (Nakicenovic et al., 2000) and 2 RCP emission scenarios for the CMIP5 GCMs (Moss et al., 2010). The SRES scenarios are based on socioeconomic story lines and differ in the resulting atmospheric CO₂-equivalent concentrations, which includes the net effect of all anthropogenic forcing agents. We used the SRES scenarios B1, A1B and A2 with the respective atmospheric CO₂-equivalent concentrations of 600 ppm, 850 ppm and 1250 ppm by the year 2100. For comparison, CO₂-equivalent for the year 2005 is estimated with 375 ppm (IPCC, 2007).

Representative Concentration Pathways (RCPs) project future radiative forcings without defining new socioeconomic scenarios. RCPs are compatible with the full range of stabilization, mitigation, and reference emissions scenarios available in the current scientific literature with an adequate separation of the radiative forcing pathways. There are 4 RCPs in total (RCP2.6, 4.5, 6.0 and 8.5), each named after their radiative forcing reached by 2100. We used RCP4.5 and RCP8.5, corresponding to a radiative forcing of 4.5 W m⁻² and 8.5 W m⁻² by 2100 respectively. The resulting CO₂-equivalent concentrations in the year 2100 for RCP4.5 and RCP8.5 are 650 ppm and 1370 ppm respectively (Moss et al., 2010).

3.3 Methods

Table 3.1: Overview of the CMIP3 GCMs used in this study for the validation period of 1961-1990 (20C3M) and for the scenarios SRES B1, A1B, A2. Not all GCMs were available for all scenarios. GCMs available at the time of writing and used in this study are denoted with an “x”.

Country	GCMs	ID	1961-1990	2070-2099 (SRES)		
			20C3M	B1	A1B	A2
Norway	BCCR-BCM2.0	A	x	x	x	x
Canada	CGCM3.1(T47)	B	x	x	x	x
Canada	CGCM3.1(T63)	C	x	x	x	-
France	CNRM-CM3	D	x	x	x	x
Australia	CSIRO-Mk3.0	E	x	x	x	x
Australia	CSIRO-Mk3.5	F	x	x	x	x
USA	GFDL-CM2.0	G	x	x	x	x
USA	GFDL-CM2.1	H	x	x	x	x
USA	GISS-AOM	I	x	x	x	-
USA	GISS-EH	J	x	-	x	-
USA	GISS-ER	K	x	x	-	x
China	FGOALS-g1.0	L	x	x	x	-
Russia	INM-CM3.0	M	x	x	x	x
France	IPSL-CM4	N	x	x	x	x
Japan	MIROC3.2(hires)	O	x	x	x	-
Japan	MIROC3.2(medres)	P	x	x	x	x
Ger./Korea	ECHO-G	Q	x	x	x	x
Germany	ECHAM5/MPI-OM	R	x	x	x	x
Japan	MRI-CGCM2.3.2	S	x	x	x	x
USA	CCSM3	T	x	x	x	x
USA	PCM	U	x	x	x	x
UK	UKMO-HadCM3	V	x	x	x	x
UK	UKMO-HadGEM1	W	x	-	x	x
Sum			23	21	22	18

3.3.3. Validation

We quantified the ability of each GCM to reproduce historic temperature, precipitation and SW radiation patterns for Bolivia. For this purpose we compared modeled against observed monthly values averaged over 1961 to 1990, and plotted the correlation coefficient, centered root-mean-square error (RMSE) and standard deviation of each GCM in a Taylor diagram (Taylor, 2001). Altitudinal differences between grid cells and meteorological stations may lead to large differences in temperature. To cor-

Table 3.2: Same as Tab. 3.1 but for CMIP5 GCMs and the respective scenarios RCP4.5 and 8.5.

Country	GCMs	ID	1961-1990	2070-2099 (RCP)	
			historic	4.5	8.5
Canada	CanESM2	a	x	x	x
France	CNRM-CM5	b	x	x	x
Russia	INM-CM4	c	x	x	x
France	IPSL-CM5A-LR	d	x	x	x
Japan	MIROC5	e	x	x	x
Japan	MIROC-ESM	f	x	x	x
Germany	MPI-ESM-LR	g	x	x	x
Japan	MRI-CGCM3	h	x	x	x
USA	GFDL-ESM2G	i	x	x	-
USA	GISS-E2-R	j	x	x	x
UK	HadGEM2-CC	k	x	x	x
UK	HadGEM2-ES	l	x	x	x
Sum			12	12	11

rect for this orographic effect we calculated local lapse rates for each individual GCM ($3.1^\circ\text{C km}^{-1}$ on average) and used these lapse rates in conjunction with the models' surface elevation to bring modeled temperatures to the altitude of the meteorological stations. In addition to Taylor diagrams we used boxplot diagrams to assess whether errors were random or systematic.

3.3.4. Ensemble weighting

Comparing modeled and observed temperature, precipitation and SW radiation, we calculated skill scores ($S_{k,l}$) for each GCM (k) and each variable (l) according to Taylor (2001):

$$S_{k,l} = \frac{4(1 + R_{k,l})^4}{(\hat{\sigma}_{fk,l} + 1/\hat{\sigma}_{fk,l})^2(1 + R_{0k,l})^4}, \quad (3.1)$$

where R is the correlation coefficient, R_0 is the maximum attainable correlation coefficient and $\hat{\sigma}_f$ is the standard deviation of the GCM divided by the standard deviation of the observation. After quantifying $S_{k,l}$ for each GCM and variable, $S_{k,l}$ was normalized for each variable by dividing through the sum of all $S_{k,l}$ from all GCMs, leading

to scores between 0 and 1:

$$\hat{S}_{k,l} = \frac{S_{k,l}}{\sum_{k=1}^{35} S_{k,l}}. \quad (3.2)$$

The final weight of each GCM (\hat{w}_k) was then taken as the normalized product of the three normalized scores from temperature, precipitation and SW radiation:

$$\hat{w}_k = \frac{w_k}{\sum_{k=1}^{35} w_k}, \quad (3.3)$$

where

$$w_k = \prod_{l=1}^3 \hat{S}_{k,l}. \quad (3.4)$$

Weights were used to develop boxplots of likely ranges of climate change by calculating the weighted 5th, 17th, 50th, 83rd and 95th percentiles of projected yearly and monthly changes for each region. The IPCC considers changes to be likely if their probability is estimated with 66% (Mastrandrea et al., 2010), corresponding to the range enclosed by the 17th and 83rd percentiles. Changes in the mean were tested for significance using a weighted t -test with a probability level of 95%.

3.3.5. Multi-model agreement

We assessed if GCMs projected significant changes in interannual variability and whether or not GCMs agreed on the directional changes of rainfall and SW radiation. After regriding all GCMs to a common spatial resolution of $2^\circ \times 2^\circ$, changes in interannual variability were tested for significance with the F -test:

$$F_{calc} = \max(\sigma_1^2/\sigma_2^2, \sigma_2^2/\sigma_1^2), \quad (3.5)$$

where F_{calc} is the calculated F -value, σ^2 is the variance with 1 and 2 denoting the two periods 1961-1990 and 2070-2099, respectively. Changes in the mean were tested

for significance with the t -test:

$$t_{calc} = (\bar{x}_2 - \bar{x}_1) / \sqrt{\frac{\sigma_2^2}{n_2} + \frac{\sigma_1^2}{n_1}}. \quad (3.6)$$

Finally, we plotted for each grid cell the number of GCMs with significant changes in interannual variability, significant increases and decreases in precipitation and SW radiation.

3.4. Results

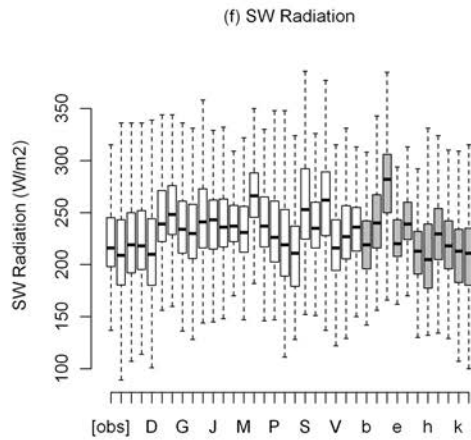
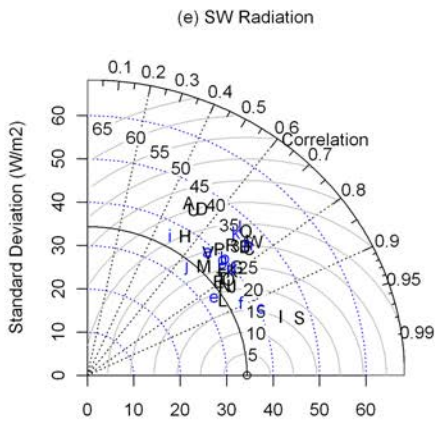
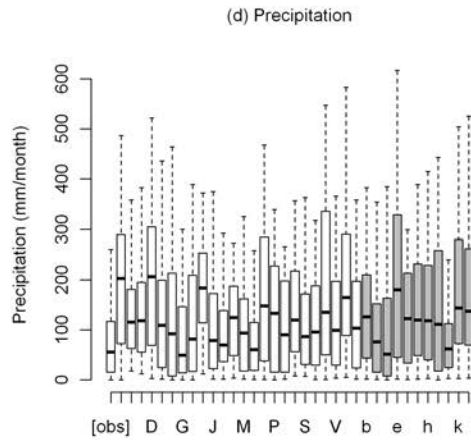
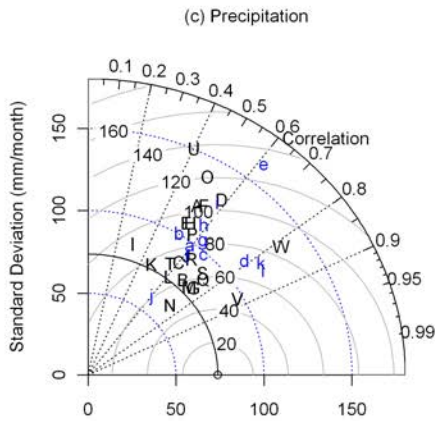
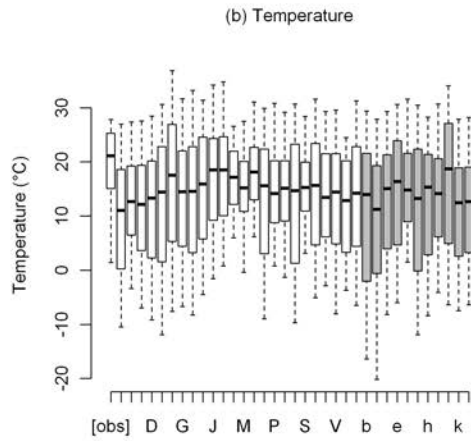
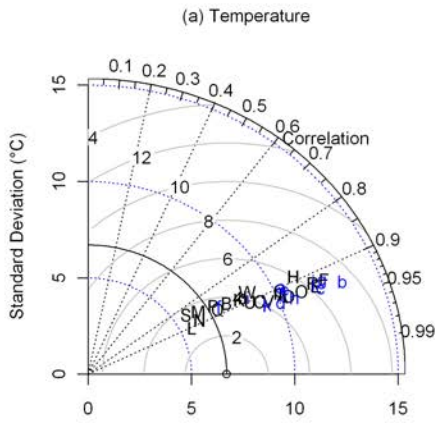
3.4.1. Validation and ensemble weighting

GCMs revealed an overall cold bias with RMSE ranging from 3 to 7°C and strong correlations ranging from 0.85 to 0.95 (Fig. 3.2). Most GCMs overestimated spatial and/or temporal variability, with higher standard deviations (5 to 13°C) compared to the observed overall standard deviation of 7°C.

Regarding rainfall, GCMs revealed an overall wet bias with RMSE ranging from 40 to 140 mm month⁻¹. Correlations strongly varied among GCMs, with coefficients ranging from 0.3 to 0.9. Most GCMs modeled higher standard deviations (60 to 160 mm month⁻¹) compared the observed overall standard deviation of 75 mm month⁻¹. Concerning SW radiation, GCMs revealed an overall positive SW radiation bias with RMSE ranging from 15 to 40 W m⁻². As for rainfall, correlations strongly varied among GCMs, with coefficients ranging from 0.5 to 0.96. Most GCMs had higher standard deviations (30 to 50 W m⁻²) compared the observed overall standard deviation of 35 W m⁻².

Figure 3.2: Taylor and boxplot diagrams of (a, b) monthly mean air temperature, (c, d) monthly precipitation and (e, f) monthly SW radiation. Black upper case and blue lower case letters correspond to GCMs from CMIP3 and CMIP5, respectively. Horizontal bars of the boxplots present the median, the boxes the interquartile ranges and the whiskers the minimum and maximum values. White boxes correspond to CMIP3, while gray shaded to CMIP5 GCMs.

3.4 Results



GCMs differed most with respect to precipitation, less by radiation and least by temperature, but none of the GCMs performed best in all 3 variables (Fig. 3.3). The highest and lowest final weights differed by a factor of 9. The 10 best GCMs consisted of 7 CMIP3 and 3 CMIP5 GCMs, with the Japanese CMIP3 model MRI-CGCM2.3.2 (S) having achieved the highest weight. Some GCMs improved from CMIP3 to CMIP5 (e.g. MIROC-ESM), some hardly changed (e.g. MPI-ESM-LR) and others worsened (e.g. CanESM2) in reproducing Bolivia's historic climate. The mean weights of CMIP3 and CMIP5 were about equal (0.029 and 0.028 respectively), while the mean weight of the 12 GCMs from the CMIP3 subsample had a slightly higher weight of 0.035. Hence, the skill to reproduce the historic climate of Bolivia has on average not improved from CMIP3 to CMIP5.

3.4.2. Temperature projections

Changes in temperature were statistically significant throughout Bolivia and coincided with CO₂ concentrations, with increasing values from B1, RCP4.5, A1B, A2 to RCP8.5. Weighted median changes of annual mean temperature were 2.6, 2.9, 3.8, 4.4 and 5.6°C for the emission scenarios B1, RCP4.5, A1B, A2 and RCP8.5 respectively, with slightly higher medians in the Andes (Fig. 3.4). Changes in monthly temperatures were generally higher during the late dry season (August to November) and less high during the wet season (December to February) (Fig. 3.5). Monthly weighted median changes ranged from 2°C (SRES B1) to 8°C (RCP8.5) in the northern lowlands and from 2°C (SRES B1) to 6°C (RCP8.5) in both southern lowlands and Andes. Weighting GCMs had no major impact on the resulting temperature scenarios.

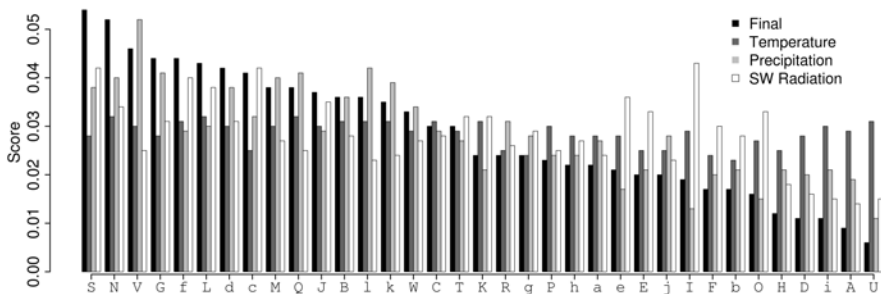


Figure 3.3: GCM scores for reproducing temperature (dark grey), precipitation (light grey) and SW radiation (white) and the corresponding final weights (black).

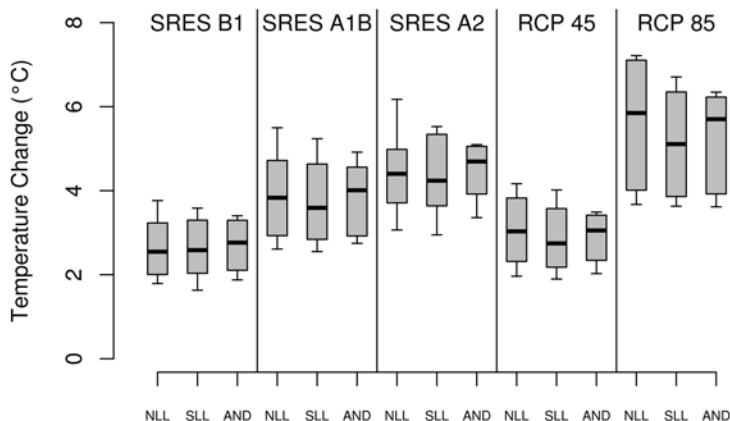


Figure 3.4: Changes in annual mean temperature ($^{\circ}\text{C}$) of the weighted ensemble comparing 1961-1990 with 2070-2099 for the regions NLL, SLL and AND under the emission scenarios SRES B1, A1B, A2, RCP4.5 and RCP8.5. The central line within each box represents the weighted median value of the model ensemble. The top and bottom of each box shows the weighted 83th and 17th percentiles, enclosing 66% of the data, and the top and bottom of each whisker displays the weighted 95th and 5th percentiles, respectively. Grey boxes denote statistically significant changes with a 95% probability (t -test).

3.4.3. Precipitation projections

Annual precipitation

Counting the number of GCMs agreeing on statistically significant changes in annual precipitation revealed that most GCMs projected no significant changes under SRES B1, and the number of GCMs with significant increases and decreases was about equal (not shown). Under SRES A1B and A2, about half of the GCMs projected significant changes, but also here there was no clear preference for either in- or decreases. This also applied to the reduced SRES sample of 12 GCMs which only included predecessors of the CMIP5 GCMs used in this study (Fig. 3.6a, d). Under RCP4.5, most GCMs projected no significant changes, however, among the remaining GCMs there were more models with statistically significant decreases than increases in both the northern and southern lowlands (Fig. 3.6b, e). Periods of comparison are 1961-1990 and 2070-2099. Significance was tested with a t -test with a 95% probability. Under RCP8.5, more than half of the GCMs (up to 7 out of 11 GCMs) projected significant decreases in the lowlands, with mean changes of up to -15% (Fig. 3.6i). This tendency for

less rainfall was not just restricted to the Bolivian lowlands, but was also present in large parts of the Amazon basin with mean decreases of up to -20% at the equator (Fig. 3.6g-i). Most GCMs from both ensembles did not project significant changes in interannual variability of annual precipitation (not shown).

The decrease of annual rainfall projected by the CMIP5 ensemble in the Bolivian lowlands was largest for RCP8.5 (-9% median, -17% 5th percentile) (Fig. 3.7). In the Andes, the CMIP3 ensemble tended to slightly less (-3% median, -7% 5th percentile), while the CMIP5 ensemble to slightly more annual rainfall (+3% median, +5% 83rd percentile). However, the projections of the individual GCMs varied so much that changes of the weighted ensembles were not statistically significant. Weighting GCMs had no major impact on the projected changes.

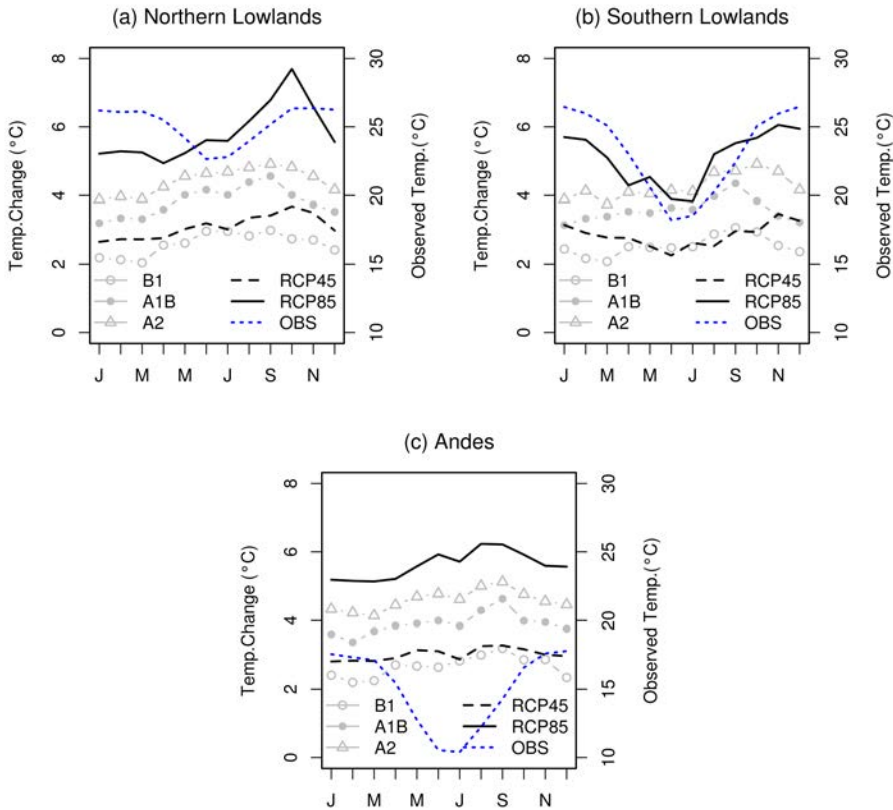


Figure 3.5: Changes in monthly mean temperatures (°C) from 1961-1990 to 2070-2099 for the emission scenarios SRES B1, A1B and A2, as well as RCP4.5 and RCP8.5. Also given are observed mean temperatures (OBS) from 1961-1990 for each region.

3.4 Results

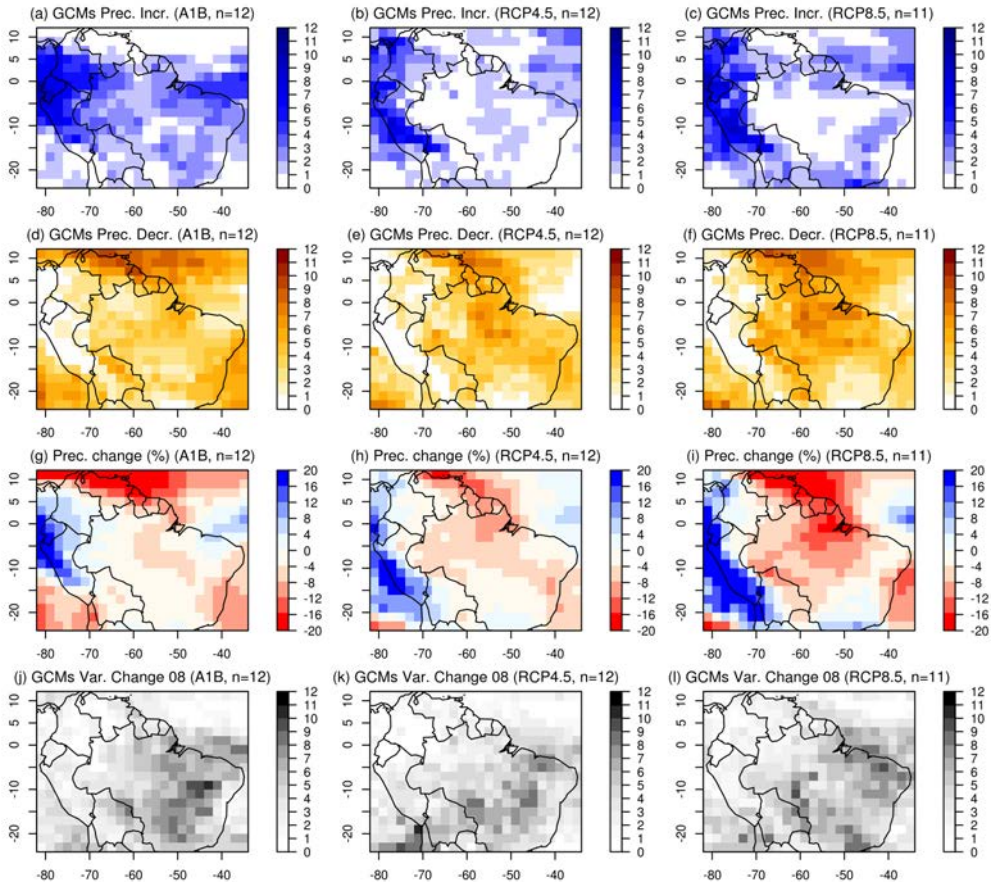


Figure 3.6: Number of GCMs per grid cell agreeing on significant (a-c) increases and (d-f) decreases of annually accumulated precipitation. (g-i) Mean changes (%) of annually accumulated precipitation (not weighted) and (j-l) number of GCMs per grid cell agreeing on significant changes in interannual variance in August. The left, central and right columns correspond to the emission scenarios SRES A1B, RCP4.5 and RCP8.5 respectively. The CMIP3 ensemble was reduced to 12 GCMs, using models with corresponding versions in CMIP5 (B, D, G, J, M, N, O, P, R, S, V and W). Periods of comparison are 1961-1990 and 2070-2099. Significance was tested with a t -test with a 95% probability.

In summary, changes in annual rainfall remained uncertain in the lowlands for CMIP3, while CMIP5 GCMs were more inclined to project decreases (-9%) there, as well as in most of the Amazon basin. In the Andes, CMIP3 GCMs tended to slightly less (-3%), while CMIP5 to slightly more annual rainfall (+3%).

Monthly precipitation

Counting the number of GCMs agreeing on statistically significant changes in monthly precipitation revealed that both ensembles were clearly more inclined to project less rainfall from July to November in the lowlands, as well as in most of the Amazon. This was most evident in October under RCP8.5 with 6 to 10 out of 11 GCMs projecting statistically significant decreases throughout most of the Amazon basin, and no model projecting significant increases (not shown). In Bolivia the decrease of monthly precipitation was strongest in the northern lowlands with changes of the median by $-29 \text{ mm month}^{-1}$ (-19%) in November under RCP8.5 (Fig. 3.8). This decrease was accompanied by significant changes in interannual variability, projected by more than half of the GCMs from both ensembles mainly during JJA (up to 10 out of 12 GCMs under RCP8.5) (Fig. 3.6j-1). During the wet months of January to March, CMIP3 GCMs projected mainly an increase of rainfall in the lowlands (up to 8 out of 18 GCMs under SRES A2), as well as in most of the Amazon basin (not shown). In Bolivia this increase was biggest under SRES A2 ($+15 \text{ mm month}^{-1}$, +8%), and absent for the CMIP5 ensemble (Fig. 3.8). In the Andes, the CMIP3 ensemble tended to less ($-11 \text{ mm month}^{-1}$, -9%), while the CMIP5 ensemble to more rainfall ($+24 \text{ mm month}^{-1}$, +20%) in parts of the wet season. As for annual totals, the projections of the individual GCMs varied so much that changes of the weighted ensembles were not statistically significant. Weighting GCMs had no major impact on the projected changes. In summary, both ensembles agreed on less rainfall (-19%) in the lowlands during drier months (JJA, SON), with significant changes in interannual rainfall variability, but disagreed on changes during wetter months (JFM). In the Andes, CMIP3 GCMs tended to less (-9%), while CMIP5 to more (+20%) monthly rainfall during parts of the wet season.

3.4.4. Shortwave radiation projections

Under all scenarios, at least half of the GCMs predicted a significant increase, and only very few a decrease of annual SW radiation in the northern lowlands (not shown). This signal became stronger from the SRES to the RCP scenarios, the latter predicting more annual SW radiation also in the southern lowlands. In the Andes, no clear signal was visible under the SRES scenarios, while under the RCP scenarios, most GCMs predicted a significant increase here.

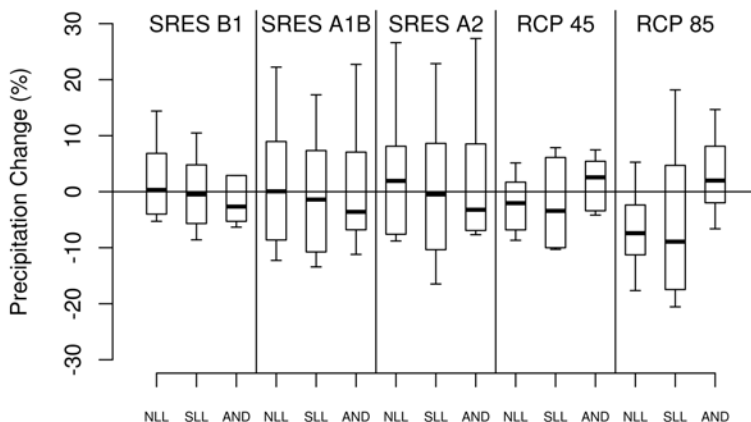


Figure 3.7: Same as Fig. 3.4 but for relative changes in annually accumulated precipitation (%).

The medians of the regional changes in annual SW radiation of the weighted ensemble were positive across all regions and scenarios, with 66% of the ensemble predicting an increase under the emission scenarios SRES B1, RCP 45 and 85 (Fig. 3.9). Weighted median changes of annual mean SW radiation ranged from 1 to 3%, with likely changes as big as +11%.

Projected changes in monthly SW radiation showed biggest increases for scenarios and seasons with decreases in rainfall. Increases in the median were as large as 20 W m⁻² (9%) in September in the northern lowlands, 9 W m⁻² (3%) in February in the southern lowlands and 13 W m⁻² (5%) in December in the Andes (Fig. 3.10). Despite the overall trend for more radiation, changes were not statistically significant.

3.5. Discussion

We validated 35 GCMs against observed surface air temperature, precipitation and incoming SW radiation, and analyzed climate change projections from 5 emission scenarios, distinguishing among 3 climatologically contrasting regions in Bolivia. GCMs revealed an overall cold, wet and positive SW radiation bias and showed no substantial improvement from the CMIP3 to the CMIP5 ensemble for the Bolivian case. Models projected an increase in temperature (2.5 to 5.9°C) and SW radiation (1 to 5%) with seasonal and regional differences. In the lowlands, changes in annual rainfall remained

uncertain for CMIP3, while CMIP5 GCMs were more inclined to project decreases (-9%). This also applied to most of the Amazon basin, suggesting a higher risk of partial biomass loss for the CMIP5 ensemble. Both ensembles agreed on less rainfall (-19%) during drier months (JJA, SON), with significant changes in interannual rainfall variability, but disagreed on changes during wetter months (JFM). In the Andes, CMIP3 GCMs tended to less (-9%), while CMIP5 to more (+20%) rainfall during parts of the wet season.

Our approach included the following limitations. (i) We are aware that climate change projections have only limited validity in mountainous regions due to the coarse spatial resolution of GCMs. High resolution regional climate modeling would therefore be more appropriate in the Andes. Forcing a regional climate model with multiple lateral boundary conditions however is very resource intensive, leading to very few model

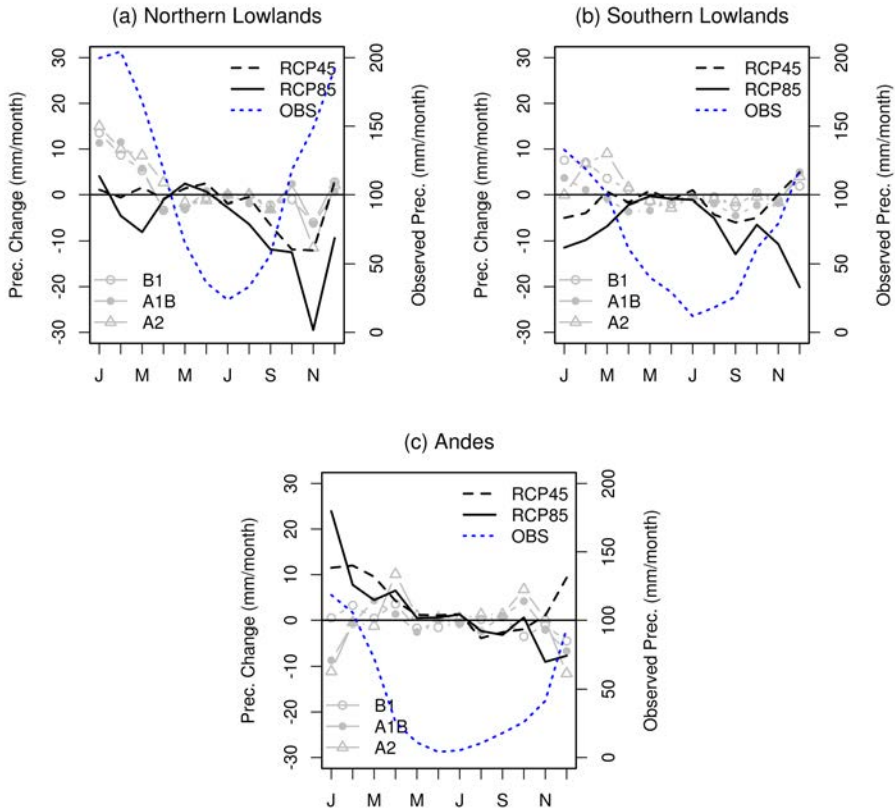


Figure 3.8: Same as Fig. 3.5 but for changes in monthly precipitation (mm month^{-1}).

runs currently available (e.g. Soares and Marengo, 2009; Urrutia and Vuille, 2009; Marengo et al., 2010). Most of these regional climate change scenarios are based on very few lateral boundary conditions (mainly HadAM3), limiting their robustness in a region with little agreement among GCMs on the directional change of rainfall. We therefore consider our approach to be a necessary precursor to future downscaling efforts in the region.

(ii) The stratification of Bolivia into the 3 regions northern lowlands, southern lowlands and Andes corresponded to the coarse spatial resolution of most GCMs, but strongly simplified the true heterogeneity of the country. Having merged parts of the Andean slopes with the Altiplano into one region neglected the contrasting precipitation regimes caused by the steep orography of the Andes. However, given the coarse resolution such processes were hardly reproduced, making our stratification reasonable.

(iii) The final weights assigned to each GCM were to some extent subjective. We combined the weights related to temperature, precipitation and SW radiation by forming the product, whereas a sum of the weights would have been an equally valid option. We preferred the product over the sum because it led to stronger differences among weights. However, since weighting the ensembles had no major impact, uncertainties related to choices of the method may be neglected.

(iv) Significance of monthly changes was tested with the Welch t -test for weighted samples, despite that for some cases data were not normally distributed. We therefore tested significance for critical months with the non-parametric Mann-Whitney-Wilcoxon test, which did not lead to much different results. Unfortunately though, we were not able to implement this test for the weighted, but only for the unweighted ensemble and therefore adhered to the t -test for weighted samples.

(v) Finally, the observation period of SW radiation lasted only from 1979 to 1990. We assumed that this period was sufficiently long for obtaining mean values representative for the complete period 1961 to 1990.

Our results confirm numerous findings from Christensen et al. (2007), Soares and Marengo (2009), Urrutia and Vuille (2009) and Marengo et al. (2010), including (i) a cold and wet bias for the Andean region, (ii) stronger temperature increases during the austral winter, (iii) great uncertainty associated with the directional change of annual rainfall, and (iv) a tendency for an intensification of the hydrological cycle for CMIP3 GCMs, with more rainfall during the wet season. Concerning SW radiation, our positive SW radiation bias agreed with the positive bias of 6 W m^{-2} global average found for multiple CMIP3 GCMs, which was most likely determined by processes in the cloud-free atmosphere rather than by an anomalous absorption through clouds Wild (2008).

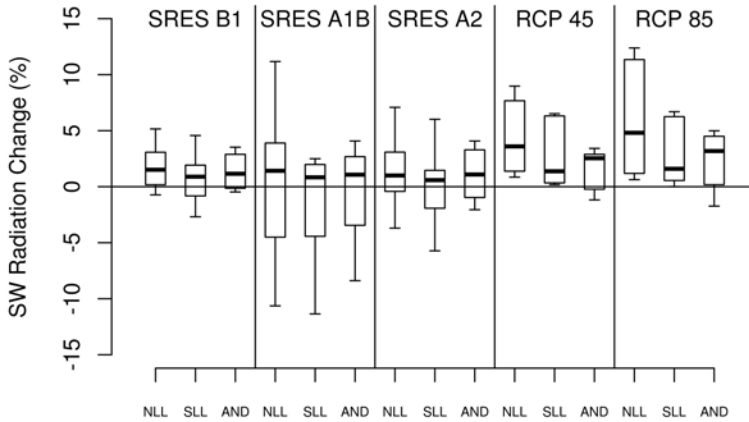


Figure 3.9: Same as Fig. 3.4 but for relative changes in annually accumulated SW radiation (%).

Differences between projections from the CMIP3 and CMIP5 ensembles may emerge from differences in the emission scenarios, resolution or processes. Given the lack of a common scenario, both ensembles cannot be compared directly. To make a comparison nevertheless, Knutti and Sedláček (2012) calibrated the simple climate model MAGICC to 19 CMIP3 models and ran it for the RCP scenarios. On a global scale, CMIP5 projections seem to be largely consistent with CMIP3 projections. The same study however reveals different rainfall projections for both ensembles in the Amazon region, suggesting that differences are not due to differences in the scenarios alone, but also due to the addition of new processes. Additional analysis will be required to determine which processes are responsible for differences in rainfall projections.

The projected changes may heavily affect human and natural systems in Bolivia. However, climate change impact studies are required to further assess the potential implications for different sectors under different scenarios. Such studies could address potential risks for drinking water supply from glaciers, hydropower, agricultural production and ecosystem stability. Given the large uncertainty of rainfall projections, it will be essential to incorporate a wide range of climate models in these studies. Furthermore it is recommended to try to identify the factors which lead to a decrease in rainfall, as well as changes in interannual rainfall variability during JJA in the Amazon. This requires a detailed analysis on how well GCMs reproduce the synoptic scale systems of South America, and on how these systems change under climate change scenarios.

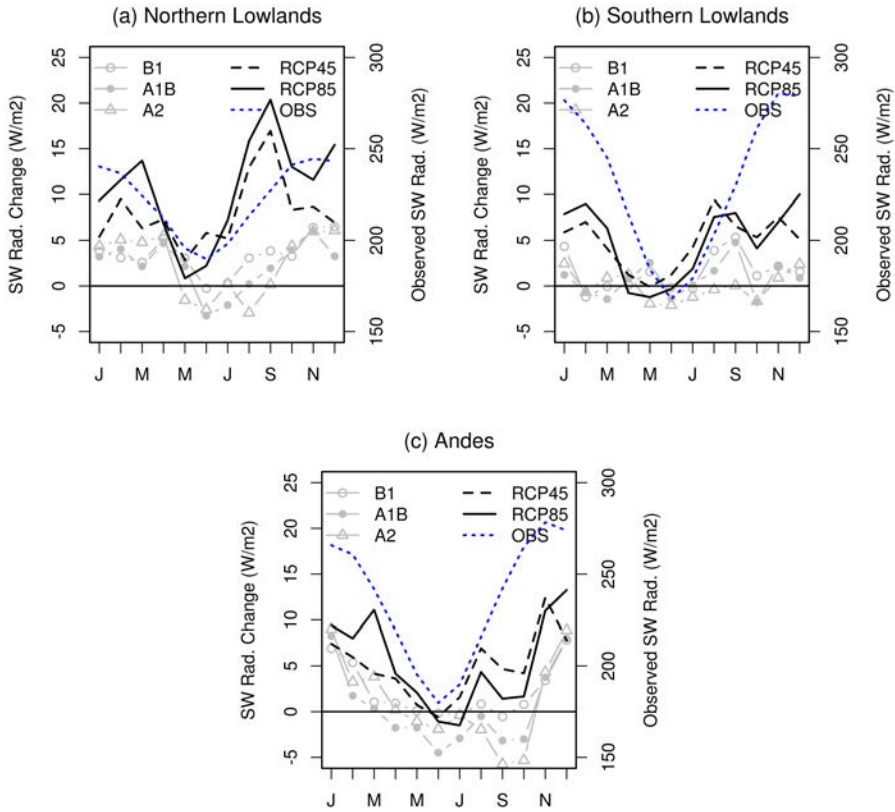


Figure 3.10: Same as Fig. 3.5 but for changes in monthly SW radiation ($W m^{-2}$)

To conclude, we hope this research contributed to a better understanding of climate change projections in Bolivia, providing a basis for a discussion on climate change impacts and adaptation. Our findings may provide inputs to further assess how resilient human and natural systems are under different climate change scenarios.

Acknowledgments

This research was supported by the Departmental Pilot Program of Adaptation to Climate Change (PDACC) as well as the project Raising the Alert about Critical Feedbacks between Climate and Land Use Change in Amazonia (AMAZALERT). PDACC is carried out by the Fundación Amigos de la Naturaleza (FAN) as well as the departmental government of Santa Cruz and funded by the embassy of the Nether-

lands. AMAZALERT is jointly funded by the European 7th Framework programme and national organizations. We thank the Bolivian National Service of Meteorology and Hydrology (SENAMHI) for the provision of the meteorological data. MERRA data used in this study was provided by the Global Modeling and Assimilation Office (GMAO) at NASA Goddard Space Flight Center. We acknowledge the World Climate Research Programme's Working Group on Coupled Modelling, which is responsible for CMIP, and we thank the climate modeling groups (listed in Tab. 3.1 and Tab. 3.2 of this paper) for producing and making available their model output. For CMIP the U.S. Department of Energy's Program for Climate Model Diagnosis and Intercomparison provides coordinating support and leads development of software infrastructure in partnership with the Global Organization for Earth System Science Portals. We are grateful for the comments from 3 anonymous reviewers who have helped us to improve the quality of this paper.

4. Measuring and Modeling Carbon Stocks from Wet to Dry Tropical Forests

Abstract

Dynamic vegetation models have been used to assess the resilience of tropical forests to climate change, but the large scale scope of these modeling experiments often misrepresent carbon dynamics at a regional level, limiting the validity of future projections at such scale. Limited attention has been paid to transition zones, where evergreen trees compete with deciduous trees along environmental gradients. Here, a dynamic vegetation model (LPJ-GUESS) was adapted to simulate present day potential vegetation as a baseline for climate change impact assessments in the evergreen and deciduous forests of Bolivia. Results were compared to biomass measurements (21 new, and 798 previous plots), and remote sensing data. Using regional parameter values for allometric relations, specific leaf area, wood density and disturbance interval, a realistic transition from the evergreen Amazon to the deciduous dry forest was simulated. This transition coincided with threshold values for precipitation (1400 mm yr^{-1}) and water deficit (-830 mm yr^{-1}), beyond which leaf abscission became a competitive advantage. The model reproduced reasonable values for seasonal leaf abscission, vegetation carbon, and forest fires. Modeled Gross Primary Productivity (GPP) and remotely sensed Normalized Difference Vegetation Index (NDVI) showed that dry forests were more sensitive to rainfall anomalies than wet forests. GPP was positively correlated to the El Niño Southern Oscillation index in the Amazon, and negatively correlated to consecutive dry days. Decreasing rainfall trends were simulated to reduce GPP in the Amazon. The current model setup provides a baseline for assessing the potential impacts of climate change in the transition zone from wet to dry tropical forests in Bolivia.

This chapter has been published as:

Seiler, C., R.W.A. Hutjes, B. Kruijt, J. Quispe, S. Añez, V.K. Arora, J.R. Melton, T. Hickler, and P. Kabat, 2014: Modeling forest dynamics along climate gradients in Bolivia, *Journal of Geophysical Research - Biogeosciences*, **119**.

4.1. Introduction

The Plurinational State of Bolivia is rich in biodiversity, hosting approximately 20,000 plant-, 1398 bird-, 600 fish-, 356 mammal-, 266 reptile-, and 204 amphibian species (Ibisch and Mérida, 2003). Ecosystems are threatened by numerous pressures, including deforestation, fires, livestock grazing, and climate change. Total deforestation from 2000 to 2010 was 1,821,153 ha (0.67% per year) (Cuéllar et al., 2012), with 49,884 ha (2.7%) located inside protected areas. During the same period, 22,012,910 ha of vegetation were burnt, from which 20% corresponded to forests (Rodríguez, 2012a). The grazing pressure in Bolivia's Chaco is among the highest in all South America (Jarvis et al., 2010). Climate change scenarios from 35 global circulation models (GCMs) project an increase in annual temperature between 2.5° and 5.9°C, and a decrease of rainfall during drier months (-19%) in Bolivia by the end of this century (Seiler et al., 2013b). The potential impacts of climate change in the Amazon remain highly uncertain, and range from a severe loss, to a substantial increase of biomass (Rammig et al., 2010; Huntingford et al., 2013). The largest uncertainty is associated with plant physiological responses, and then with future emissions scenarios, while uncertainties from differences in climate projections are significantly smaller (Huntingford et al., 2013). The possibility of a biomass loss implies also a potential risk for carbon stocks from forest conservation projects related to the climate change mitigation mechanism on reducing emissions from deforestation and forest degradation (REDD) (UNFCCC, 2010). Two such projects are currently implemented in Bolivia, namely the Noel Kempff Mercado Climate Action Project (Virgilio, 2009), and the indigenous REDD program in the Bolivian Amazon (Quispe and Añez, 2010).

Carbon stocks in the Amazon may be affected not only by long-term climate change, but also by short-term extreme climate events (e.g. Asner et al., 2000; Behrenfeld et al., 2001; Phillips et al., 2009; Holmgren et al., 2013). Climate variability in Bolivia is heavily influenced by the El Niño Southern Oscillation (ENSO) (Seiler et al., 2013a). During the La Niña related drought of 2010, Bolivia's Amazon was amongst the most affected regions within the entire Amazon basin (Lewis et al., 2011). The total area of forest and savanna fires in Bolivia was unusually high during this year, as well as during the previous severe, and El Niño related drought of 2005 (Rodríguez, 2012a). Precipitation in Bolivia has decreased over the 1985 to 2004 period by 4% during the wet, and 10% during the dry season, while temperatures are rising at 0.1°C per decade (Seiler et al., 2013a).

Understanding carbon dynamics may help to assess the resilience of ecosystems to current and future pressures. Carbon dynamics in tropical South America have been studied in multiple ways, including biometric measurements (e.g. Baker et al., 2004), flux tower measurements (e.g. Andreae et al., 2002), remote sensing (e.g. Saatchi et al. 2007) and dynamic vegetation modeling (e.g. Cox et al., 2013). Complementing each other, such results can be integrated to provide a better understanding of past and future dynamics. Most modeling studies were designed to assess large-scale carbon dynamics of the entire Amazon basin, focusing mainly on tropical evergreen trees and

grasslands, and lacking detail due to coarse spatial resolutions (e.g. Cox et al., 2004; Salazar et al., 2007; Huntingford et al., 2008; Rammig et al., 2010; Castanho et al., 2013). Limited attention has been paid to transition zones, where evergreen trees compete with deciduous trees along environmental gradients. A global application of the dynamic vegetation model LPJ simulated grasslands instead of deciduous trees in Bolivia's semi-dry and dry forests (Sitch et al., 2003). Similarly, the potential vegetation model CPTEC-PVM (Oyama and Nobre, 2004) simulated mainly savanna in Bolivia's Amazon forest under present day climate (Salazar et al., 2007), limiting the validity of any future projections for the region. Also, model results are based on empirical parameter values derived from studies not necessarily representative of the Amazon. In the case of LPJ-GUESS (see sec. 4.3.1) this includes allometric relations, which were derived from 16 tree species growing in the boreal forest of Canada (Huang et al., 1992). In other cases, the sources of the parameter values are unclear, or values are based on expert judgment (e.g., wood density, fire resistance, and disturbance interval).

Previous modeling studies are only of limited use for regional climate change impact assessments due to their large scale scope. This motivated us to implement a dynamic vegetation model explicitly for Bolivia, and to evaluate its performance for current climatic conditions, using carbon stock measurements and remote sensing data. Special attention was paid to the distribution of Plant Functional Types (PFTs), seasonal leaf abscission, and fires (sec. 4.4.1), carbon stocks (sec. 4.4.2), and the model's sensitivity to climate variability (sec. 4.4.3). The latter included assessing the impacts of ENSO and extreme events, as well as to rising atmospheric concentrations in carbon dioxide ($[\text{CO}_2]$). Model performance was improved through the use of regional parameter values related to the physical structure of trees, and tree mortality (Tab. 4.1).

4.2. Study area

Bolivia is a tropical country measuring more than one million km^2 . With its main altitudinal divisions being lowlands (<800 m MSL), Andean slopes (800-3,200 m MSL) and highlands (Altiplano) ($>3,200$ m MSL), Bolivia's climate varies with increasing altitude from a wet tropical to a cold desert climate, with annual mean surface air temperatures ranging from 0 to 30°C (Fig. 4.1). Rainfall ranges from <300 to >3500 mm yr^{-1} , and varies from high to low from the northern Andean slopes, northern lowlands, southern lowlands and southern Andean slopes to the Altiplano, with the north-south division roughly at 18°S . The austral summer (DJF) and winter (JJA) coincide with the wet and dry season, respectively. Incoming daily mean net short wave (SW) radiation at the surface ranges from 160 to 280 W m^{-2} , with higher values in the Altiplano and southern lowlands.

Spatial gradients in climate lead to the formation of contrasting vegetation units at different elevation levels. In the lowlands this includes the evergreen rain forest of the Amazon, the semi-deciduous Chiquitania forest and the deciduous Chaco dry forest

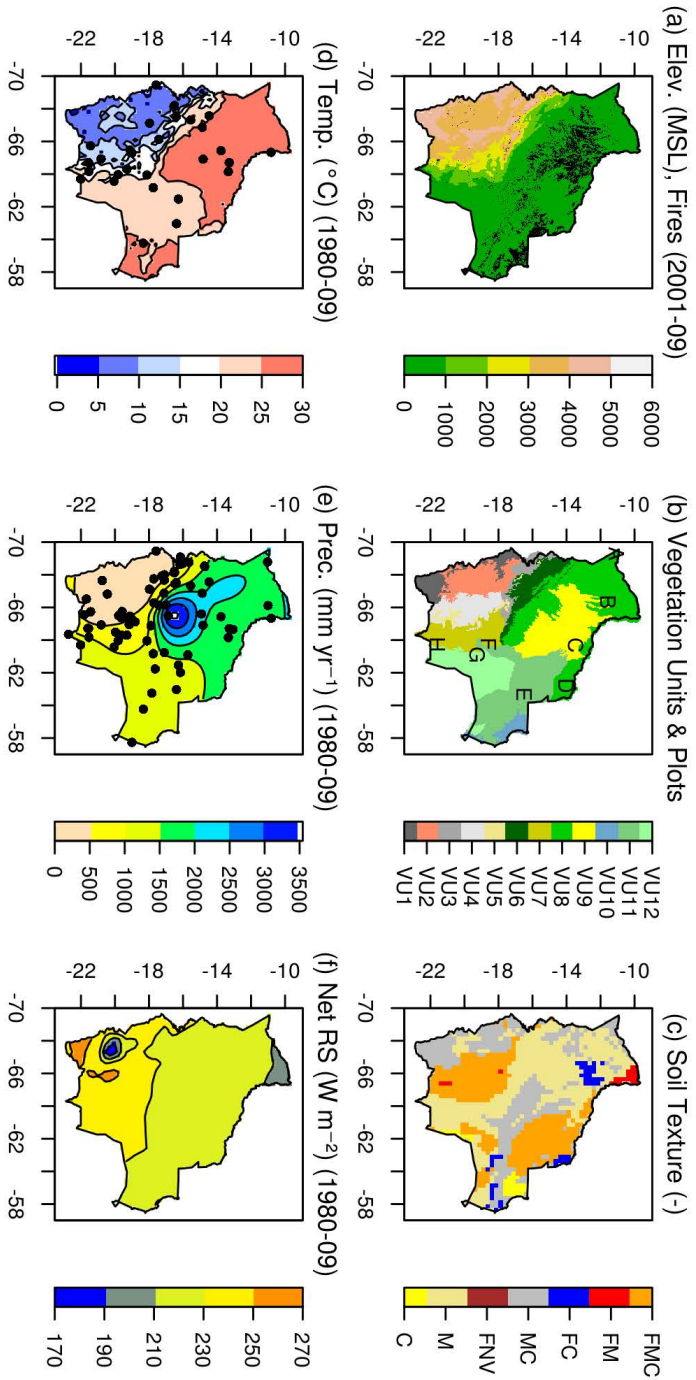


Figure 4.1: (a) Surface elevation (m MSL) and location of fires from 2001-2009, (b) vegetation units (VU1 = Western Cordillera, VU2 = Altiplano, VU3 = Eastern Cordillera and Northern Altiplano, VU4 = Eastern Cordillera and Central and Southern Altiplano, VU5 = Prepuna, VU6 = Yungas, VU7 = Tucumano Forest, VU8 = Amazon, VU9 = Beni savannas, VU10= Pantanal, VU11 = Chiquitania, VU12 = Chaco (Navarro and Ferreira, 2004)) with biomass measurement sites (A-H), (c) annual mean temperature (°C) and meteorological stations from 1980-2009, (d) annual mean precipitation (mm year⁻¹) and meteorological stations from 1980-2009, (e) annual mean SW radiation (W m⁻²) from 1980-2009 and (f) soil texture (F = fine, M = medium, C = coarse, NV = non-veretisol) (FAO, 2012).

(Fig. 4.1d). Evergreen and deciduous tree species in these forests have adapted to their environment in different ways, leading to differences in functional traits. Deciduous tree species have lower wood densities and higher specific leaf area (SLA) compared to evergreen tree species, allowing for a faster vertical growth and more carbon gain during the reduced growing season (Markesteijn et al., 2011). The same also applies to shade-intolerant compared to shade-tolerant species of both, evergreen and deciduous trees (Markesteijn et al., 2011). Large parts of the lowlands (111,000 km²) are also covered by the tropical savannas of Beni, which are affected by seasonal flooding, drought, and land use (Larrea et al., 2010). The cloud forests of the Yungas grow on the north-facing slopes of the Andes, while the Tucumano forest can be found along the east-facing slopes. The highlands host the alpine grasslands and bare lands of the Altiplano and cordilleras. More information on the ecological characteristics of Bolivia's vegetation zones can be found in Navarro and Ferreira (2004) and Josse et al. (2007).

Numerous biomass measurements in Bolivia already indicate the spatial variability of carbon stocks in lowland Bolivia. Dauber et al. (2000) estimated aboveground vegetation carbon of trees with a diameter at breast height (DBH) > 10 cm from 74 forest inventories in Bolivia, with decreasing median values from the lowland Amazon (8.6 kgC m⁻²), to the pre-Andean Amazon (6.4 kgC m⁻²), and the Chiquitania forest (5.7 kgC m⁻²). Measurements from Mostacedo et al. (2009) were similar, but do not confirm a decrease from the evergreen to the deciduous forest, with 7.0 kgC m⁻² in the Amazon (-11.00°S, -68.00°W), 8.7 kgC m⁻² in the northern Chiquitania (-15.78°S, -62.92°W) and 9.0 kgC m⁻² in the southern Chiquitania (-16.12°S, -61.72°W). In the Amazon of the Itenez, Baker et al. (2004) measured 6.2 to 14.2 kgC m⁻² (-14.5°S, -61.1°W). Differences among measurements may result from natural variability, as well as from differences in methods, and different degrees of human interventions. The limited meta-data, and since only living trees with a DBH > 10 cm were considered, motivated us to use these numbers as additional references only, and not for model evaluation purposes. Instead, we used biomass measurements with a consistent method from previous campaigns carried out by the Fundación Amigos de la Naturaleza (FAN, www.fan-bo.org) (798 plots, see sec. 4.3.2 Methods for details). To obtain comparable values in other vegetation units, additional measurements in 21 plots were made explicitly for this study in the forests of the Chiquitania, Chaco, and northern Tucumano, as well as in the tropical savannas of Beni.

4.3. Methods

4.3.1. Model description

The dynamic vegetation model LPJ-GUESS (Lund Potsdam Jena General Ecosystem Simulator) (Smith et al., 2001; Ahlström et al., 2013) simulates the exchange of water and carbon between soil, plants and atmosphere, as well as the resulting terrestrial

ecosystem composition and structure. Model inputs consist of temperature, precipitation, solar radiation, $[\text{CO}_2]$, and soil texture. Plants are grouped into plant function types (PFTs) according to structural and phenological differences. The structure of a tree is simplified to a cylinder with fine roots, sapwood and heartwood, a crown area and a leaf area index (LAI). Grasses lack a structure and consist of roots and LAI only. Soils consist of an upper (0-0.5 m) and a lower layer (0.5-1.5 m) of identical soil texture. One grid cell represents the average of several replicate patches, typically of 0.1 ha in size each. A patch may contain several PFT cohorts, each represented by an average individual. Replicate patches are driven by the same input data; however, processes differ due to stochastics in establishment, mortality and disturbance processes. The following paragraphs outline the model's main computation steps, with special emphasis on processes related to parameters (listed in Tab. 4.1) altered in this study.

Gross photosynthesis is calculated according to the coupled photosynthesis and water balance scheme of BIOME 3 (Haxeltine and Prentice, 1996). Leaf respiration is subtracted, and the resulting net photosynthesis is used together with $[\text{CO}_2]$ to calculate non-water-stressed canopy conductance. Together with equilibrium evapotranspiration, non-water-stressed canopy conductance is used to estimate the transpirational demand. The counterpart of the demand is the supply of water to the plant, which is computed as follows.

Precipitation enters the soil until the upper layer is saturated, while any additional precipitation is lost as surface runoff. Soil water evaporates from the upper 20 cm, depending on potential evaporation and soil water content. Soil water percolates from the upper to the lower soil layer, until the lower soil layer is saturated, in which case excess water is lost as drainage. Water contained in the lower soil layer can leave the soil as base flow at a given rate. The amount of water potentially accessible to plants (w_r) depends of the amount of water in the soil, the available water capacity, the distribution of roots, and a maximum transpiration rate (em_{max}). The supply of water to the plant is estimated to equal the product of w_r and em_{max} . If the demand exceeds the supply, plants experience water stress, in which case the previously calculated non-water-stressed canopy conductance is reduced to the water-stressed canopy conductance, which is further used to calculate the water-stressed photosynthesis.

Leaf abscission of deciduous PFTs occurs if the ratio of water supply and demand (ω) falls below 0.35. After subtracting the amount of carbon used for respiration (leaf, maintenance and growth), as well as for a constant fraction for reproduction, the remaining carbon is distributed to leaves, sapwood and fine roots, satisfying four allometric constraints. The first constraint determines the ratio (k_{latosa}) between the total leaf area (LA) and the total sapwood area (SA) (Equation 4.1). The second relates the amount of carbon invested into leaves and roots, depending on ω (not shown). The last two determine the relation of DBH and tree height (H), as well as

crown area (CA):

$$LA = k_{latosa} * SA, \quad (4.1)$$

$$H = k_{allom2} * DBH^{k_{allom3}}, \quad (4.2)$$

$$CA = k_{allom1} * DBH^{k_{rp}}, \quad (4.3)$$

where k_{allom1} , k_{allom2} , k_{allom3} and k_{rp} are empirical constants applied to all tree PFTs (Tab. 4.1). A maximum crown area limits the growth of tree crowns. Equation 4.2 is actually not used to calculate H , but is solved for DBH instead. H is calculated from the ratio of volume and area. Since a volume equals the ratio of its corresponding mass and density, H can be expressed from the mass (c_{sap}), divided by the density (ρ_{sap}) and SA. Calculating SA from Equation 4.1, and considering that the specific leaf area (SLA) equals the ratio of LA and leaf mass (c_{leaf}), H is calculated as follows:

$$H = \frac{c_{sap} * k_{latosa}}{\rho_{sap} * c_{leaf} * SLA}. \quad (4.4)$$

Since higher values of SLA imply more LA at a given c_{leaf} , and since a greater LA needs to be supported by more sapwood area (Equation 4.1), trees become wider, and hence less tall, with increasing values of SLA.

Next to tree height, SLA is also used to calculate LAI:

$$LAI = \frac{c_{leaf}}{\rho_{trees}} * \frac{SLA}{CA}, \quad (4.5)$$

where ρ_{trees} is the density of trees (number of individuals m⁻²).

The competition among PFTs is assumed to be proportional to their ability to absorb light, which increases with increasing CA, tree density and LAI. The structure of the forest feeds back on the photosynthesis in two ways. Tree height and LAI determine the fraction of photosynthetically active radiation absorbed by foliage (FPAR), and soil moisture is reduced through interception and transpiration.

When newly produced carbon enters the vegetation pool, part of the sapwood converts to heartwood, and fractions of leaves and roots enter the litter pool. Litter is converted

to soil organic carbon at a rate depending on the relative soil water content of the upper soil layer, as well as soil temperature. The sapling establishment rate depends on the amount of light reaching the forest floor. A PFT-specific minimum temperature threshold value determines conditions suitable for establishment and survival (t_{cmin}). The performance of tree growth is expressed through growth efficiency, the ratio of annual Net Primary Productivity (NPP) and total leaf area. Tree mortality occurs via age, stress associated with high temperatures, unsuitable climatic conditions, fire, too low growth efficiency or disturbance. The latter may represent the death of trees related to multiple causes, including windthrow or pests. Daily fire probability increases with decreasing relative soil water content in the upper soil layer. The length of the fire season is the sum of these probabilities, and determines the fractional area affected by fire. Fire occurs in a patch if a randomly generated fraction is below the calculated fire probability, while the number of individuals killed depends on the fire resistance of the respective PFT. A more detailed model description can be found in Sitch et al. (2003) and Gerten et al. (2007).

4.3.2. Data

Forcing data

Model inputs consisted of daily temperature, precipitation, SW radiation, annual mean $[\text{CO}_2]$ and soil texture. Daily temperature and precipitation data consisted of spatially interpolated station observations covering the period 1980 to 2009. Station data were provided by Bolivia's National Service of Meteorology and Hydrology (SENAMHI) and homogenized by Seiler et al. (2013a). To improve the spatial interpolation of rainfall, we added two stations located at the foothills of the northern Andean slopes, where annual rainfall rates are highest in Bolivia. Also, in case of five stations we replaced the homogenized with the original time series, because the annual mean precipitation of both series differed by $>25\%$. The respective stations were Cobija, Copacabana, Sanjoaquin, Uyuni, and Yacuiba. The final number of stations was 29 with respect to temperature, and 70 in case of rainfall. Temperature was spatially interpolated using an inverse distance weighting function (IDW) (Pebesma, 2004). Orographic effects on temperature were included by bringing actual temperature down to sea level before, and back to real height, after the spatial interpolation. For this we used a local lapse rate of $-4.4^\circ\text{C km}^{-1}$ derived from our data, as well as station heights, and a digital elevation model from Jarvis et al. (2008). Precipitation was spatially interpolated using a thin plate spline function (TPS) (Furrer et al., 2012), and compared against remotely sensed rainfall estimates ($R^2 = 0.87$) from the Tropical Rainfall Measuring Mission (TRMM3B43) (Huffman et al., 2010) (<http://trmm.gsfc.nasa.gov/>). Other interpolation techniques were tested as well, but were rejected because of lower coefficients of determination. Daily incoming net solar radiation at the surface was obtained from the Modern-Era Retrospective Analysis for Research and Applications (MERRA), a NASA reanalysis for the satellite era using

the Goddard Earth Observing System Data Assimilation System Version 5 (GEOS-5) (Rienecker et al., 2011) (<http://disc.sci.gsfc.nasa.gov>). Data covered the period from 1980 to 2009, and were spatially interpolated from $0.67^\circ \times 0.50^\circ$ to $0.25^\circ \times 0.25^\circ$ using a bilinear interpolation technique (van Etten, 2012). Annual mean observed $[\text{CO}_2]$ from 1765-2005 was obtained from (<http://www.iiasa.ac.at>) and updated for 2006-2009 from (<http://www.esrl.noaa.gov/gmd/>). Soil texture was obtained from the Harmonized World Soil Database FAO (2012).

Regional parameter values

Regional parameter values were obtained from field measurements and literature. Allometric relations between DBH, tree height and crown area were measured from 139 trees located in the sites of the Amazon (D, Fig. 4.1b), Chiquitania (E), Northern Tucumano (F) and Chaco (G), covering all major forest types in Bolivia (Tab. 4.1).

A temperature threshold value for establishment and survival (t_{cmin}) was calculated from observed minimum monthly mean temperatures from 1980-2009, and from the spatial distribution of forest in Bolivia given by a recent land cover map (Glob-Cover2009, Arino et al., 2010). Values for SLA and wood density were obtained for each tree PFT from Markesteijn et al. (2011) (their Table 2). The respective values originate from 40 species, and were measured in a sample plot located in the Chiquitania (16.12°S , 61.72°W). A fire resistance of 40% (*i.e.* the percentage of trees which survive a fire) was measured by Pinard et al. (1999) from 500 trees located in a semi-humid tropical forest dominated by evergreen tree species in Bolivia's lowlands (15.78°S , 62.63°W). We applied the reported value of 40% to evergreen PFTs, and approximated fire resistance of deciduous PFTs with a slightly higher value of 50%. The selection of these parameters was limited to a number of practical constraints, including our ability to measure variables, available literature, and knowledge of processes of regional importance.

Validation data

Aboveground biomass was measured in 819 sample plots located in the following vegetation units: (i) Amazon (704 plots; sites A, B, D; Fig. 4.1b), (ii) Savannas (6 plots; C), (iii) Chiquitania (6 plots; E), (iv) Chaco (4 plots; G), and (v) Northern- (5 plots; F), and Southern Tucumano forest (94 plots; H). All plots used in this study were located in natural forests, which, to our knowledge, have not experienced significant human interventions. Sites A and B belonged to the Indigenous REDD program, with details presented in Quispe (2008) and Quispe and Añez (2010). Site D presented measurements from the Noel Kempff Mercado Climate Action Project, documented in FAN (2005). Measurements in site H were made for the carbon project San Antonio San Alberto, presented in FAN (2003). The remaining sites C, E, F and G were installed for this study, with further details documented in Quispe (2011). We

measured the aboveground biomass of living and dead trees, palm trees, liana and cacti, as well as under-story woody and herbaceous vegetation and litter from 819 sample plots. Earlier measurements of sites D and H were based on nested circular plots, with an inner radius of 4 m, and an outer radius of 14 m. For all other sites we used rectangular plots of 1 ha in size. These 1 ha plots contained 3 types of subplots of varying size (5x5 m, 2x2 m and 1x1 m). Subplots were installed in the 4 corners, as well as in the center of the sample plot, resulting in 15 subplots per plot. In the 1 ha sample plots we measured the diameter of all trees with a DBH > 10 cm, as well as the height of palm trees, the diameter of liana and cacti, and the length and diameters of dead wood. In the 5x5 m subplots we measured the diameter of trees with a DBH ranging from 5-10 cm. Thinner trees with a height >1.3 m in the 2x2 m subplots were cut and weighted. The ratio of fresh to dry wood was calculated from wood samples. The biomass of all remaining woody, and of all herbaceous vegetation was measured in the 1x1 m subplots. In the circular plots we measured all woody vegetation with a DBH > 20 cm. Woody vegetation with a DBH between 5 and 20 cm was measured in the inner plot only. Woody vegetation with a DBH < 5 cm, as well as under-story vegetation and litter, was measured in four circular subplots of 0.28 m² in size. Measurements were taken for every plot once during the period 1997 till 2011.

A set of biometric equations were used to convert measurements to dry biomass of individual plants (Tab. 4.2). Some species belonging to the *Bombacaceae* family in the drier regions of Bolivia had very large stem diameters for water storage. The calculated total biomass for these species was reduced by a factor of 0.5 to avoid an overestimation of the actual biomass. Belowground biomass was estimated to be 20% of the aboveground biomass (Cairns et al., 1997). Dry biomass was converted to mass of carbon by using a carbon fraction of dry matter equal to 0.5 (Penman et al., 2003). Tree heights and crown areas used to obtain regional allometric relations were measured for a random selection of trees of varying sizes. Soil organic carbon content of soil samples from 0 to 30 cm depth was quantified applying the Walkley-Black method (Walkley and Black, 1934).

For additional validation purposes, we also made use of the following remote sensing products. The distribution of evergreen and deciduous broad leaved PFTs was compared to a global 1-km resolution remotely sensed data set from DeFries et al. (1999). The distribution of grass PFTs was compared to the land cover map GlobCover 2009 from Arino et al. (2010), where the extension of the lowland savannas was improved with an eco-regional map presented in Ibisch and Mérida (2003). The seasonality of simulated LAI was compared to remotely sensed LAI from MOD15 (Knyazikhin et al., 1999) (<http://neo.sci.gsfc.nasa.gov>) from the Moderate Resolution Imaging Spectroradiometer (MODIS) for the period 2001-2009. The fractional area burnt was examined against the remote sensing product MCD45A2 (Roy et al., 2008) (<http://modis-fire.umd.edu>) for the same period. The climate sensitivity of modeled Gross Primary Productivity (GPP) was compared to remotely sensed Normalized Difference Vegetation Index (NDVI) from 1981 till 2006. The data was obtained from

the Global Inventory Modeling and Mapping Studies (GIMMS) (Pinzon et al., 2005) (<http://glcf.umd.edu/data/gimms/index.shtml>).

4.3.3. Experimental design and analysis

We used the model's three tropical broadleaved PFTs (i) evergreen shade-intolerant (EGSI), (ii) evergreen shade-tolerant (EGST), and (iii) deciduous shade-intolerant (DESI), as well as the two grass PFTs with C3 and C4 photosynthetic pathways. Due to the existence of shade-tolerant deciduous tree species in Bolivia (e.g. *Aspidosperma cylindrocarpon*, *Casearia gossypiosperma*, *Pogonopus tubulosus*, and *Simira rubescens*; Markesteijn et al., 2011), we also added a deciduous shade-tolerant PFT (DEST). Deciduous PFTs have a shorter leaf life span, with all leaves entering the litter pool within 1 year ($\text{turnover}_{\text{leaf}}$), a higher SLA, and a higher fire resistance compared to evergreen PFTs (Tab. 4.3). Shade-intolerant PFTs have a faster growth rate ($\text{turnover}_{\text{sap}}$) and a higher sapling establishment rate (est_{max}), but the demand for photosynthetically active radiation ($\text{parff}_{\text{min}}$), as well as the decrease of establishment rates with decreasing PAR at the forest floor (α_r), are higher. Also, shade-intolerant PFTs are more likely to die when growth efficiency is low ($\text{greff}_{\text{min}}$). The lifespan of deciduous PFTs is estimated to be 400 years, while EGST and EGSI can live up to 500 and 200 years, respectively. In addition to the differences listed above, this study also introduces PFT-specific wood densities (Tab. 4.1). Such PFT traits influence the competition for light and water, and hence the overall success of a PFT under given environmental conditions.

We initiated the model with a 1000 year spin-up with a constant $[\text{CO}_2]$ of 286 ppm, corresponding to the observed value for 1860. After the spin-up, we forced the model with observed $[\text{CO}_2]$ for 149 years, corresponding to the period from 1861 to 2009, with a $[\text{CO}_2]$ of 387 ppm by 2009. To isolate the impact of rising $[\text{CO}_2]$, we also conducted a second model run where $[\text{CO}_2]$ was kept constant at 286 ppm. Climate data were taken from the period 1980 to 2009 for the entire model run. To avoid periodic trends previous to 1980, the data was arranged in a random sequence of years before 1980.

The model was first run for the entire study region with default parameter values provided with the model code. After identifying the main limitations, we tested the impacts of regional parameter values listed in Tab. 4.1 for 40 grid cells, coinciding with the locations of our measurement plots. Impacts were assessed for each parameter separately, as well as for all parameters combined. Since the model was not able to reproduce tropical savannas, we forced it to grow only grass in the savanna region. After this analysis, we ran the model again for the entire study region, but this time with all regional parameter values combined. Results were averaged over the last 30 years (1980-2009), and compared to measured carbon stocks, and remotely sensed

Table 4.1: Regional Parameter Values, with abbreviations of parameters and PFTs provided in sec. 4.3.2 and sec. 4.3.3, respectively.

Parameter	PFT	Default	Bolivia	Unit	Source
disturbance interval	all	100	200	years	estimation
t_{min}	all trees	15.5	10	°C	this study
k_{allom1}	all trees	250	374	(-)	this study
k_{allom2}	all trees	60	36	(-)	this study
k_{allom3}	all trees	0.67	0.58	(-)	this study
k_p	all trees	1.6	1.5	(-)	this study
maximum crown area	all trees	50	650	m ²	this study
SLA	EGST	21.7	33.92	m ² kgC ⁻¹	Markstreijn et al. (2011)
SLA	EGSI	21.7	34.77	m ² kgC ⁻¹	Markstreijn et al. (2011)
SLA	DEST	41.1	39.50	m ² kgC ⁻¹	Markstreijn et al. (2011)
SLA	DESI	41.1	41.23	m ² kgC ⁻¹	Markstreijn et al. (2011)
SLA	C3G, C4G	29.9	19.2	m ² kgC ⁻¹	den Hollander (2008)
wood density	EGST	200	288	kgC m ⁻³	Markstreijn et al. (2011)
wood density	EGSI	200	174	kgC m ⁻³	Markstreijn et al. (2011)
wood density	DEST	200	228	kgC m ⁻³	Markstreijn et al. (2011)
wood density	DESI	200	161	kgC m ⁻³	Markstreijn et al. (2011)
fire resistance	EGST, EGSI	10	40	%	Pinard et al. (1999)
fire resistance	DEST, DESI	30	50	%	estimation

Table 4.2: Equations used to calculate above-ground biomass of individual plants, where b is the dry biomass (kg) per individual plant, d is the diameter (cm) at breast height (1.3 m), h is the plant height (m), ρ is the dead wood density (kg m⁻³), a_1 is the area at the stump, a_2 is the area at the crown bottom, and $dist$ is the distance between stump and crown bottom.

Biometric equations	Group	R ²	Source
$b = 12.764 + 0.2588 * d^{2.0515}$	<i>Cecropia</i> species	0.91	FAN (2005)
$b = 6.666 + 12.826 * \sqrt{h} * \ln(h)$	<i>Euterpe oleracea</i> (palm tree)	0.75	FAN (2005)
$b = 23.487 + 41.851 * \ln(h)^2$	<i>Scheelea princeps</i> (palm tree)	0.62	FAN (2005)
$b = \exp(-2.289 + 2.649 * \ln(d) - 0.021 * \ln(d)^2)$	All other tree species	0.98	Penman et al. (2003)
$b = 10^{(0.12+0.91*\log_{10}(\pi(d/2)^2))}$	Liana species	0.82	Putz (1983)
$b = 0.001 * d^{3.2327}$	Cacti species	0.70	Sampaio and Silva (2005)
$b = ((dist * (a_1 + \sqrt{a_1 * a_2 + a_2}))/3)/1000000 * \rho$	Laying dead wood	NA	FAN (2005)

Table 4.3: Differences between tropical tree PFTs. Parameters marked with an asterisks show regional values adapted for this study.

Parameter	PFTs				Unit
	EGST	EGSI	DEST	DESI	
leaf life span	2	2	0.5	0.5	years
turnover _{leaf}	0.5	0.5	1	1	fraction yr ⁻¹
SLA*	33.92	34.77	39.50	41.23	m ² kgC ⁻¹
fire resistance*	40	40	50	50	%
tree longevity	500	200	400	400	years
turnover _{sap}	0.05	0.1	0.05	0.1	fraction yr ⁻¹
est _{max}	0.05	0.2	0.05	0.2	indiv m ⁻² yr ⁻¹
parff _{min}	350,000	2,500,000	350,000	2,500,000	J m ⁻² day ⁻¹
a_r	3	10	3	10	(-)
greff _{min}	0.04	0.08	0.04	0.08	kgC m ⁻² leaf yr ⁻¹
wood density*	288	174	228	161	kgC m ⁻³

PFT distribution. In addition, LAI seasonality and the occurrences of fires were compared to remote sensing data for the period from 2001 to 2009. We assessed the model's sensitivity to climate variability based on regression analyses of annual GPP and temperature, precipitation, and SW radiation anomalies, as well as ENSO and extreme precipitation events. Relations were critically examined by using remotely sensed NDVI as a proxy for GPP. We also evaluated the impact of rising atmospheric [CO₂] on forests and savanna by comparing the evolution of vegetation carbon over time between model runs with observed and constant [CO₂]. In addition, we assessed how forests responded to the observed negative precipitation trend since 1985.

4.4. Results

4.4.1. Plant Functional Types

Applying the model with its default parameter values resulted in an unrealistic distribution of PFTs. In this model run, deciduous PFTs were dominating the Amazon, no forest was growing along the Andean slopes, grasslands were dominating the dry forest, and the model simulated forests in the tropical savannas of Beni (Fig. 4.2 top row). Replacing default parameter values with those specific to the region (Tab. 4.1), improved PFT distribution significantly (Fig. 4.2 second row), with SLA, wood density and disturbance interval being the most important parameters.

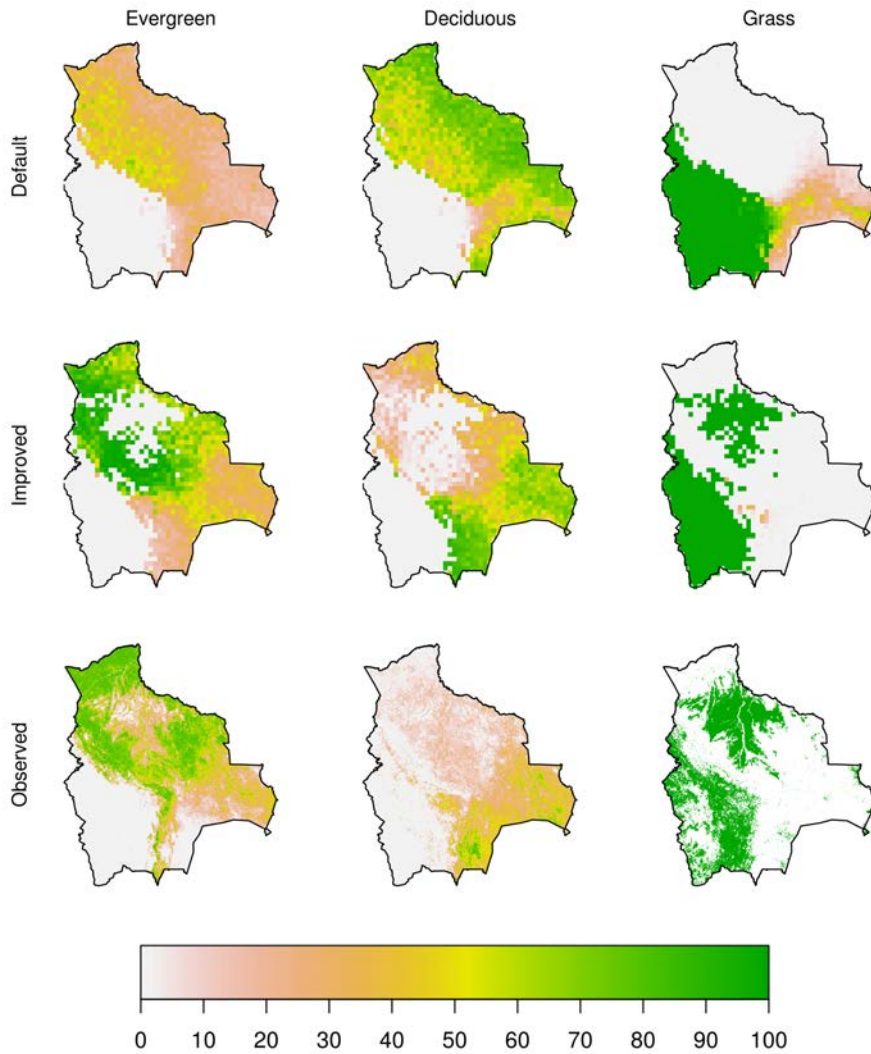


Figure 4.2: Distribution (%) of evergreen, deciduous and grass PFTs (columns) based on the default parameter value settings, improved parameter value settings and according to observations (rows) from DeFries et al. (1999), Arino et al. (2010) and Ibisch and Mérida (2003).

Regional values for SLA were higher than the default values for evergreen PFTs, favoring evergreen over deciduous PFTs (Fig. 4.3a, row 2). This is because of an increase in SLA, which increased LAI, FPAR and eventually NPP, resulting in a higher growth efficiency. Measured wood densities were higher for shade-tolerant and for evergreen PFTs. Since higher wood densities imply slower vertical growth, the application of the regional wood densities favored the growth of deciduous PFTs (Fig. 4.3a, row 3). Using a regional value for t_{cmin} resulted in an accurate tree line, allowing trees to grow at higher altitudes (Fig. 4.3a, row 4). Measured fire resistance (40%) was much higher than the default value of 10% of evergreen PFTs. The smaller difference of fire resistance between evergreen and deciduous PFTs favored the growth of evergreen PFTs (Fig. 4.3a, row 5). Increasing the disturbance interval from the default value of 100 to 200, 300 and 400 years decreased gap dynamics, and favored therefore the shade-tolerant PFTs (Fig. 4.3a, row 6-8). Since this particular experiment only included a shade-intolerant, and no shade-tolerant deciduous PFT, the evergreen PFTs dominated. Including the new PFT DEST, favored the growth of deciduous over evergreen PFTs (Fig. 4.3, row 9). Combining all regional parameter values, and having set the disturbance interval to 200 years, favored the growth of evergreen PFTs in all sites, and suppressed the growth of deciduous PFTs in the Amazon (Fig. 4.3, bottom row). Growth efficiency of evergreen PFTs increased in the Amazon, and decreased in Chiquitania and Chaco, while the opposite occurred for deciduous PFTs.

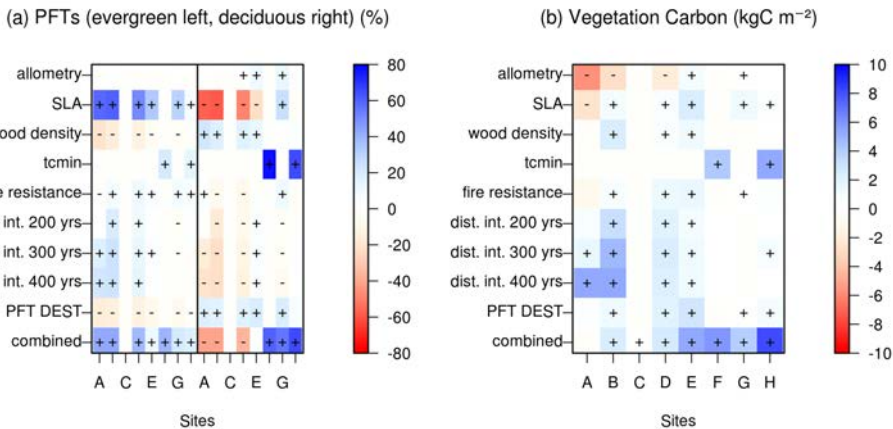


Figure 4.3: Impact of regional parameter values on (a) the distribution of evergreen and deciduous PFTs, and (b) vegetation carbon for 8 sites (A-H). Values show the difference between the regional and the default run. Statistically significant increases and decreases are denoted with (+) and (-), respectively (t -test, 95% probability).

4.4 Results

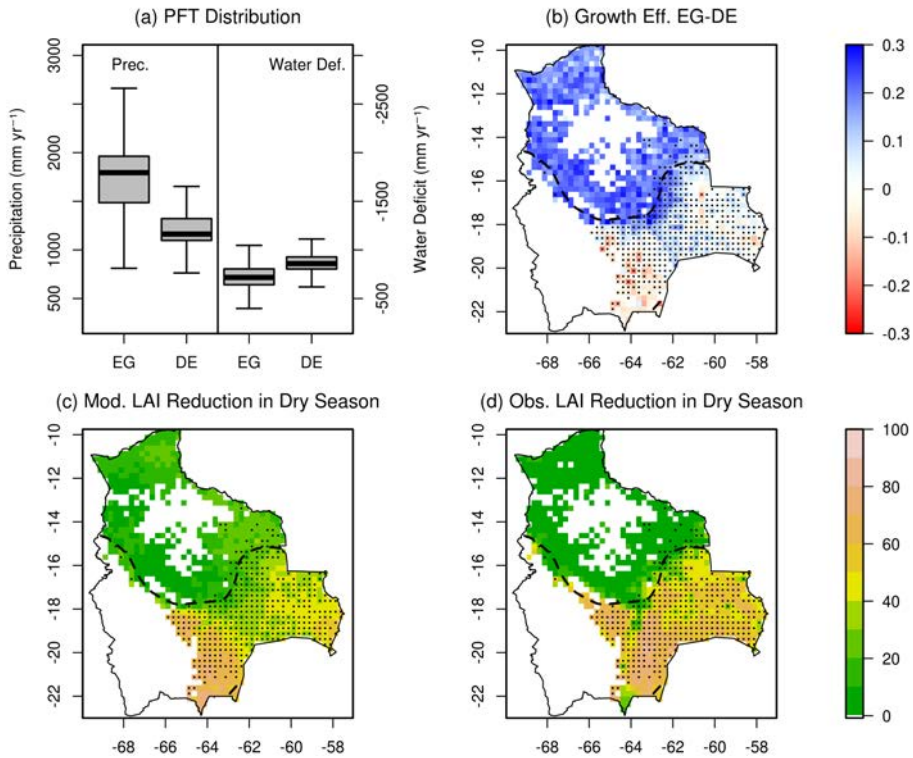


Figure 4.4: (a) Distribution of evergreen (EG) and deciduous (DE) PFTs versus annual precipitation and water deficit; (b) evergreen minus deciduous PFT growth efficiency ($\text{kgC m}^{-2} \text{yr}^{-1}$); and relative reduction of LAI (%) from February (wet) to September (dry) (2001-2009) (c) as modeled and (d) as observed from remote sensing data (MOD15). The dashed line denotes the precipitation contour of 1400 mm yr^{-1} , while stipples mark regions with an annual water deficit below -830 mm yr^{-1} .

Running the model for all Bolivia with the regional parameter values allowed for a realistic distribution of PFTs. Evergreen PFTs dominated the Amazon region, while deciduous PFTs dominated the Chiquitania and Chaco region (Fig. 4.2, second row). The modeled transition from mainly evergreen to mainly deciduous forest spatially coincided with an annual precipitation threshold of 1400 mm yr^{-1} (Fig. 4.4 a and b). Computing the monthly difference of potential evapotranspiration and precipitation, and summing up all negative values over a year, gives an estimate of the annual water deficit. The region dominated by deciduous PFTs experienced an annual moisture deficit below -830 mm yr^{-1} . In this region seasonal leaf abscission was a competitive

advantage, leading to a higher growth efficiency of deciduous trees. The modeled reduction of LAI from the end of the wet season (February) to the end of the dry season (September) mainly agreed with observations from remote sensing data (Fig. 4.4c and d). While simulated LAI values were accurate for the Chaco, the model underestimated the seasonality of LAI in the Chiquitania. The distribution of grasslands in the Andes was modeled correctly, with the exception for some regions with bare land. The model simulated the growth of trees in regions actually covered by savanna, as a result we forced the model to grow only grass in this particular region.

The model reproduced reasonable values of burnt forest during most years, but overestimated fires by 57% on average, mainly due to a large overestimation in a particular year (2002) (Fig. 4.5). Also, the spatial distribution of fires did not match observations with too many fires in the Chaco and too few in the Chiquitania. In the savannas, the model systematically underestimated fires (not shown).

4.4.2. Carbon stocks

Our field measurements found highest total carbon stocks in the cloud forest of northern Tucumano (44 kgC m^{-2}), with high values in the vegetation (25 kgC m^{-2}) and soil pool (17 kgC m^{-2}) (Tab. 4.4). Lowest values were found in the savannas (6 kgC m^{-2}), where most of the carbon was stored in the soil. Vegetation carbon decreased from the lowland Amazon (12 to 14 kgC m^{-2}) to the Chiquitania (11 kgC m^{-2}), Chaco (9 kgC m^{-2}) and southern Tucumano forests (6 kgC m^{-2}). With the exception of the

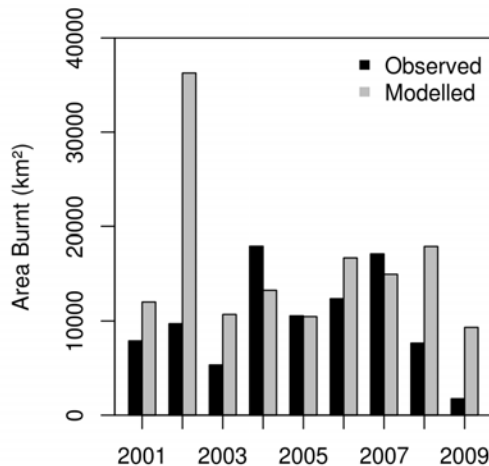


Figure 4.5: Modeled and remotely sensed (MCD45A2) areas of burnt forest.

savannas, the vegetation pool contained most of the carbon (61%), followed by the soil (31%), and litter pool (8%). The uncertainty of the mean values was high, with a coefficient of variation of around 40% for the vegetation, 46% for the litter, and 47% for the soil pool in forests.

Using the default parameter values, the model reproduced accurate quantities of vegetation carbon in the Amazon, but systematically underestimated vegetation carbon in the dry forests of the Chiquitania and Chaco, and in the Tucumano forest (not shown). Regional parameter values affected vegetation carbon significantly, especially with respect to allometric relations and disturbance interval.

Our field measurements of DBH, tree height and crown area revealed that trees in Bolivia were not as tall at a given DBH, but had a greater crown than predicted by the default parameter values (Fig. 4.6). Also, the maximum crown area in the Bolivian Amazon was much larger (650 m²) than the default value of 50 m². Replacing default with regional allometric parameter values (*i.e.* k_{allom1} , k_{allom2} , k_{allom3} , k_{TP} and maximum crown area, Tab. 4.1) lead therefore to smaller trees with larger crowns. This caused a reduction of vegetation carbon in the Amazon (Fig. 4.3b, top row), because larger crowns increased tree mortality that occurs as a result of light competition, thereby lowering tree density. This did not occur in southern Bolivia, as tree density was already low there.

Regional values of evergreen SLA (34 m² kgC⁻¹) were higher than the default value of 22 m² kgC⁻¹. Greater values of SLA enhanced photosynthesis, and lead to more vegetation carbon in most sites (Fig. 4.3b, row 2). Using a lower temperature threshold value of 10°C for establishment and survival allowed trees to grow in the higher elevated Tucumano forest, increasing vegetation carbon there (Fig. 4.3b, row 4). Measured fire resistance (40%; Pinard et al., 1999) was much higher than the default value of 10% of evergreen PFTs, lowering fire related mortality, and hence increasing vegetation carbon. Increasing the disturbance interval from the default value of 100 to 200, 300 and 400 years decreased mortality, allowing trees to grow taller, and to accumulate more vegetation carbon (Fig. 4.3b, row 6-8). Combining all regional parameter values, and having set the disturbance interval to 200 years, increased vegetation carbon in nearly all sites, with greater relative increases in the dry than in the wet forests (Fig. 4.3b, bottom row).

Running the model with regional parameter values for the entire study region showed that modeled vegetation carbon was highest in the cloud forests of the northern Andean slopes, and decreased from the northern Amazon to the Chiquitania, Chaco, savanna and Altiplano (Fig. 4.7b). Modeled vegetation carbon was correlated significantly (99% level) with observations ($R^2 = 0.31$), with a tendency for a positive bias (Fig. 4.7a). Only for one site (F, Northern Tucumano forest) did the model have inaccurate values, for reasons addressed in the Discussion section. Regional parameter values did not affect the litter and soil pool significantly (not shown). In both cases, modeled and observed values were not correlated, but at least of the same magnitude. In case of litter, observed and modeled values were below 4 kgC m⁻², with underes-

timates in one Amazon site (B) and overestimates in the savanna (C). In the case of soils, carbon stocks were accurate for most sites, and too low in the Amazon site (B) and northern Tucumano forest (F).

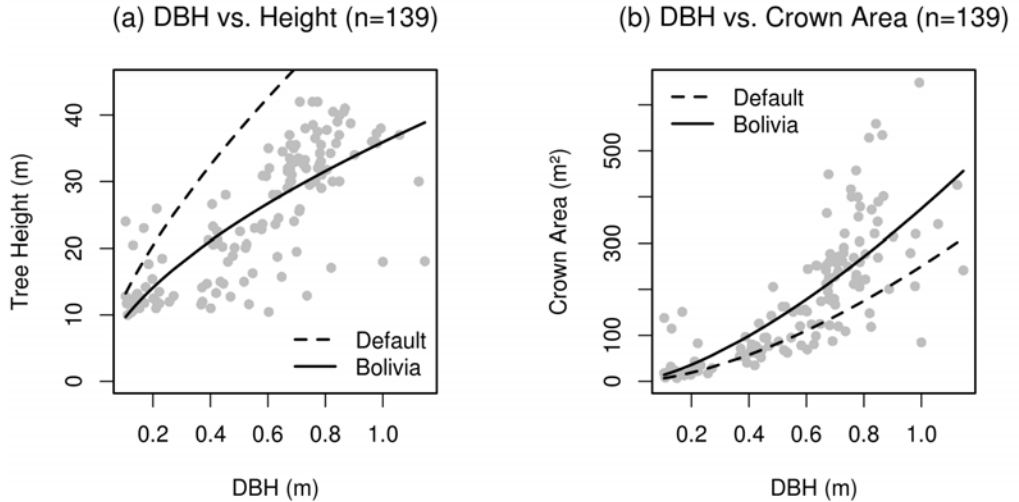


Figure 4.6: Allometric relations of DBH and (a) tree height and (b) crown area for 139 trees in Bolivia. The dashed lines show functions based on default coefficients used in the model, while the solid lines show functions based on regional coefficients used in this study. The respective coefficients are listed in Tab. 4.1.

4.4.3. Climate sensitivity

Modeled GPP and remotely sensed NDVI were significantly correlated in most of the dry forests and part of the Amazon (Fig. 4.8 a). Annual GPP anomalies were strongly correlated with annual precipitation anomalies, with a higher coefficient of determination in the dry forests ($R^2 = 0.8$), than in the wet forests ($R^2 = 0.5$) (Fig. 4.9). Correlations of GPP with temperature and SW radiation were weaker ($R^2 < 0.3$) than with precipitation. The dry forests responded most sensitively to precipitation anomalies, where an increase in rainfall by 1% caused an increase in GPP by about 1% (Fig. 4.8 b). This enhanced sensitivity was also found for remotely sensed NDVI (Fig. 4.8 c).

Table 4.4: Mean and standard deviation (sd) of measured carbon stocks (kgC m^{-2}) of vegetation, litter and soil, as well as total number of plots for each site (N).

(Site)	Veg. unit	Lon	Lat	Vegetation		Litter		Soil		Total		N
				mean	sd	mean	sd	mean	sd	mean	sd	
(A)	Amazon	-69.28	-11.06	12.36	6.46	1.41	0.70	2.68	1.04	16.45	7.09	62
(B)	Amazon	-66.34	-11.57	14.23	3.51	3.11	0.85	10.05	9.06	27.39	9.38	30
(C)	Savanna	-63.69	-13.49	0.25	0.20	0.23	0.22	5.63	1.16	6.12	1.29	6
(D)	Amazon	-61.22	-14.04	12.16	7.89	1.54	1.05	3.21	1.98	16.91	8.70	612
(E)	Chiquitania	-60.68	-16.48	10.91	1.57	1.53	0.41	6.77	1.61	19.21	3.17	6
(F)	Tucumano N	-63.77	-18.58	25.35	8.87	1.44	0.31	17.06	3.76	43.84	10.77	5
(G)	Chaco	-63.11	-19.27	8.64	2.49	1.28	0.54	5.58	2.13	15.50	3.54	4
(H)	Tucumano S	-63.73	-21.60	5.81	3.48	0.72	0.65	3.75	1.91	10.28	4.49	94
Sum											819	

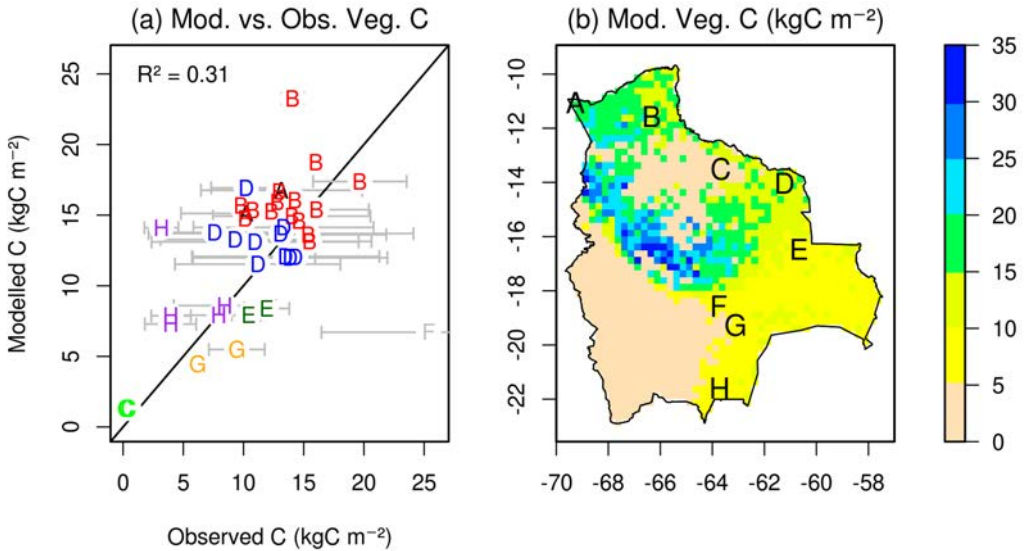


Figure 4.7: (a) Modeled versus observed vegetation carbon for 8 sites; and (b) modeled vegetation carbon (kgC m^{-2}) for Bolivia with site locations (A-H, see Tab. 4.4). Grey bars denote the standard deviation of the observations, in case several plots shared a single grid cell.

The ENSO index showed significant positive correlations with GPP in Bolivia's Amazon region, where an El Niño year with an annual mean ENSO index of 1 could increase GPP by up to 15% (Fig. 4.8 d). The reason for this was a positive correlation of ENSO and annual precipitation in lowland Bolivia. While this correlation was the general pattern, impacts of ENSO varied considerably (Fig. 4.9). Remotely sensed NDVI also revealed a positive slope when regressed against the ENSO index, but correlations were not significant (Fig. 4.8 e). Another important climate mode for Bolivia, the Pacific Decadal Oscillation (PDO) (Garreaud et al., 2009; Seiler et al., 2013a), had no significant impact on GPP anomalies.

Consecutive dry days (CDD) affected GPP significantly, where an increase of CDD by 1 day could decrease GPP by up to 1.2% (Fig. 4.8 f). Remotely sensed NDVI also revealed a negative slope when regressed against CDD, but correlations were significant for few grid cells only (Fig. 4.8 g).

Precipitation is currently decreasing in Bolivia since about 1985 (Seiler et al., 2013a), resulting in a significant reduction of modeled GPP in Bolivia's Amazon (Fig. 4.8 h). Remotely sensed NDVI revealed a different pattern, with positive trends in the Amazon, and negative trends in the dry forests (Fig. 4.8 i).

4.4 Results

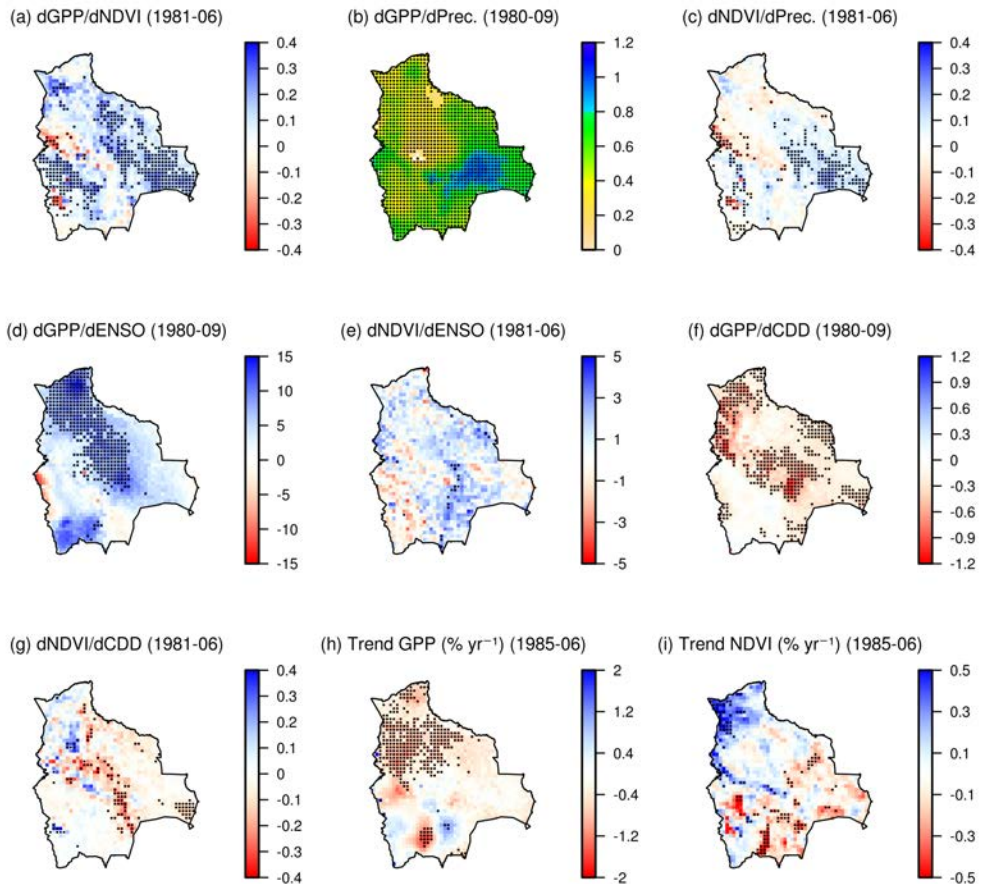


Figure 4.8: Linear regressions of (a) annual GPP and NDVI, (b) annual GPP and precipitation, (c) NDVI and precipitation, (d) GPP and ENSO, (e) NDVI and ENSO, (f) GPP and CDD and (g) NDVI and CDD; and annual trends in (h) GPP and (i) NDVI. Dots denote grid cells where the regressions (a-g) and trends (h,i) are statistically significant at the 95% level.

Forcing the model with the observed rise of $[\text{CO}_2]$ led to a significant increase of vegetation carbon throughout most of Bolivia. The dry forests of the Chaco and Chiquitania were more susceptible to rising $[\text{CO}_2]$ than the wet forests of the Amazon and the Yungas, with 24% and 45% more vegetation carbon due to rising $[\text{CO}_2]$ by 2009 in the Amazon and Chaco, respectively (Fig. 4.10). This was to be expected,

as an increase in $[\text{CO}_2]$ implies lower stomatal conductance, increasing the water use efficiency of plants. Since this is a greater benefit in water limited regions, the CO_2 -fertilizing effect is bigger in dry compared to wet forests.

4.5. Discussion

We adapted the dynamic vegetation model LPJ-GUESS to simulate present day potential vegetation as a baseline for climate change impact assessments for Bolivia. Results were compared to biomass measurements (21 new, and 798 previous plots) and remote sensing data. Using regional parameter values for allometric relations, specific leaf area, wood density and disturbance interval, a realistic transition from the evergreen Amazon to the deciduous dry forest was simulated. This transition coincided with threshold values for precipitation (1400 mm yr^{-1}) and water deficit (-830 mm yr^{-1}), beyond which leaf abscission became a competitive advantage. The model reproduced reasonable values for seasonal leaf abscission, vegetation carbon, and forest fires. Modeled GPP and remotely sensed NDVI showed that dry forests were more sensitive to rainfall anomalies than wet forests. Modeled GPP was positively correlated to ENSO in the Amazon, and negatively correlated to consecutive dry days. Decreasing rainfall trends are simulated to decrease GPP in the Amazon.

Our biomass measurements in Bolivia's Amazon and Chiquitania were comparable to values reported by Dauber et al. (2000), Mostacedo et al. (2009) and Baker et al. (2004), considering that our values also included roots (assumed to be 20% of above-ground living biomass), as well as trees with a $\text{DBH} < 10 \text{ cm}$. The high spatial variability within some measurement sites (A, D) indicated the existence of important regional factors not captured by the model, such as soil nutrients, varying soil depth, lateral water transport, or local disturbances. The large amounts of vegetation carbon measured in the cloud forests of the Northern Tucumano (site F) contradicted findings from Girardin et al. (2010) and Moser et al. (2011), who reported decreasing values with increasing altitude in the tropical Andes. Model results for this site were much lower than measurements, likely due to an underestimation of the precipitation forcing data, given that the closest meteorological station was located in a much drier area (Mairana, 1300 mm yr^{-1}). However, the model did reproduce comparably high values of vegetation carbon in the cloud forests of the northern Andean slopes, where the presence of meteorological stations lead to a more realistic interpolation of rainfall. Remotely sensed estimates from Saatchi et al. (2011) however cannot confirm such high values. Additional biometric measurements in Bolivia's cloud forest may clarify if the large amounts of vegetation carbon measured in the Tucumano forest, and modeled in the Yungas, are representative for Bolivia's cloud forests.

Modeled GPP and remotely sensed NDVI showed similar responses to climate variability, but revealed opposing trends in Bolivia's Amazon. While the model simulated a decrease of GPP due to decreasing rainfall, remotely sensed NDVI showed an increasing trend from 1985 to 2006. Numerous reasons may be responsible for this,

including that NDVI is only a proxy for GPP, the saturation of NDVI for high LAI, the imperfect spatial interpolation of rainfall measurements, and a range of potentially important processes not represented in the model. These processes include the horizontal water transport from the Andes to the lowlands (McClain and Naiman, 2008), capillary rise (Romero-Saltos et al., 2005), shallow groundwater tables directly tapped by roots (Miguez-Macho and Fan, 2012), and water withdrawal from greater soil depths through deep roots (Bruno et al., 2006). Such processes would make forests more resilient to water stress, and motivated vegetation modelers to increase soil depth for model experiments in the Amazon (e.g. Baker et al., 2008). In case of LPJ-GUESS, a greater soil depth implies less runoff, as soils are less likely to become saturated. In a side analysis of this study we compared modeled against observed runoff from 1984 to 2010 for the upper Mamoré river basin in Puerto Siles (12.80°S, 65.00°W). Our modeled runoff systematically underestimated annual runoff by 37% on average, for which we were reluctant to further decrease our runoff by increasing soil depth. Also, a deeper soil layer reduces modeled soil moisture, as rain water is distributed over a larger volume. This in return increases fire probability, and decrease vegetation carbon. Given that groundwater levels may be shallow, increasing the model's soil depth might only lead to improvements if groundwater hydrology is considered.

The strong sensitivity of LPJ-GUESS and other DGVMs to rising $[\text{CO}_2]$ has been reported previously, especially under tropical, but also drier climates (Hickler et al., 2008). This sensitivity is most probably exaggerated, because the response of plants to rising $[\text{CO}_2]$ is limited by nutrients, which are currently not included in most DGVMs (Körner, 2006). Furthermore, field experiments suggest that additional $[\text{CO}_2]$ is not necessarily accumulated in long-lived biomass pools, but is instead transported faster through the trees (Körner et al., 2005). A new free-air CO_2 enrichment (FACE) experiment in the Amazon will soon provide more insights on the true sensitivity of tropical plants to rising $[\text{CO}_2]$ (Tollefson, 2013).

Few studies quantified natural disturbance related to windthrow in the Amazon. Espirito-Santo et al. (2010) estimated the return interval of windthrows from Landsat satellite data to range between 27,000 and 90,000 years in the Amazon, resulting in an insignificant contribution to CO_2 emissions when compared to deforestation. Negrón-Juárez et al. (2010) on the other hand showed that storms during the year of 2005 produced a tree mortality equivalent to 23% of the mean annual biomass accumulation, and an equivalent to 30% of the observed annual deforestation reported for the same year and region. We are not aware of a widely accepted natural disturbance interval for the Amazon, for which we tested the impacts of different intervals. Our final choice of 200 years was higher than the default value, but still allowed for sufficient gap dynamics important for the growth of deciduous trees. The current model version assumes a uniform disturbance interval for the entire globe, except for fires. This may be improved by quantifying spatially varying disturbance intervals (Chambers et al., 2013), or by incorporating a physically based approach as proposed by Lagergren et al. (2012).

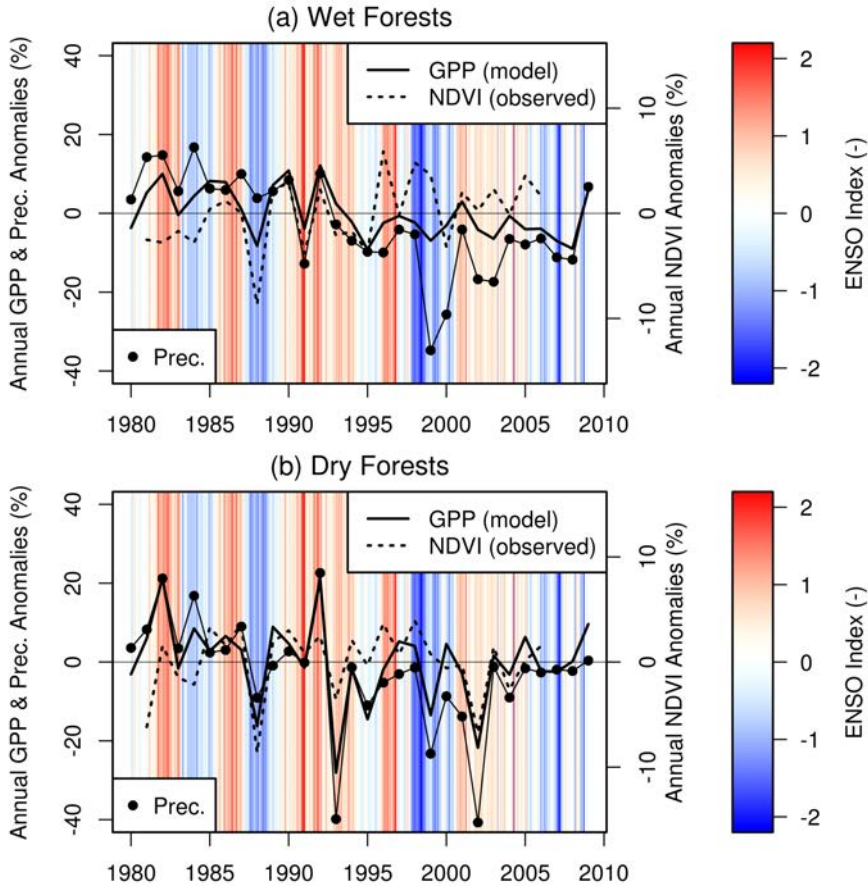


Figure 4.9: Modeled GPP, remotely sensed NDVI and precipitation anomalies averaged over the (a) wet forests (Amazon and Yungas) and (b) dry forests (Chaco and Chiquitania). Vertical lines in blue and red shades represent the monthly ENSO index.

Fire resistance reported by Pinard et al. (1999) was averaged over all species, regardless of leaf phenology. Their site was located in a semi-humid forest (15.78°S, 62.63°W) containing both evergreen and deciduous trees, but was dominated by evergreen trees. We therefore applied the reported value of 40% to evergreen PFTs, and assigned a slightly higher value of 50% to deciduous PFTs. This choice was motivated by the fact that the default values for fire resistance were higher for deciduous than for evergreen PFTs. Additional measurements in the deciduous forest could improve this approximation. The high fire frequency in the savannas, and the spatial distribution

of forest fires in general, could not be reproduced properly in the model, as many of these fires are man-made (Rodriguez, 2012a).

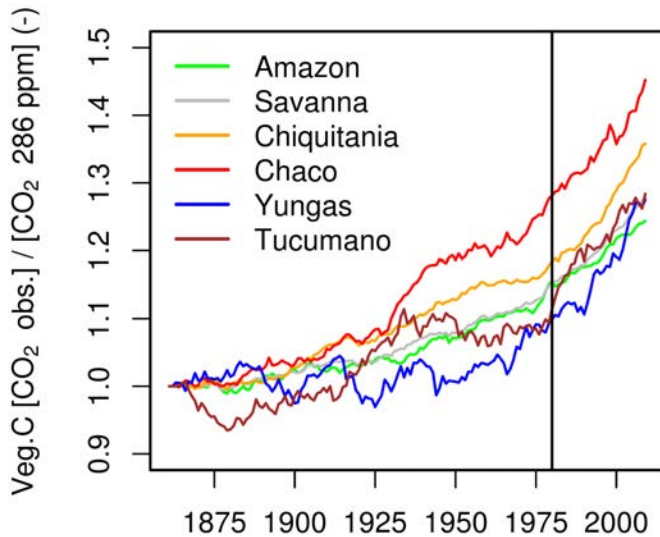


Figure 4.10: Ratios of vegetation carbon forced with observed $[\text{CO}_2]$ and constant $[\text{CO}_2]$ at 286 ppm from 1861 to 2009 for different vegetation units presented in Fig. 4.1b. The vertical black line marks the year of 1980, dividing the observed (1980-2009) from the constructed (1861-1997) climate data.

Further limitations and potentials for improvement include the following aspects. (i) We expressed the distribution of PFTs by the relative amount of carbon stored by a PFT, and compared this to the data from DeFries et al. (1999). This comparison was only an approximation, as the data from DeFries et al. (1999) show the fractional area covered by a PFT, with a potential maximum of 80%. We consider our approach to be valid nevertheless, as we used this data as a reference for the general spatial patterns only. (ii) Tropical savannas could not be reproduced by the model, as one of the main mechanisms, seasonal flooding, was missing in the model. Additional model components would be required to model seasonal floodings, and its impacts on plant growth. (iii) Regional parameter values of SLA and wood density were measured in a single site located in the Chiquitania, where shade tolerant and intolerant evergreen and deciduous tree species were present. While this allowed us to obtain values from trees growing under the same environmental conditions, values are not necessarily representative for other forests. Additional measurements in other locations could

inform on the variability of these values. (iv) Some tree species in the Bolivian Andes belong to coniferous PFTs (e.g. *Prumnopitys exigua* and *Podocarpus parlatorei*). We excluded coniferous PFTs in the modeling experiments, as we focused on the transition of evergreen to deciduous forests in the lowlands. (v) The period of climate observations from 1980-2009 was very short, ignoring potentially important climate variability previous to 1980. Choosing a random order of years for the spin-up may have exaggerated the true interannual climate variability.

Climate change may lead to more water deficit, potentially shifting the current boundaries between evergreen and deciduous PFTs at the edge of the Amazon, affecting not only carbon stocks, but also species distribution. Since dry forests show a greater sensitivity to rainfall anomalies than wet forests, the probability of forest die-back may be larger at the edge of the Amazon basin, at least for the Bolivian case. Climate change impact assessments on tropical forests could pay more attention to these sensitive transition zones.

To conclude, we adapted and evaluated the dynamic vegetation model LPJ-GUESS for the historic climate conditions of Bolivia. Special attention was paid to the transition of evergreen to deciduous forests, seasonal leaf abscission, vegetation carbon, forest fires, the response of GPP to climate variability, and the model's sensitivity to rising [CO₂]. The current model setup provides a baseline for assessing the potential impacts of climate change in the transition zone from wet to dry tropical forests in Bolivia.

Acknowledgments

This research was supported by the Departmental Pilot Program of Adaptation to Climate Change (PDACC) as well as the project Raising the Alert about Critical Feedbacks between Climate and Land Use Change in Amazonia (AMAZALERT, project number: 282664). PDACC is carried out by the Fundación Amigos de la Naturaleza (FAN) and the departmental government of Santa Cruz, and is funded by the embassy of the Netherlands. AMAZALERT is jointly funded by the European 7th Framework programme and national organizations. The research funding programme LOEWE provided financial support for the simulations, which were carried out at the LOEWE Frankfurt Centre for Scientific Computing (LOEWE-CSC). C.S, J.R.M. and T.H. were supported by a WIMEK grant, an NSERC Visiting Postdoctoral Fellowship, and the LOEWE initiative, respectively. We thank the Bolivian National Service of Meteorology and Hydrology (SENAMHI) for the provision of the meteorological data. We are grateful for the technical support from Dr. Matthew Forrest from the Biodiversity and Climate Research Centre (BiK-F), and thank Dr. Sassan Saatchi from the Jet Propulsion Laboratory (JPL, NASA) for discussions. Field data collection was only possible due to the tremendous efforts from over 60 community members from Baures, Churcos, El Espino, Posttrervalde, Santa Ana de Velasco and Tierras Nuevas.

5. The Sensitivity of Wet and Dry Tropical Forests to Climate Change in Bolivia

Abstract

Bolivia's forests contribute to the global carbon and water cycle, as well as to global biodiversity. The survival of these forests may be at risk due to climate change. To explore the associated mechanisms and uncertainties, a regionally adapted dynamic vegetation model (LPJ-GUESS) was implemented for the Bolivian case, and forced with two contrasting climate change projections. Mechanisms of change were evaluated by changes in carbon stocks and fluxes, factoring out the individual contributions of atmospheric carbon dioxide ($[\text{CO}_2]$), temperature and precipitation. Special attention was paid to the effect of rising temperatures on photosynthesis, respiration, and the atmospheric demand for transpiration. Impacts ranged from a strong increment to a severe loss of vegetation carbon (c_v), depending on differences in climate projections, as well as the physiological response to rising $[\text{CO}_2]$. The loss of c_v was primarily driven by a reduction in gross primary productivity, and secondarily by enhanced emissions from fires and autotrophic respiration. In the wet forest, less precipitation and higher temperatures equally reduced c_v , while in the dry forest, the impact of precipitation was dominating. The temperature-related reduction of c_v was mainly due to a decrease in photosynthesis, and only to lesser extent because of more autotrophic respiration and less stomatal conductance as a response to an increasing atmospheric demand. Tropical dry forests were simulated to virtually disappear, regardless of the fertilizing effect of rising $[\text{CO}_2]$, suggesting a higher risk for forest loss along the drier southern fringe of the Amazon. Implications for two Bolivian projects on reducing emissions from deforestation and forest degradation (REDD) are discussed.

This chapter has been submitted as:

Seiler, C., R.W.A. Hutjes, B. Kruijt, T. Hickler, 2014: The Sensitivity of Wet and Dry Tropical Forests to Climate Change in Bolivia. *submitted*.

5.1. Introduction

The important contribution of the Amazon rainforest to the global carbon cycle (Pan et al., 2011), water cycle (Salati et al., 1979) and biodiversity (Gaston, 2000) motivates extensive research on the sensitivity of these forests to climate change. This sensitivity can be explored by forcing dynamic vegetation models (DGVMs) with climate change projections from general circulation models (GCMs) for a range of emission scenarios (Huntingford et al., 2008). The impacts of climate change however remain highly uncertain, and range from severe losses (Cox et al., 2004) to substantial increases in biomass (Huntingford et al., 2013). Uncertainties arise from conflicting climate change projections (Poulter et al., 2010), as well as different physiological responses of plants to rising concentrations of atmospheric carbon dioxide ($[\text{CO}_2]$), increasing temperatures, and water stress (Galbraith et al., 2010).

Climate change scenarios from 35 global circulation models (GCMs) project an increase in mean annual temperature between 2° and 7°C in Bolivia by the end of this century, with conflicting projections for annual precipitation ($\pm 20\%$) (Seiler et al., 2013b). Conflicting rainfall projections arise from spatial shifts in convective mass fluxes associated with different SST pattern responses to enhanced greenhouse gas emissions (Chadwick et al., 2013).

Rising $[\text{CO}_2]$ can affect the plant by directly enhancing photosynthesis, and by reducing the plant's water use efficiency. Free-Air CO_2 Enrichment (FACE) experiments showed that plant growth under elevated $[\text{CO}_2]$ is constrained by a decreasing availability of nitrogen as carbon and nitrogen are sequestered in long-lived plant biomass and soil organic matter (Reich et al., 2006; Norby et al., 2010). While comparable field experiments for the Amazon are still in preparation (Tollefson, 2013), it can be expected that the fertilizing effect of rising $[\text{CO}_2]$ is most likely exaggerated in most DGVMs due to missing nutrient cycles, including nitrogen and phosphorus, in these models (Oren et al., 2001; Körner, 2006; Hickler et al., 2008; Wang et al., 2010). The impact of rising $[\text{CO}_2]$ on water use efficiency however is not affected by nutrients, but may be limited by phenotypic plasticity (de Boer et al., 2011).

The response of photosynthesis to rising leaf temperatures can be described with a bell-shaped curve (Hickler et al., 2008). The associated uncertainty arises from the exact shape and plasticity of this curve, as plants are known to adapt their temperature optimum to changes in their environment (Berry and Bjorkman, 1980; Medlyn et al., 2002; Atkin and Tjoelker, 2003). This is of great relevance, as model experiments for the Amazon show that the projected rise in temperature can cause the same amount of biomass loss as caused by the projected reductions in precipitation (Galbraith et al., 2010). Two thirds of this loss were associated with a reduction of photosynthesis, and one third with an increase of respiration in the case of the LPJ model (Sitch et al., 2003).

Uncertainties related to water stress are mainly associated with a number of sub-surface processes observed in the field, but not commonly incorporated in DGVMs.

This includes capillary rise (Romero-Saltos et al., 2005), shallow groundwater tables directly tapped by roots (Miguez-Macho and Fan, 2012), and water withdrawal from greater soil depths through deep roots (Bruno et al., 2006).

The focus of previous studies has been mainly on the Amazon basin as a whole, and less on the drier transition zones from evergreen to deciduous forests along the southern margin of the basin. The impacts of climate change however may actually be higher in these transition zones, as species are closer to the extreme limits of their ecological requirements (Killeen et al., 2006). The border line of the Amazon basin cuts through the lowlands of Bolivia, with evergreen wet forests in the north, and deciduous dry forests towards the south. Also, large parts of the Bolivian lowlands (111,000 km²) are covered by the tropical savannas of Beni. Studying Bolivia gave us the opportunity to assess carbon dynamics in a transition zone where evergreen and deciduous tree species, as well as grasses are competing for resources. The presence of two large scale carbon offset projects eligible under REDD (Reducing Emissions from Deforestation and Forest Degradation; UNFCCC, 2010) was an additional motive to study this region, since the risk of a climate change induced forest die-back has triggered a discussion on the permanence of carbon stocks protected by REDD (Malhi et al., 2008; Gumpenberger et al., 2010). It must be noted that at the time of writing the Bolivian government opposes the carbon trading scheme of REDD projects, and is promoting an alternative mechanism without the sale of carbon credits instead, namely the joint mitigation and adaptation mechanism for the comprehensive and sustainable management of forest and the mother earth (JMA; RREE, 2012). For simplicity, we continue referring to both projects as REDD, as they originally were designed as such.

A regional climate change impact analysis requires detailed information which cannot easily be provided by previous studies of global or continental scale. In the Bolivian case, a global application of the DGVM LPJ simulated grasslands instead of deciduous trees in Bolivia's semi-dry and dry forests for present-day climate (Sitch et al., 2003). Similarly, the DGVM CPTEC-PVM (Oyama and Nobre, 2004) simulated mainly savanna in Bolivia's Amazon forest for current climatic conditions (Salazar et al., 2007), limiting the validity of any future projections for the region. Seiler et al. (2014) therefore implemented the DGVM LPJ-GUESS (Smith et al., 2001; Ahlström et al., 2013) explicitly for Bolivia, and evaluated its performance for current climatic conditions with carbon stock measurements and remote sensing data. Using regional parameter values for allometric relations, specific leaf area, wood density and disturbance interval, Seiler et al. (2014) simulated a realistic transition from the evergreen Amazon to the deciduous dry forest, as well as reasonable carbon stocks for different forest types.

Using the same model configuration, we explored the sensitivity of Bolivian forests to climate change for two contrasting climate change scenarios generated by two different GCMs forced with the same emission scenario (RCP8.5, see sec. 5.3.2). The uncertainty of climate change projections was addressed by comparing the impacts of a wet scenario with little temperature increase, against a dry scenario with a strong

temperature increase (sec. 5.4.1). Since LPJ-GUESS did not include nutrient cycling at the time of writing, experiments were conducted with both constant, and with rising $[\text{CO}_2]$. The actual fertilizing effect is estimated to lie somewhere between these two runs. Mechanisms of forest loss were identified by focusing on the dry scenario, and by quantifying the individual contributions of precipitation and temperature (sec. 5.4.2). Special attention was paid to the physiological response of plants to rising temperature by distinguishing the impacts of rising temperature on photosynthesis, respiration, and stomatal conductance related to an increasing atmospheric demand. Implications for the carbon stocks protected by the two Bolivian REDD projects are discussed in sec. 5.5.

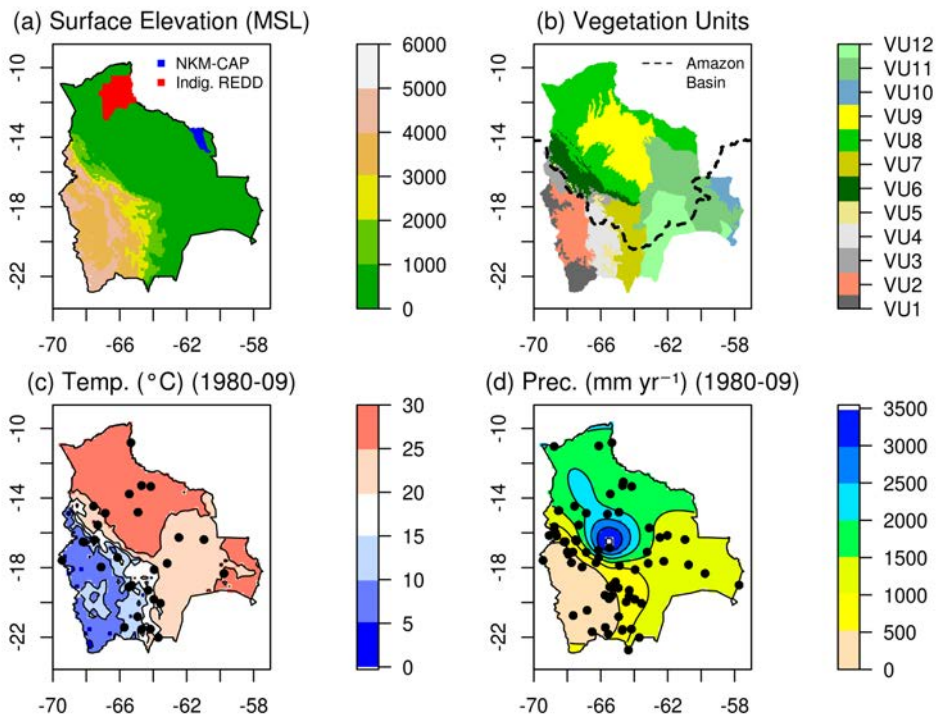


Figure 5.1: (a) Surface elevation (m MSL), (b) vegetation units (VU1 = Western Cordillera, VU2 = Altiplano, VU3 = Eastern Cordillera and Northern Altiplano, VU4 = Eastern Cordillera and Central and Southern Altiplano, VU5 = Prepuna, VU6 = Yungas, VU7 = Tucumano Forest, VU8 = Amazon, VU9 = Beni savannas, VU10= Pantanal, VU11 = Chiquitania, VU12 = Chaco (Navarro and Ferreira, 2004)), (c) annual mean temperature (°C) and meteorological stations from 1980-2009, (d) annual mean precipitation (mm yr⁻¹) and meteorological stations from 1980-2009.

5.2. Study area

The Plurinational State of Bolivia is a tropical country measuring more than one million km². About half of this area is covered by forest (Morales et al., 2001), including the evergreen rain forest of the Amazon (hereafter referred to as wet forest), the semi-deciduous Chiquitania forest, and the deciduous Chaco dry forest (both hereafter referred to as dry forest) (Fig. 5.1). The transition from wet to dry forests occurs along a precipitation gradient, with decreasing annual rainfall, and increasing seasonality towards the south (Seiler et al., 2014). Cloud forests (Yungas) grow along the Andean slopes where rainfall rates are highest in Bolivia. Large parts of the Bolivian lowlands (111,000 km²) are also covered by the tropical savannas of Beni, which are affected by seasonal flooding, drought, and land use (Larrea et al., 2010).

Bolivian forests store approximately 6 Gt of carbon (Saatchi et al., 2011), and affect the water cycle of the Madeira river basin, providing about 10% of the total discharge of the Amazon river (Roche and Jauregui, 1988). Holding a National Biodiversity Index of 0.724 (CBD, 2001), Bolivia hosts around 20,000 plant-, 1,398 bird-, 600 fish-, 356 mammal-, 266 reptile-, and 204 amphibian species (Ibisch and Mérida, 2003). Protected areas, as well as two large-scale REDD projects, intend to protect forests from human pressures. The respective projects are the Climate Action Project Noel Kempff Mercado (CAP-NKM) (Virgilio, 2009), and the Indigenous REDD Program in the Bolivian Amazon (FAN, 2010).

5.3. Methods

5.3.1. Model description

The dynamic vegetation model LPJ-GUESS (Smith et al., 2001; Ahlström et al., 2013) simulates the exchange of water and carbon between soil, plants and atmosphere, as well as the resulting terrestrial ecosystem composition and structure (Fig. 5.2). Model inputs consist of temperature, precipitation, solar radiation, [CO₂], and soil texture. Plants are grouped into plant functional types (PFTs) according to structural and phenological differences. One grid cell represents the average of several replicate patches, typically of 0.1 ha in size each. A patch may contain several PFT cohorts, each represented by an average individual. Replicate patches are driven by the same input data, however, vegetation dynamics differ due to stochasticity in establishment, mortality and disturbance processes. Soils consist of an upper (0-0.5 m) and a lower layer (0.5-1.5 m) of identical soil texture. The following paragraphs outline the model's main computation steps relevant to this study.

(0.08), p_i is the internal partial pressure of CO₂, [O₂] is the partial pressure of oxygen, t_{scal} is a temperature scalar, Γ^* is the CO₂ compensation point, and K_c and K_o are the Michaelis constants for CO₂ and O₂, respectively. K_c , K_o , Γ^* and t_{scal} are temperature dependent, and together lead to a bell-shaped response of A_{nd} to temperature. K_c , K_o and Γ^* increase exponentially with temperature following a Q₁₀ relationship, and t_{scal} is calculated from PFT-specific temperature values for minimum, low, high and maximum photosynthesis rate. A_{nd} is maximized by optimizing V_{max} for a given K_c , K_o , Γ^* , t_{scal} , APAR and p_i .

The internal partial pressure of CO₂ (p_i) depends on the closure of the plant's stomata, which in return depends on the balance of transpirational demand and water supply. The transpirational demand (d) is estimated from non-water stressed canopy conductance (g_c) and the equilibrium evaporation (E_q). Based on Monteith (1995):

$$d = E_q * \alpha_m * g_c / (g_c + g_m), \quad (5.4)$$

where a_m and g_m are empirical parameters (1.391 and 3.26, respectively), and g_c is calculated as an iterative solution to the photosynthesis and water balance. E_q increases with temperature and SW radiation according to Monteith and Unsworth (2007) (their equation 13.37):

$$E_q = [s / (s + \gamma)] * R_n / \lambda, \quad (5.5)$$

where s is the change of saturation vapour pressure with temperature, R_n is the instantaneous net radiation (W m⁻²) estimated from incoming net solar radiation and air temperature, γ is the temperature-dependent psychrometer constant, and λ is the temperature-dependent latent heat of vaporization.

The supply of water to the plant is simulated as follows. Precipitation enters the soil until the upper layer is saturated, while any additional precipitation is lost as surface runoff. Soil water evaporates from the upper 20 cm, depending on potential evaporation and soil water content. Soil water percolates from the upper to the lower soil layer, until the lower soil layer is saturated, in which case excess water is lost as drainage. Water contained in the lower soil layer can leave the soil as base flow at a given rate. The fraction of water potentially accessible to plants (w_r) depends of the amount of water in the soil, the available water capacity, the distribution of roots, and a maximum transpiration rate (e_{max}). The supply of water to the plant is estimated to equal the product of w_r and e_{max} . If the demand exceeds the supply, plants experience water stress, leading to less canopy conductance, less p_i and hence less A_{nd} .

A_{nd} is equal to Gross Primary Productivity (GPP) minus leaf respiration, and is reduced to Net Primary Productivity (NPP) by subtracting the amount of carbon

respired for the maintenance and growth of sapwood and roots. Maintenance respiration (R_m) is modeled to increase with biomass and temperature as follows:

$$R_m = 0.095218 * \frac{C}{C:N} * g(T), \quad (5.6)$$

where C is the carbon mass of either sapwood or roots, and $C:N$ is the constant ratio of carbon and nitrogen of either sapwood ($C:N = 330$) or roots ($C:N = 29$). g is a dimensionless temperature response function adapted from Lloyd and Taylor (1994):

$$g = \exp \left[308.56 * \left(\frac{1}{56.02} - \frac{1}{T + 46.02} \right) \right], \quad (5.7)$$

where T is the air temperature in the case of sapwood and soil temperature in the case of roots. Growth respiration is estimated to be 25% of the difference of GPP and maintenance respiration.

A constant fraction of NPP is used for reproduction, while the rest is distributed to leaves, sapwood and fine roots satisfying four allometric constraints. When newly produced carbon enters the vegetation pool, part of the sapwood converts to heartwood, and fractions of leaves and roots enter the litter pool. Litter is converted to soil organic carbon at a rate depending on the relative soil water content of the upper soil layer, as well as soil temperature.

Tree mortality occurs via age, stress associated with high temperatures, unsuitable climatic conditions, fire, too low growth efficiency or disturbance. The latter may represent the death of trees related to multiple causes, including windthrow or pests. Daily fire probability increases with decreasing relative soil water content in the upper soil layer. The length of the fire season is the sum of these probabilities, and determines the fractional area affected by fire. Fire occurs in a patch if a randomly generated fraction is below the calculated fire probability, while the number of individuals killed depends on the fire resistance of the respective PFT. The structure of the forest feeds back on the photosynthesis in two ways. Tree height and LAI determine the fraction of photosynthetically active radiation absorbed by foliage (FPAR), and soil moisture is reduced through interception and transpiration. A more detailed model description can be found in Sitch et al. (2003) and Gerten et al. (2007).

5.3.2. Data

Model inputs comprised of daily temperature, precipitation, SW radiation, annual mean $[\text{CO}_2]$ and soil texture. Annual mean observed $[\text{CO}_2]$ from 1765-2005 was obtained from (<http://www.iiasa.ac.at>) and updated for 2006-2009 from (<http://www.esrl>).

noaa.gov/gmd/). Future $[CO_2]$ from 2010 to 2099 for RCP8.5 were downloaded from (<http://www.iiasa.ac.at>). Soil texture was taken from the Harmonized World Soil Database FAO (2012). Climate data consisted of spatially interpolated station observations, reanalysis data, and climate model outputs. Observed temperature and precipitation data covered the period of 1980 to 2009, and were taken from 29 and 70 stations, respectively (Fig. 5.1). These data were provided by Bolivia's National Service of Meteorology and Hydrology (SENAMHI), homogenized by Seiler et al. (2013a), and spatially interpolated by Seiler et al. (2014). Daily incoming net short wave radiation at the surface was obtained from the Modern-Era Retrospective Analysis for Research and Applications (MERRA), a NASA reanalysis for the satellite era using the Goddard Earth Observing System Data Assimilation System Version 5 (GEOS-5) (Rienecker et al., 2011) (<http://disc.sci.gsfc.nasa.gov>). MERRA data covered the period from 1980 to 2009, and were spatially interpolated from $0.67^\circ \times 0.50^\circ$ to $0.25^\circ \times 0.25^\circ$ using a bilinear interpolation technique (van Etten, 2012). Climate change projections of temperature and precipitation were provided by two GCMs participating in the Fifth Phase of the Coupled Model Inter-comparison Project (CMIP5), namely the Coupled Global Climate Model, version 5 (CNRM-CM5) (Voldoire et al., 2012), and the IPSL Coupled Model, version 5 (IPSL-CM5A-LR) (Dufresne et al., 2013). Both models share a similar radiative scheme, but differ in their dynamical core resolution, land surface scheme, and set of physical parameterizations (Cattiaux et al., 2013). They perform about equally well when compared to historic temperature observations from 1961-1990 in Bolivia ($R = 0.92$), but differ when compared to observed precipitation, with R equal to 0.50 for CNRM-CM5 and 0.80 for IPSL-CM5A-LR (Seiler et al., 2013b). Model output data were downloaded from (<http://cmip-pcmdi.llnl.gov/cmip5/>), and bias corrected and statistically downscaled to a resolution of 0.25° following the approach from Piani et al. (2010), which improved the historic temperature and precipitation patterns of both models ($R = 0.95$). As climate change scenario we selected the Representative Concentration Pathway 8.5 (RCP8.5), projecting a future radiative forcing of 8.5 W m^{-2} by 2100 (Moss et al., 2010). The two models CNRM-CM5 and IPSL-CM5A-LR were chosen because of large differences in their projections for RCP8.5, covering a wide range of uncertainty. Annual mean air temperatures are projected to increase by 4°C in the case of CNRM-CM5, and by 6°C in the case of IPSL-CM5A-LR from 1961-1990 to 2070-2099 (Fig. 5.3). Temperature projections are within the likely range of changes projected by an ensemble of 11 CMIP5 GCMs for RCP8.5 in Bolivia (Seiler et al., 2013b). Concerning annual precipitation, CNRM-CM5 projects an increase of about 5% in lowland Bolivia, while IPSL-CM5A-LR projects a decrease of about 17% in the wet, and 26% in the dry forests from 1961-1990 to 2070-2099 (Fig. 5.3). These rainfall scenarios cover a large range of uncertainty, as they exceed the likely ranges of change projected by the previously mentioned ensemble by about 6% on average. Projections of SW radiation were not used given a strong bias of the radiation of CNRM-CM5 and IPSL-CM5A-LR when compared to our MERRA data. Instead we used MERRA data from 1980 to 2009 in a random sequence of years for the period 2010 to 2099. This choice can be justified, given that the projected changes of the median from 1961-1990 to 2070-2099

were only between 1 and 3% (Seiler et al., 2013b).

5.3.3. Experimental design

We initiated the model with a 1000 year spin-up with a constant $[\text{CO}_2]$ of 286 ppm, corresponding to the observed value for 1860. After the spin-up, we forced the model with observed $[\text{CO}_2]$ for 149 years, corresponding to the period from 1861 to 2009, with a $[\text{CO}_2]$ of 387 ppm by 2009. Up to 2009, the model was forced with daily climate observations of temperature, precipitation and incoming solar radiation at the surface from 1980 to 2009. To avoid periodic trends previous to 1980, the data was arranged in a random sequence of years before 1980. A set of model experiments summarized in Tab. 5.1 assessed the impacts of changes in temperature, precipitation and $[\text{CO}_2]$, as well as the importance of the temperature dependence of photosynthesis, respiration and transpirational demand. The role of temperature dependence was quantified by setting temperature-dependent variables to constant values. In the case of photosynthesis we set t_{scal} to a constant value of 0.9 (-), and K_c , K_o and Γ^* to 30, 30,000 and 1.73 Pa respectively, corresponding to values valid for 25°C (Haxeltine and Prentice, 1996). This way A_{nd} was independent of temperature, but still varied with APAR and stomatal conductance. Concerning respiration, we set g to a constant value of 3.2 (-), corresponding to the value valid for 25°C. The role of transpirational demand was assessed by setting E_q equal to 5.6 mm day⁻¹, corresponding to the value valid for 25°C and 250 W m⁻². In some of these model runs we used observed climate data not only up till 2009, but also for the period 2010-2099. We did this by arranging the observed data from 1980 to 2009 in a random sequence of years for the period 2010 to 2099. To study the impacts of rainfall reduction more closely, most experiments were conducted with the climate projections from IPSL-CM5A-LR. These runs were compared to control runs for the period 2070 to 2099. All control runs were based on observed climate data and constant $[\text{CO}_2]$ after 2009 (387 ppm). If the model variables K_c , K_o , Γ^* , g and E_q were set to constant values in the experiments, they were also set constant in the corresponding control runs (Tab. 5.1).

5.4. Results

5.4.1. Changes in carbon pools

The impacts of climate change on c_v differed strongly between runs based on CNRM-CM5 and IPSL-CM5A-LR, and were heavily affected by the potential fertilizing effect of rising $[\text{CO}_2]$. Forcing LPJ-GUESS with temperature and precipitation projections from CNRM-CM5 (RCP8.5), and rising $[\text{CO}_2]$ till 2099, lead to an increase of c_v by about 10 kgC m⁻² in both wet and dry forests (Fig. 5.4). Keeping $[\text{CO}_2]$ at 387 ppm after 2009, caused c_v to remain more or less constant under CNRM-CM5. Forcing LPJ-GUESS with IPSL-CM5A-LR (RCP8.5), and keeping the potential CO₂-fertilization

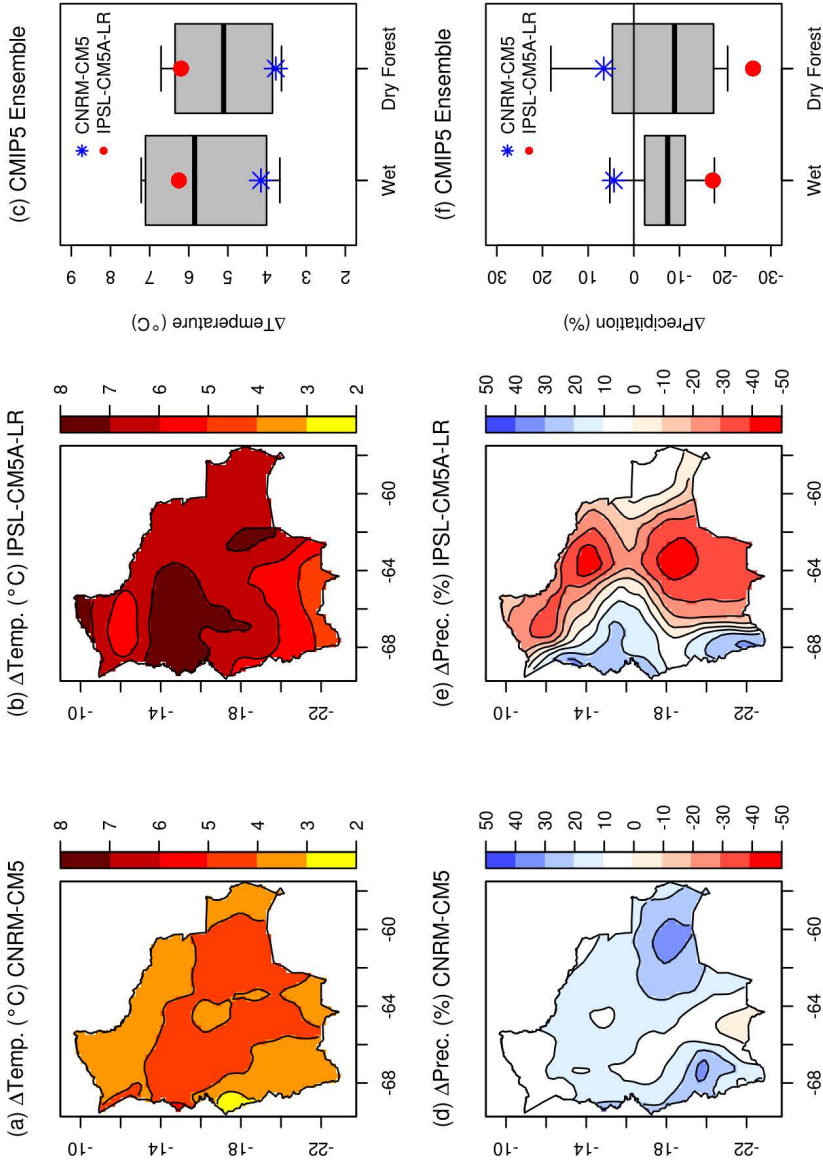


Figure 5.3: Changes in mean annual temperature from 1980-2009 to 2070-2099 as projected by (a) CNRM-CM5 and (b) IPSL-CM5A-LR for RCP8.5 (statistically downscaled and bias-corrected); (c) changes in annual mean temperature from 1961-1990 to 2070-2099 as projected from both models in comparison to changes projected by 11 GCMs in wet and dry forests for RCP8.5 presented in Seiler et al. (2013b). The central line within each box represents the weighted median value of the model ensemble. The top and bottom of each box show the weighted 83rd and 17th percentiles, enclosing 66% of the data, and the top and bottom of each whisker display the weighted 95th and 5th percentiles, respectively. (d) to (f) same as (a) to (c) but for annual precipitation.

Table 5.1: Overview of experiments.

Experiment IDs	Input Variables (2010-2099)			Model Variables (spinup+1980-2099)		
	Temperature	Precipitation	[CO ₂]	K_c, K_o, I^*, t_{scal}	g	E_q
$\Delta T + \Delta P + \Delta CO_2$	CNRM, IPSL	CNRM, IPSL	RCP8.5			
$\Delta T + \Delta P$	CNRM, IPSL	CNRM, IPSL	387 ppm			
ΔP	observed	IPSL	387 ppm			
ΔT	IPSL	observed	387 ppm			
$\Delta T + A_{nd}$	IPSL	observed	387 ppm	constant		
$\Delta T + g$	IPSL	observed	387 ppm		constant	
$\Delta T + E_q$	IPSL	observed	387 ppm			constant
$\Delta T + A_{nd} + g + E_q$	IPSL	observed	387 ppm	constant	constant	constant
$\Delta T + \Delta P + \Delta CO_2$	observed	observed	387 ppm			
$\Delta T + \Delta P$	observed	observed	387 ppm			
ΔP	observed	observed	387 ppm			
ΔT	observed	observed	387 ppm			
$\Delta T + A_{nd}$	observed	observed	387 ppm	constant		
$\Delta T + g$	observed	observed	387 ppm		constant	
$\Delta T + E_q$	observed	observed	387 ppm			constant
$\Delta T + A_{nd} + g + E_q$	observed	observed	387 ppm	constant	constant	constant

off, reduced c_v by 10 kgC m⁻² (46%) in the wet forest, and by 9 kgC m⁻² yr⁻¹ (81%) in the dry forest (Fig. 5.4 and Fig. 5.5; $\Delta T + \Delta P$). In the wet forest, most vegetation loss under IPSL-CM5A-LR could be avoided by the potential CO₂-fertilization effect, while in the dry forest, 62% of c_v was lost regardless of the potential fertilization of CO₂. Vegetation carbon protected by both REDD projects changed correspondingly, ranging from 99% more to 41% less c_v , as summarized in Tab. 5.2. The biggest absolute changes occurred in the transition zone between evergreen forests, deciduous forests and savannas (-15 kgC m⁻²), suggesting an expansion of grasslands in the future, with and without the potential fertilizing effect of CO₂ (Fig. 5.6). Some parts of the cloud forests of the Yungas experienced an increment in c_v due to the projected increase of rainfall in this particular region, as well as due to the positive impact of rising temperatures on GPP for colder climates. Evergreen and deciduous PFTs were about equally affected by the overall reduction of c_v (Fig. 5.7). Grasses on the other hand became more dominant, storing about 25% of the c_v in the dry forest by 2100, when the potential CO₂-fertilization was turned off. Litter and soil pools reduced in both forests, with greater reductions when the potential CO₂-fertilization was turned off (22-49% litter, and 16-34% soil pool).

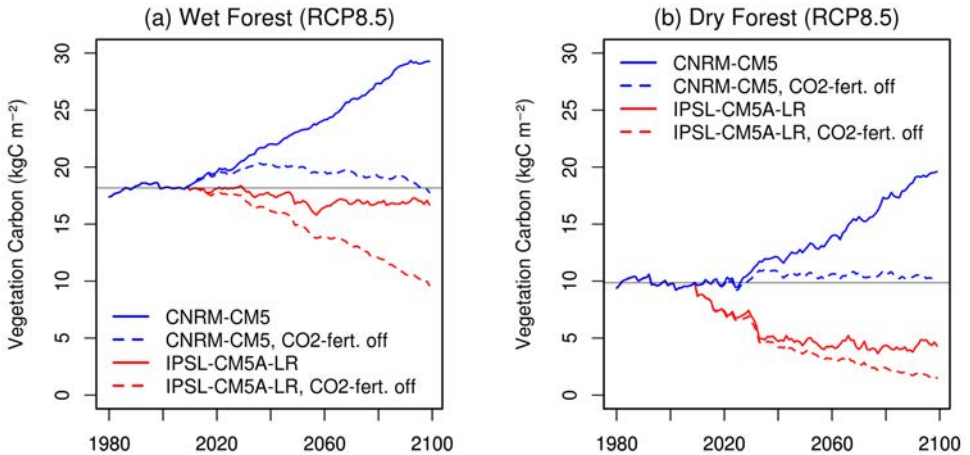


Figure 5.4: Vegetation carbon (c_v) from 1980 to 2099 in (a) wet and (b) dry forests for RCP8.5. The black horizontal line resembles the mean c_v for the period 1980-2009.

5.4.2. Mechanisms of forest loss

We analyzed the mechanisms of forest loss as projected under the dry scenario of IPSL-CM5A-LR (RCP8.5). Using this forcing, both forests were simulated to convert from a carbon sink to a carbon source, as illustrated in Fig. 5.7, where the blue shaded area presents the accumulated net amount of carbon released into the atmosphere.

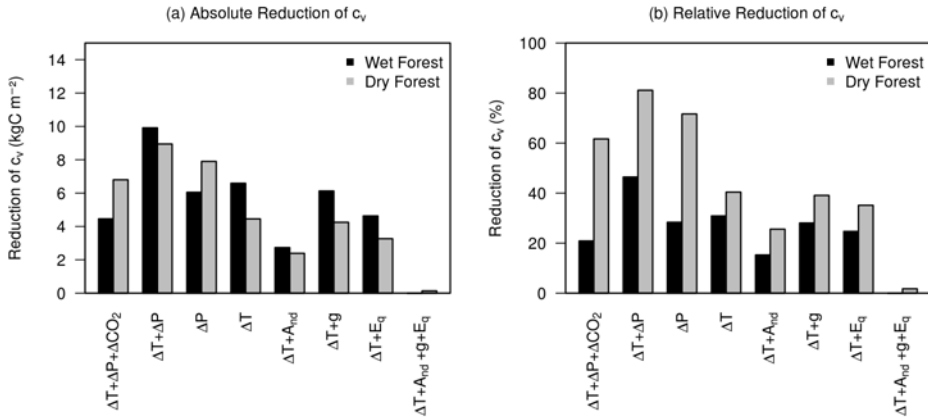


Figure 5.5: Absolute (a) and relative (b) reduction of vegetation carbon (c_v) when forcing the model with climate change projections from IPSL-CM5-LR (RCP8.5) for eight different model runs (x -axis), where ΔT , ΔP and ΔCO_2 are changing temperature, precipitation and $[CO_2]$, and A_{ind} , g and E_q are temperature independent photosynthesis, respiration and equilibrium evaporation, respectively. Changes are calculated for the period 2070 to 2099, and are relative to the same period of the corresponding control runs listed in Tab. 5.1.

By 2099, this accumulated carbon loss was about 1.6 kgC m^{-2} (359 million tC) in the wet forest, and 7.0 kgC m^{-2} (2,041 million tC) in the dry forest when the potential CO_2 -fertilization was turned on, and about 10 kgC m^{-2} in both forest types when the potential CO_2 -fertilization effect was turned off (2320 and 2807 million tC in wet and dry forests, respectively). The following mechanisms were responsible for the conversion from carbon sink to carbon source.

When the potential CO_2 -fertilization effect was turned on, the loss of c_v in the wet forest was driven by an increase in carbon emissions related to autotrophic respiration and fires (Fig. 5.8a). Autotrophic respiration increased due to higher temperatures, while emissions from fires increased due to the reduction of rainfall and hence soil water content (Fig. 5.9, column $\Delta T + \Delta P + \Delta CO_2$). Rising $[CO_2]$ fully compensated the impact of less soil water on photosynthesis. GPP increased due to the combined effect of rising $[CO_2]$ on photosynthesis and water use efficiency. The reduction of stomatal conductance decreased transpiration per unit of LAI, increasing water use efficiency (GPP / transpiration) by 31%. The increase in GPP dampened the effect of rising emissions from autotrophic respiration and fires.

In the dry forest, the conversion from sink to source was mainly related to a reduction of GPP (Fig. 5.8a). The potential CO_2 -fertilization effect was not strong enough to

Table 5.2: Projected mean changes from 1980-2009 to 2070-2099 in vegetation carbon (Δc_v) and the corresponding standard deviations (sd) resulting from spatial variability for both REDD projects, under climate change scenarios projected by two GCMs (RCP8.5), with and without the CO₂-fertilizing effect.

Project	CO ₂	CNRM-CM5		IPSL-CM5A-LR	
		on	off	on	off
CAP-NKM	Δc_v (%)	99	19	-16	-43
	sd (%)	31	22	25	11
Ind. REDD	Δc_v (%)	53	6	-18	-40
	sd (%)	35	22	21	15

compensate for the reduction of soil water, despite an increase of water use efficiency by 38%. GPP per unit of LAI increased nevertheless, due to a shift from trees with a C3 to grasses with a C4 photosynthetic pathway (Fig. 5.9, column $\Delta T + \Delta P + \Delta CO_2$).

When the potential CO₂-fertilization effect was turned off, the loss of c_v was driven by a strong reduction in GPP in both forest types (Fig. 5.8b). While autotrophic respiration per unit of LAI increased due to higher temperatures, total values decreased because of the reduction in biomass (Fig. 5.9, column $\Delta T + \Delta P$).

The described losses of c_v result from the combined effect of rising temperatures and decreasing rainfall. To quantify the importance of each variable, model runs were also conducted for projections in precipitation and temperature separately (IPSL-CM5A-LR, RCP8.5). In the wet forest, less precipitation and higher temperatures reduced c_v equally, while in the dry forest, the impact of precipitation was dominating (Fig. 5.5; ΔP and ΔT). Decreasing rainfall reduced c_v by 6 kgC m⁻² (28%) in the wet and by 8 kgC m⁻² (72%) in the dry forest. The drier conditions led to a significant decrease of the soil water content of the upper soil layer (-20% in the wet, -28% in the dry forest), leading to less transpiration (-13% wet, -23% dry forest), less GPP (-15% wet, -31% dry forest), and more carbon loss through fires in the wet forest (96%) (Fig. 5.9, column ΔP). Evergreen PFTs suffered most from the drier conditions, while the amount of carbon stored in grass, increased. Less precipitation caused an increment of GPP per unit of LAI in the dry forest due to the increasing presence of C4 grasses.

Rising temperatures reduced c_v by 6.6 kgC m⁻² (31%) in the wet forest, and by 4.5 kgC m⁻² (40%) in the dry forest (Fig. 5.5; ΔT). The temperature dependence of A_{nd} contributed most to this reduction, where 16% (14%), of the loss of c_v in the wet (dry) forest was avoided when A_{nd} was forced to be independent from temperature (Fig. 5.5; $\Delta T + A_{nd}$). Setting E_q constant avoided only about 5% of the reduction of c_v in both forest types ($\Delta T + E_q$). The temperature-dependence of respiration showed the lowest impact, avoiding only 3% of the reduction of c_v in the wet, and 1% in the

dry forest when assigning a constant value to g ($\Delta T + g$). The sum of these numbers is smaller compared to the relative carbon loss of the ΔT -experiment, suggesting an important non-linear interaction between A_{nd} , g , and E_q . Soil water content was not significantly affected by rising temperatures (Fig. 5.9, column ΔT).

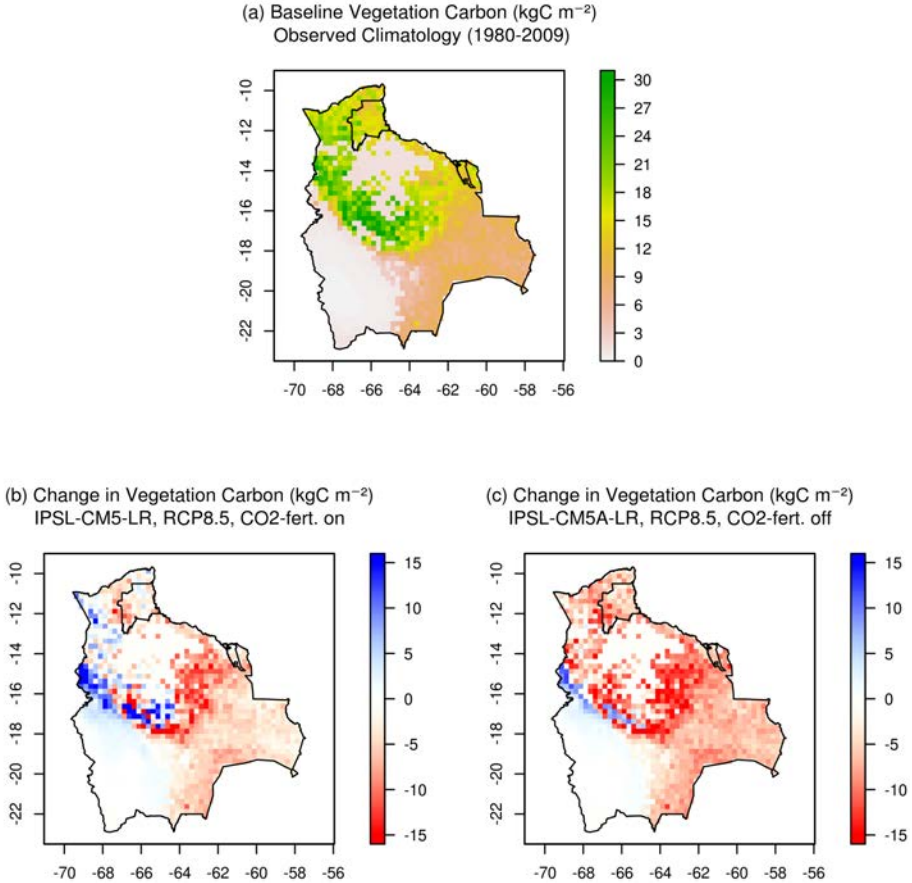


Figure 5.6: (a) Vegetation carbon (c_v) modeled for observed daily climate from 1980 to 2009; change in c_v from 1980-2009 to 2070-2099 for climate change projections simulated by IPSL-CM5-LR (RCP8.5) when the potential CO₂-fertilization effect is (b) included and (c) excluded.

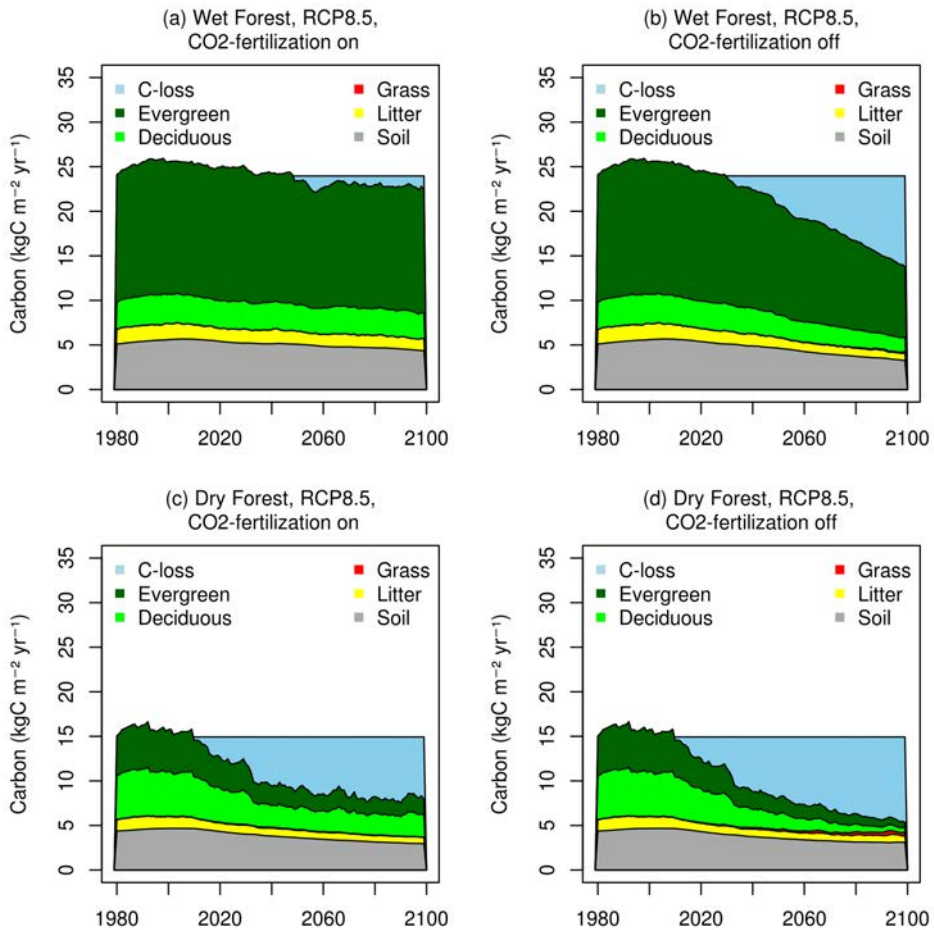


Figure 5.7: Carbon pools and accumulated carbon loss modeled from 1980 to 2100 for climate change projections simulated by IPSL-CM5-LR (RCP8.5) in (a, b) wet forests and (c, d) dry forests when the potential CO₂-fertilization effect is (a, c) included and (b, d) excluded. The blue shaded area presents the accumulated net flux of carbon from vegetation and soils to the atmosphere. This net flux is added on top of the pools.

5.5. Discussion

A regionally adapted version of LPJ-GUESS was implemented for the Bolivian case, and forced with two contrasting climate change projections. Mechanisms of forest loss were evaluated by quantifying carbon fluxes, as well as the individual contributions of $[\text{CO}_2]$, temperature and precipitation. Special attention was paid to the role of temperature-dependent processes, namely photosynthesis, respiration, and the atmospheric demand for transpiration. Impacts ranged from a strong increment to a severe loss of c_v , depending on differences in climate projections, as well as the physiological response to rising $[\text{CO}_2]$. The loss of c_v was primarily driven by a reduction in GPP, and secondarily by enhanced emissions from fires. In the wet forest, less precipitation and higher temperatures equally reduced c_v , while in the dry forest, the impact of precipitation was dominating. The temperature-related reduction of c_v was mainly due to a decrease in photosynthesis, and only to lesser extent because of more autotrophic respiration and less stomatal conductance as a response to an increasing atmospheric demand. Tropical dry forests were simulated to virtually disappear, regardless of the potential fertilizing effect of rising $[\text{CO}_2]$, suggesting a higher risk for forest loss along the drier southern fringe of the Amazon.

The greater sensitivity of the dry forests to climate change as simulated under IPSL-CM5A-LR (RCP8.5) was due to a combination of mechanisms. Similar absolute reductions of c_v in both forests caused a greater relative loss in the dry forest simply because the dry forests stored about 44% less c_v under present day climate. Also, projections in rainfall differed between both forest types, with about 10% less precipitation in the dry forest. These stronger projections, in combination with the dry climatology of the region, created extremely water-limited conditions, which could not be compensated by the fertilizing effect of rising $[\text{CO}_2]$. The large uncertainty of the potential CO_2 -fertilizing effect found for the wet forest is in accordance with previous studies (e.g. Rammig et al., 2010), and should be constrained through observations in the Amazon (Tollefson, 2013). Measurements at FACE sites in temperate forests suggest that an increase of water use efficiency by up to 38% is possible (De Kauwe et al., 2013), indicating that rising $[\text{CO}_2]$ may indeed buffer some of the forest loss. The modeled increase of GPP due to rising $[\text{CO}_2]$ on the other hand is most likely to be exaggerated, and could be limited by including nutrient cycles of nitrogen and phosphorus (Körner, 2006).

The importance of rising temperatures versus precipitation, and the dominating affect of climate change on GPP versus other processes, confirm findings for the LPJ model presented in Galbraith et al. (2010). Our simulations however neglected a possible thermal acclimation of plants (Atkin and Tjoelker, 2003; Medlyn et al., 2002). An acclimation of respiration to rising temperatures however is unlikely to change our results, as respiration played only a minor role (Fig. 5.5). A thermal acclimation of photosynthesis on the other hand could have a substantial impact, as this is one of the main processes of c_v loss. Additional field experiments in tropical forests should address this question by exposing leaves to higher temperatures, as e.g. currently

done in the context of the AMAZALERT project (www.eu-amazalert.org).

We used a random sequence of years of observed climate data to spin-up the model. While this prevented periodic trends, it introduced an artificial interannual climate variability. Also, we used a random sequence of years of observed incoming solar radiation for the period 2010-2099, which allowed us to avoid a discontinuity between observed and simulated radiation. This approach also introduced an artificial inter-annual variability of solar radiation, and caused inconsistencies with temperature and precipitation projections. However, we consider impacts to be minor, as we analyzed changes in carbon pools and fluxes averaged over 30 year periods.

The discharge of rainwater from the Andes to the lowlands and the related flooding of forests (McClain and Naiman, 2008) may present an important supply of moisture, potentially compensating part of the projected precipitation decrease. Also, the true sensitivity of forests to less rainfall may be affected through capillary rise (Romero-Saltos et al., 2005), shallow groundwater tables directly tapped by roots (Miguez-Macho and Fan, 2012), and water withdrawal from greater soil depths through deep roots (Bruno et al., 2006), not included in the model. In the case of LPJ-GUESS, a greater soil depth implies less runoff, as soils are less likely to become saturated. Modeled annual runoff however already systematically underestimated observations by 37% on average when compared to observations from 1984 to 2010 for the upper Mamoré river basin in Puerto Siles (12.80°S, 65.00°W) (Seiler et al., 2014). While this may be related to misrepresentations of soil hydrology in the savannas, we were reluctant to further decrease our runoff by increasing soil depth. Also, a deeper soil

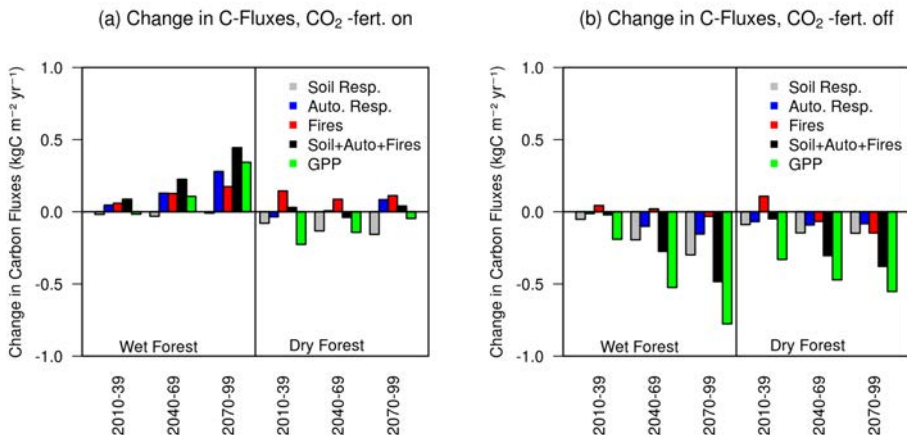


Figure 5.8: Changes in carbon fluxes between 1980-2009 and 2010-2039, 2040-2069, and 2070-2099, for climate change projections simulated by IPSL-CM5-LR (RCP8.5), with (a) and without (b) the potential CO₂-fertilization effect, in wet and dry forests.

layer reduces modeled soil moisture, as rain water is distributed over a larger volume. This in return increases fire probability, and decreases vegetation carbon. Given that groundwater levels may be shallow, increasing the model's soil depth might only lead to improvements if groundwater hydrology is considered. Other processes not included in the model are expected to decrease ecosystem resilience to climate change through enhanced fragmentation (Cochrane and Barber, 2009), such as deforestation, anthropogenic fires and livestock grazing.

Field experiments on the sensitivity of photosynthesis to rising $[\text{CO}_2]$ (Tollefson, 2013) and temperatures in the Amazon are required to reduce the uncertainty of the response of tropical forests to climate change. New model components on land use and subsurface processes related to soil water and nutrients could explore the importance of these factors. Future modeling and experimental studies could pay more attention to carbon dynamics along the southern fringe of the Amazon, where trees are already coping with a stronger rainfall seasonality, and hence more intense periods of drought.

The large uncertainties related to climate change projections and the physiological response to rising $[\text{CO}_2]$ implies an unsure fate of the carbon stocks protected by the two Bolivian REDD projects. An ensemble of about 20 GCMs from the Third Phase of the Coupled Model Inter-comparison Project (CMIP3) reveal an equal likelihood for future increases and decreases of annual rainfall in Bolivia's wet forests for the emission scenarios B1, A1B and A2 (Seiler et al., 2013b). The same study found a likely decrease of rainfall in the region for the emission scenario RCP8.5 only (ensemble of 11 CMIP5 GCMs). The true fertilizing effect of rising $[\text{CO}_2]$ is likely to be somewhere in between the two extreme cases where the effect is either turned on or off. At this stage, it is not possible to judge whether the carbon stocks in both projects will either increase or decrease. In any case, conservation efforts like REDD and protected areas avoid fragmentation from land use and land use change, supporting natural forest structures. As these natural forests are more likely to be resilient to climate change (Cochrane and Barber, 2009), conservation efforts can serve both, climate change mitigation, and adaptation purposes.

To conclude, we assessed the sensitivity of carbon dynamics in the wet and dry tropical forests of Bolivia for two contrasting climate change projections. Drivers of change were evaluated by quantifying the changes in carbon fluxes (GPP, autotrophic and heterotrophic respiration, and fires), as well as the individual contributions of changes in $[\text{CO}_2]$, temperature and precipitation. Special attention was paid to the impacts of temperature on photosynthesis, respiration, and transpirational demand. Our results contribute to the understanding of the mechanisms and uncertainties of climate change induced carbon losses in wet and dry tropical forests. Tropical dry forests were simulated to virtually disappear, regardless of the potential fertilizing effect of rising $[\text{CO}_2]$, suggesting a higher risk for forest loss along the drier southern fringe of the Amazon.

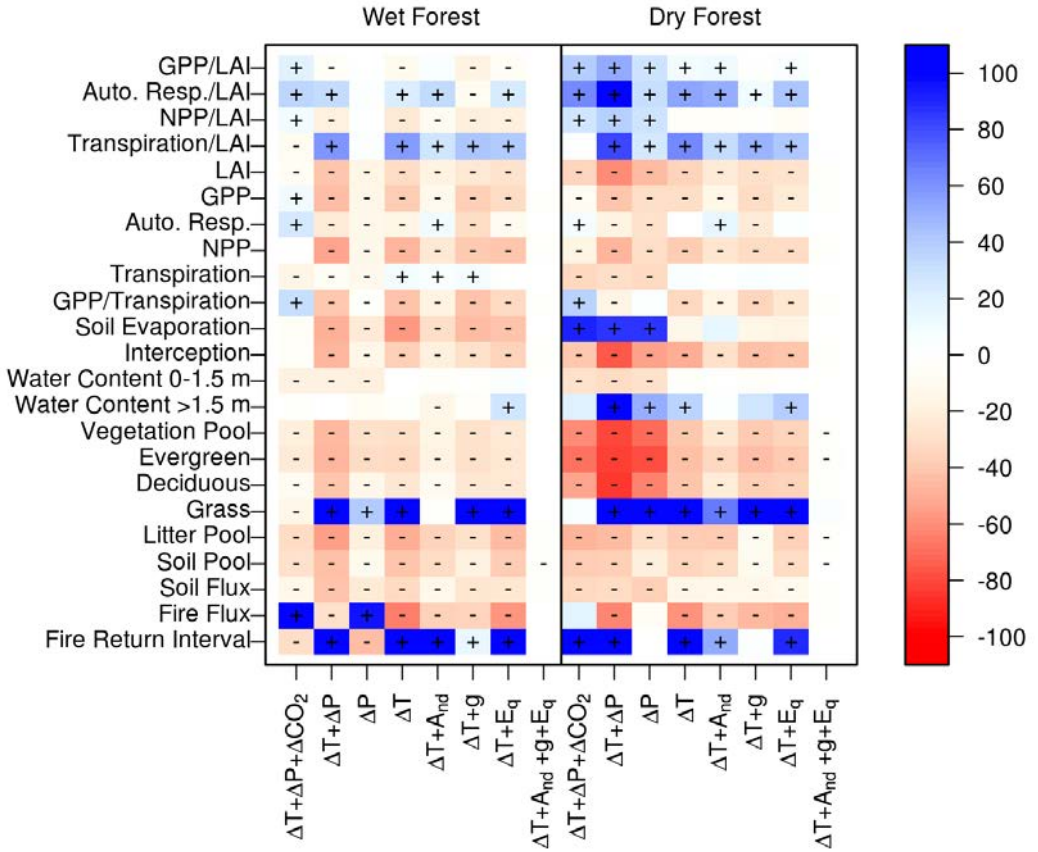


Figure 5.9: Relative changes in model output variables when forcing the model with climate change projections from IPSL-CM5-LR (RCP8.5) for eight different model runs (x -axis), where ΔT , ΔP and ΔCO_2 are changing temperature, precipitation and $[CO_2]$, and A_{nd} , g and E_q are temperature independent photosynthesis, respiration and equilibrium evaporation, respectively. Changes are calculated for the period 2070 to 2099, and are relative to the same period of the corresponding control runs listed in Tab. 5.1. Statistically significant increases and decreases are denoted with (+) and (-), respectively (t -test, 95% probability).

Acknowledgments

This research was supported by the Departmental Pilot Program of Adaptation to Climate Change (PDACC) as well as the project Raising the Alert about Critical Feedbacks between Climate and Land Use Change in Amazonia (AMAZALERT, project number: 282664). PDACC is carried out by the Fundación Amigos de la Naturaleza (FAN) and the departmental government of Santa Cruz, and is funded by the embassy of the Netherlands. AMAZALERT is jointly funded by the European 7th Framework programme and national organizations. The research funding programme LOEWE provided financial support for the simulations, which were carried out at the LOEWE Frankfurt Centre for Scientific Computing (LOEWE-CSC). C.S and T.H. were supported by a WIMEK grant, and the LOEWE initiative, respectively. We thank the Bolivian National Service of Meteorology and Hydrology (SENAMHI) for the provision of the meteorological data. We are grateful for discussions with Dr. Matthew Forrest from the Biodiversity and Climate Research Centre (BiK-F). Dr. Iwan Supit and Wietse H. P. Franssen (Climate Change and Adaptive Land and Water Management, Wageningen University and Research Centre) conducted bias corrections and statistical downscaling for this study.

6. General Discussion

6.1. Research questions

This thesis studies the sensitivity of vegetation dynamics to climate variability and change in Bolivia. The complexity of the problem was approached by integrating information from climate observations, climate projections, biomass measurements, remote sensing data, and a dynamic vegetation model. The first part of the thesis (Chapter 2 and 3) assesses the historic and possible future climates of Bolivia, providing input for the second part (Chapter 4 and 5) that explores vegetation dynamics for recent and possible future climates from a modeling perspective. Four research questions guided us through this process, the answers to which shall be summarized and discussed below.

- *Are there any trends in observed climate means and extremes, and how do they relate to global climate modes?*

Meteorological observations revealed a significant increase in close-to-surface air temperatures at a rate of about 0.1°C per decade, with stronger increases in the Andes and in the dry season (Chapter 2). Rainfall totals increased from 1965 to 1984 (12% in DJF and 18% in JJA) and decreased afterward (-4% in DJF and -10% in JJA), following roughly the pattern of PDO. Total amounts of rainfall, as well as the number of extreme events, were higher during PDO(+), EN, and LN in the lowlands. During austral summer (DJF), EN led to drier conditions in the Andes with more variable precipitation. Trends of climate extremes generally corresponded to trends of climate means. Our estimated temperature trend of 0.1°C per decade is comparable to trends shown by Vuille et al. (2003). Precipitation trends complemented findings from Vuille et al. (2003) and Ronchail (1995), and confirmed relations with PDO as also described by Marengo (2004).

Data homogenization was challenging due to a lacking documentation of changes in measurement instruments, sites, and procedures. Also, the time series of 50 years were too short in order to distinguish between natural climate variability and climate change. Finally, station density was very low in the remote areas of the northern Amazon, Chaco, and Altiplano. The quality of future monitoring and analysis of climate variability and trends would greatly benefit from documenting changes in measurement procedures. We also encourage the installation of additional meteorological stations in all areas with low station density. Our analysis could be extended

by considering time lags between climate modes and measured temperature and precipitation events. Future analysis should try to improve our understanding of the physical relation between global climate modes and the South American Monsoon System (SAMS). Significant progress in this direction has been made by combining observational monitoring data with regional climate modeling experiments in the context of the international research programs MESA (Monsoon Experiment in South America) and VAMOS (Variability of the American Monsoon Systems) (Vera et al., 2006; Marengo et al., 2012). These programs study the nature of SAMS, including its structure, life cycle and variability, as well as impacts of climate change. There is still a great need to better understand the controlling processes, how these processes may vary and change, and how they may interact with different sectors of society. Improved maintenance of the observational networks, and additional investments in human capacity building, model development and computing facilities are crucial ingredients for future advancements in this direction.

The assessment of climate observations provided us with the necessary data base required for our evaluation of GCMs in Chapter 3, as well as with the forcing data used for LPJ-GUESS in Chapter 4 and 5. Also, having detected historic trends allowed us to simulate the sensitivity of LPJ-GUESS to increasing temperatures and decreasing rainfall in Chapter 4. However, our results are not only relevant in the context of this research, but may also contribute to a discussion on disaster risk management, and adaptation to climate change. Increasing temperatures and decreasing rainfall imply challenges for wild fire management, agriculture and water supply. Potential future increases in the variability of ENSO and PDO may increase the occurrence of extreme weather events. These challenges demand a range of adaptation measures, including improved fire management, water management and diversification of crops. Such efforts could be supported through a seasonal forecasting system, which should incorporate statistical relationships between climate modes and extreme weather events.

- *How well do GCMs reproduce the current climate, and what are the projections for the future?*

After analyzing historic climate patterns in Chapter 2, we preceded with the evaluation of 35 different GCMs and 5 emission scenarios in Chapter 3. GCMs revealed an overall cold, wet and positive SW radiation bias and showed no substantial improvement from the CMIP3 to the CMIP5 ensemble for the Bolivian case. Models projected an increase in temperature (2.5 to 5.9°C) and SW radiation (1 to 5%) with seasonal and regional differences. In the lowlands, changes in annual rainfall remained uncertain for CMIP3, while CMIP5 GCMs were more inclined to project decreases (-9%), not only with respect to Bolivia, but also regarding the entire Amazon basin. Both ensembles agreed on less rainfall (-19%) during drier months (JJA, SON), with significant changes in interannual rainfall variability, but disagreed on changes during wetter months (JFM). In the Andes, CMIP3 GCMs tended to less (-9%), while CMIP5 to more (+20%) rainfall during parts of the wet season. Our results confirm numerous findings from Christensen et al. (2007), Soares and Marengo (2009), Urrutia and Vuille (2009) and Marengo et al. (2010), including (i) a cold and wet bias for

the Andean region, (ii) stronger temperature increases during the austral winter, (iii) great uncertainty associated with the directional change of annual rainfall, and (iv) a tendency for an intensification of the hydrological cycle for CMIP3 GCMs, with more rainfall during the wet season. The lacking consensus on annual rainfall projections among CMIP3 climate models has been documented previously (Christensen et al., 2007). A recent comparison of precipitation projections from CMIP3 and CMIP5 models for the Amazon highlights a weaker consensus on increased precipitation during the wet season, but a stronger consensus on a more intense dry season, supporting our findings (Joetzjer et al., 2013).

The horizontal resolution of GCMs is too coarse to properly represent processes in mountainous regions. High resolution regional climate modeling is required for improving simulations in Bolivia. Forcing a regional climate model with multiple lateral boundary conditions however is very resource intensive, leading to very few model runs currently available (e.g. Soares and Marengo, 2009; Urrutia and Vuille, 2009; Marengo et al., 2010). Most of these regional climate change scenarios are based on very few lateral boundary conditions (mainly HadAM3), limiting their robustness in a region with little agreement on the directional change of rainfall. Our study can therefore be used to interpret the existing high-resolution scenarios in the context of the overall uncertainty arising from both CMIP3 and CMIP5 ensembles. Also, our model ranking provides useful information for future downscaling and climate change impact studies, enabling users to make informed choices on suitable forcing data. The top three CMIP3 models for Bolivia were MRI-CGCM2.3.2, IPSL-CM4, and UKMO-HadCM3, while the top three CMIP5 models were MIROC-ESM, IPSL-CM5A-LR, and INM-CM4.

The great uncertainty of rainfall projections implies that future climate change impact studies will have to rely on forcing data presenting both, increasing and decreasing rainfall scenarios. Adaptation measures should be designed to satisfy immediate needs, and be robust under both scenarios. The implications of climate change for ecosystems are addressed in Chapter 5. Future studies on climate change projections for Bolivia could shift their focus from the evaluation of surface variables to the atmospheric circulation, including the thermal Chaco low, the upper-level Bolivian high, the low level jet east of the Andean slopes, and the South Atlantic Convergence Zone. In addition, GCMs should also be evaluated with respect to the relation between climate modes and extreme weather events in Bolivia. Such a comprehensive analysis might allow us to estimate the likelihood of the directional change on physical reasoning, rather than on pure ensemble statistics.

- *Can we reproduce vegetation dynamics realistically for current climate conditions?*

We adapted the dynamic vegetation model LPJ-GUESS to simulate present day potential vegetation in Chapter 4 as a baseline for our climate change impact assessment presented in Chapter 5. Results were compared to biomass measurements from 21 new, and 798 previous plots, as well as to remote sensing data. Using regional param-

eter values for allometric relations, specific leaf area, wood density and disturbance interval, a realistic transition from the evergreen Amazon to the deciduous dry forest was simulated. This transition coincided with threshold values for precipitation (1400 mm yr⁻¹) and water deficit (-830 mm yr⁻¹), beyond which leaf abscission became a competitive advantage. The model reproduced reasonable values for seasonal leaf abscission, vegetation carbon, and forest fires. Modeled GPP and remotely sensed NDVI showed that dry forests were more sensitive to rainfall anomalies than wet forests. Modeled GPP was positively correlated to ENSO in the Amazon, and negatively correlated to consecutive dry days. Decreasing rainfall trends were simulated to decrease GPP in the Amazon. Our biomass measurements in Bolivia's Amazon and Chiquitania were comparable to values reported by Dauber et al. (2000), Mostacedo et al. (2009) and Baker et al. (2004). The large amounts of vegetation carbon measured in the cloud forests contradicted findings from Girardin et al. (2010) and Moser et al. (2011), for reasons discussed in Chapter 4. The strong sensitivity of LPJ-GUESS and other DGVMs to rising [CO₂] has been reported previously, especially under tropical, but also drier climates (Hickler et al., 2008).

Regional parameter values of SLA and wood density were measured in a single site located in the Chiquitania, where shade tolerant and intolerant evergreen and deciduous tree species were present. While this allowed us to obtain values from trees growing under the same environmental conditions, values are not necessarily representative for other forests in Bolivia. Also, choosing a random order of years for the spin-up may have exaggerated the true interannual climate variability. Further, we evaluated the simulated interannual variability of GPP with remotely sensed NDVI from 1981 to 2006. This approach has some limitations, given that NDVI saturates for high LAI (Asner et al., 2004), and that the time period analyzed is short when compared to time scales of tree age and forest disturbances. Finally, tropical savannas could not be reproduced by the model, as one of the main mechanisms, seasonal flooding and its impacts on growth, was missing in the model. Additional field measurements in other forest types could inform on the variability of regional parameter values applied in this study. Our regional value for disturbance intervals could be refined from remote sensing data (Chambers et al., 2013), or be replaced by a physically based approach (Lagergren et al., 2012). The significance of the artificial variability introduced by our spinup could be tested by running the model with a de-trended time series of years in chronological order. Schöngart et al. (2004) found significant relations between tree ring width and precipitation anomalies in the Amazon. Stable isotopes in tree rings can further help to assess the long-term physiological response of rising [CO₂] to water use efficiency. Results for tropical trees suggest an increasing water use efficiency due to less stomatal conductance related to rising [CO₂] (Brienen et al., 2011; Nock et al., 2011). Similar analyses for the Bolivian case would be of great value for model evaluation purposes, and could complement our short-term evaluation based on remote sensing data. Finally, our research could be extended by developing a new LPJ-GUESS module for water logging, which would allow us to dynamically model the seasonally flooded savannas of Beni.

The regional application and evaluation of LPJ-GUESS under present-day climate is the basis for our climate change impact assessment presented in Chapter 4. We conclude that LPJ-GUESS is sufficiently flexible to make it a suitable modeling framework for regional studies on vegetation dynamics. The success of such a regional application is likely to depend on the incorporation of regional parameter values. Special attention should be paid to the disturbance interval, which is both, difficult to estimate, and highly influential. Applying one fixed value on a global scale is hardly justifiable.

- *How sensitive are forests to climate change, and what are the main drivers of change?*

Using the same model configuration, the impacts of climate change were then assessed for two contrasting projections in Chapter 5. The impacts of climate change differed strongly between runs based on the wet projection from CNRM-CM5, and the dry projection from IPSL-CM5A-LR, and were heavily affected by the potential fertilizing effect of rising $[\text{CO}_2]$. Vegetation carbon increased under the wet projections from CNRM-CM5 when the potential CO_2 -fertilizing effect was included. Turning this effect off caused c_v to remain more or less constant. Forcing LPJ-GUESS with the dry projection (IPSL-CM5A-LR), and keeping the potential CO_2 -fertilization off, substantially reduced c_v in both forests. Only in the wet forest could most of this vegetation loss be avoided by the potential CO_2 -fertilization effect. Vegetation carbon protected by both carbon offset projects changed correspondingly, ranging from 99% more to 41% less c_v . The loss of c_v was primarily driven by a reduction in GPP, and secondarily by enhanced emissions from fires. In the wet forest, less precipitation and higher temperatures equally reduced c_v , while in the dry forest, the impact of precipitation was dominating. The temperature-related reduction of c_v was mainly due to a decrease in photosynthesis, and only to lesser extent because of more autotrophic respiration and less stomatal conductance as a response to an increasing atmospheric demand. Tropical dry forests were simulated to virtually disappear, regardless of the potential fertilizing effect of rising $[\text{CO}_2]$, suggesting a higher risk for forest loss along the drier southern fringe of the Amazon. The importance of rising temperatures versus precipitation, and the dominating affect of climate change on GPP versus other processes, confirm findings for the LPJ model presented in Galbraith et al. (2010). The large uncertainty of the potential CO_2 -fertilizing effect found for the wet forest is in accordance with previous studies (e.g. Rammig et al., 2010).

Our experiments neglected numerous processes which could both enhance and decrease the resilience of tropical forests to climate change. The reduction of precipitation as projected by some GCMs may be compensated by the lateral transport of water from the Andes to the lowlands (McClain and Naiman, 2008), leading to annual inundations with extensions up to 92,100 km² in the Bolivian flood plains of Moxos (Melack and Hess, 2011). Capillary rise (Romero-Saltos et al., 2005), shallow ground water tables directly tapped by roots (Miguez-Macho and Fan, 2012), water withdrawal from greater soil depths through deep roots (Bruno et al., 2006), as well as water storage in the stem of some species (e.g. *Chorisia speciosa*), could further

increase the resilience of tropical forests to climate change. A possible thermal acclimation of photosynthesis could avoid a significant part of the simulated carbon loss. However, lacking observational data makes it difficult to estimate the importance of these processes for Bolivian forests. Other processes not included in the model are expected to decrease ecosystem resilience through enhanced fragmentation (Cochrane and Barber, 2009), such as deforestation, anthropogenic fires and livestock grazing. Also, the fertilizing effect of rising $[\text{CO}_2]$ was most likely exaggerated, as LPJ-GUESS does not account for the limitations of nutrients in the soil (Körner, 2006). Finally, the simulated large increase in water use efficiency due to rising $[\text{CO}_2]$ could in reality be limited by the plant's phenotypic plasticity (de Boer et al., 2011). LPJ-GUESS has the great potential to be extended with modules of either regional or global importance. On a global scale it will be essential to incorporate nutrients such as nitrogen and phosphorus into the model. For the Bolivian case we also recommend including the lateral transport of water from the Andes, as well as water logging. Anthropogenic fires and land use could further add more realism.

Our results demonstrate that a climate change induced forest dieback is indeed possible in the Bolivian case. The biggest absolute changes are simulated to occur in the transition zone between wet and dry tropical forest, while the forests along the Andean slopes were simulated to be less affected. A partial loss of carbon stocks protected by both Bolivian REDD projects is also possible. Results are subjects to uncertainties discussed above, and highly depend on the directional change of future annual rainfall. The possibility of a forest dieback poses a serious threat to biodiversity, as well as rural livelihoods. Implications for adaptation and mitigation measures are discussed in the following section.

6.2. Climate change adaptation and mitigation measures for Bolivian forests

Adaptation measures for Bolivian forests should prioritize actions related to deforestation, fire management, grazing, and water resource management. A reduction of deforestation will help to maintain intact, and hence presumably more resilient ecosystems. Key regions of forest protection should include the Andean slopes, ecological transition zones, and riverine zones. The forests of the Andean slopes play an important role in the regulation of the hydrological cycle of the region (Seiler and Moene, 2011). If annual precipitation will increase, Andean forests may help to prevent major floods further downstream. In the contrary dry case, the same forests may provide an essential source of water during the dry season. Additional motives to protect especially these forests are their extraordinary biodiversity (Ibisch and Mérida, 2003), and their important function as a bio-corridor (Ibisch et al., 2007). Furthermore, these forests were simulated to be less affected by climate change compared to other regions, suggesting that conservation efforts are likely to be effective despite climate change. A possible construction of a highway through these forests crossing the Indigenous

Territory of the Isiboro Sécure National Park (TIPNIS) would be highly counteractive. The second regional focus of forest conservation should support maintaining broad species migration corridors in transition zones, especially between the wet and dry forests (Chiquitania), where current and future pressures are highest. Species in these forests are likely to be more affected by climate change, as they are closer to the extreme limits of their ecological requirements (Killeen et al., 2006). These forests also experienced biggest absolute losses of carbon in our climate change impact simulations, and are expected to be most affected by future deforestation (Müller et al., 2012). A third regional focus of conservation should include the natural vegetation along riverine zones, as they support flood prevention, humid refugia, and migration corridors (Malhi et al., 2008).

Land use change and forest fires are strongly linked in Bolivia (Rodriguez, 2012a), as fires are commonly used to clear land for agriculture and livestock farming. Climate change projections tend towards a decline in precipitation during the dry season, provoking more forest fires as also shown in our simulations (Chapter 5). Since man-made forest fires already pose a severe threat to Bolivian ecosystems, improved fire management is an essential key stone in adapting Bolivian forests to climate change. Another important driver of forest degradation in Bolivia is live stock grazing (Müller et al., 2013). With an estimated total of about 7 million head of cattle (Urioste, 2012), extensive grazing practices heavily affect Bolivian dry forests through overgrazing (Jarvis et al., 2010). The expansion of the agricultural frontier (Killeen et al., 2007) in combination with a current, as well as projected intensification of the dry season (Chapter 2 and 3), presents also serious challenges to the management of hydrological resources.

Current deforestation in Bolivia is mainly driven by the expansion of mechanized agriculture for the production of soy beans (Hecht, 2005; Müller et al., 2012). Conditions favoring this development include the access to cheap land through nontransparent markets, the absence of effective environmental control, and lacking taxes on land and agro-industrial export earnings, all leading to the foreign monopolization of land (Urioste, 2012). Strong political will and enhanced public awareness will be required to turn these conditions around. Granting collective property titles to indigenous communities, as well as improved law enforcement, and higher penalties for illegal deforestation, may further help to dampen the expansion of the agricultural frontier. Further policy options to reduce deforestation and forest degradation in Bolivia are discussed in Müller et al. (2013). Improvements for water management in Bolivia are proposed by Cochrane et al. (2007), and should lead to a regulation of water extraction based on a hydrological monitoring system. Fire management should be supported by the recently developed early warning system for forest fires in Bolivia [<http://incendios.fan-bo.org>]. The current system is based on remote sensing data and meteorological observations, and could be improved by including terrestrial water storage observations from the Gravity Recovery and Climate Experiment (GRACE), as proposed by Chen et al. (2013). This information needs to be applied locally to coordinate fire activities in the region, as e.g. applied in the context of the Depart-

mental Pilot Program of Adaptation to Climate Change (PDACC) in the Chiquitania (Rodríguez, 2012b). Such activities should be expanded throughout Bolivia's lowlands with the support of the departmental and national government. Forest carbon projects could further push for conservation, while promoting sustainable forest use for indigenous communities. Since the Bolivian government opposes the carbon credit trading scheme proposed for REDD under the United Nations Framework Convention on Climate Change (UNFCCC), Bolivian carbon credits could be sold on voluntary markets instead. Our simulations show that there is a certain risk for a partial loss of carbon stocks due to climate change. The potential for non-permanence needs to be addressed in climate negotiations, e.g. by assigning a limited lifespan to carbon credits, as already the case for the clean development mechanism (UNFCCC, 2005). Additional efforts for reducing deforestation and forest degradation need to be undertaken by the international community. Land use change is increasingly driven by international trade, and the distant impacts of consumption in industrialized countries (Meyfroidt et al., 2013). These nations should therefore assume a leading role in promoting sustainability in global market trading through mechanisms such as ecolabeling, and boycotting commodities that do not meet minimum sustainability criteria.

6.3. Outlook

We studied the sensitivity of tropical forests to climate variability and change in Bolivia by integrating information from climate observations, climate projections, biomass measurements, remote sensing data, and a dynamic vegetation model. While this approach allowed us to develop a detailed picture for a specific region, it deviated our attention from processes of global scale. Climate variability has regional impacts, but is driven by anomalous circulations in oceans and atmosphere. Statistical relations presented in this thesis only indicated the importance of climate modes, but did not unravel the underlying mechanisms. Also, our analysis of CMIP3 and CMIP5 climate models described biases and uncertainties in detail, but did not further explore the corresponding processes. Furthermore, our experiments neglected any climate-vegetation feedbacks, as LPJ-GUESS was coupled off-line to climate model output data. The physics of teleconnections, biases, and climate-vegetation feedbacks can be studied more consistently when integrating DGVMs into climate models, as has been done for numerous models participating in CMIP5 (e.g. GFDL-ESM2G and GFDL-ESM2M (Dunne et al., 2012), HadGEM2-ES (Collins et al., 2011), INMCM4 (Volodin et al., 2010), MIROC-ESM (Watanabe et al., 2011), MPI-ESM-LR (Giorgetta et al., 2013)). These models, also referred to as Earth System Models (ESMs), can be driven by concentrations or by emissions. In concentration driven experiments, the carbon fluxes between land, ocean and atmosphere do not feed back to the climate system, as concentrations are prescribed. In emission driven experiments, the carbon cycle is fully coupled, and changes in fluxes feed back to the entire climate system. Friedlingstein et al. (2013) quantified this feedback by conducting concentration and

emission driven experiments for eleven CMIP5 models for the RCP8.5 scenario. Seven out of eleven models simulated an enhancement of $[\text{CO}_2]$ (on average by 44 ppm, 985 ± 97 ppm by 2100) and radiative forcing (by 0.25 W m^{-2}) when the carbon cycle was interactively coupled, suggesting that at global scale, the feedback is fairly small in relation to the impact of anthropogenic emissions. This suggests that our results may not change substantially under emission driven experiments.

Further advancements in earth system modeling include the incorporation of the nitrogen cycle in some vegetation models (CLM4CN (Oleson et al., 2010), OCN (Zaehle and Friend, 2010), SDGVM (Woodward and Lomas, 2004), TRIFFID (Cox, 2001), LPJ-GUESS (Fleischer et al., 2013)). The inclusion of the nitrogen cycle is simulated to reduce the future uptake of carbon by the vegetation, as nitrogen limits photosynthesis (IPCC, 2013). The coupling of the nitrogen and phosphor cycle in the land surface model JSBACH (Raddatz et al., 2007), is shown to reduce land carbon uptake by 25% compared to simulations without nutrients (Goll et al., 2012). The incorporation of nutrients in vegetation models is still in its early stage, and will have to be constrained through more observational data.

While important improvements are being made in the development of DGVMs, the impact of climate change on Bolivia's forests will greatly depend on the very uncertain directional change of precipitation. A better understanding of the physical mechanisms may therefore be required to interpret, and possibly reduce this uncertainty. Chadwick et al. (2013) decomposed CMIP5 precipitation for the tropics, and found two major and opposing processes related to changes in tropical precipitation. On the one hand, precipitation increases because higher temperatures allow more specific humidity in the troposphere in accordance with the Clausius–Clapeyron relationship. On the other hand, models project a weakening of the tropical circulation, decreasing divergence and convection, and hence precipitation. This weakening can occur because total tropospheric column warming is greater in climatological descent regions than in ascent regions, reducing the pressure gradient between both regions (Ma et al., 2012). Such a weakening can already be detected by observations (Vecchi et al., 2006), and is a robust feature of climate change projections from CMIP3 (Vecchi and Soden, 2007) and CMIP5 models (Chadwick et al., 2013). Both precipitation changes are of similar magnitude, canceling each other out in large parts of the tropics. Hence, smaller precipitation components end up determining the final pattern of change. This component was identified as spatial shifts in convective mass flux associated with SST pattern responses to enhanced greenhouse gas emissions (Chadwick et al., 2013). A better understanding between SST biases and precipitation projections could therefore help to constrain the current uncertainty of rainfall projections over the Amazon. The vegetation modeling community would greatly benefit from such insights, allowing for more informed choices on reasonable forcing data. Otherwise, large uncertainties will remain for climate change impact assessments in the Amazon, despite extensive model improvements.

A. Appendix

A.1. Climate Indices

The following tables provide definitions and example values of climate indices.

Table A.1: Temperature-related climate indices (Abs. = absolute, Thr. = threshold, Perc. = percentile based, Dur. = duration, and O. = others). AP and LL are values from two example stations from the Altiplano (El Alto, La Paz) and the lowlands (El Trompillo, Santa Cruz de la Sierra), averaged from 1960 to 2009.

Cat	ID	Indicator name	Definition	Unit	AP	LL
Abs.	txx	Max Tmax	Monthly maximum value of daily maximum T	°C	20	37
	tnx	Max Tmin	Monthly maximum value of daily minimum T	°C	5	25
	txn	Min Tmax	Monthly minimum value of daily maximum T	°C	6	12
Thr.	tnn	Min Tmin	Monthly minimum value of daily minimum T	°C	-10	6
	fd0	Frost days	Annual count when Tmin < 0°C	Days	190	0
	id0	Ice days	Annual count when Tmax < 0°C	Days	0	0
Perc.	su25	Summer days 25	Annual count when Tmax > 25°C	Days	0	296
	su30	Summer days 30	Annual count when Tmax > 30°C	Days	0	166
	tr20	Tropical nights	Annual count when Tmin > 20°C	Days	0	194
Dur.	tn10p	Cool nights	Tmin < 10th percentile	Days	7	9
	tx10p	Cool days	Tmax < 10th percentile	Days	8	10
	tn90p	Warm nights	Tmin > 90th percentile	Days	20	14
	tx90p	Warm days	Tmax > 90th percentile	Days	12	11
	gsl	Growing season length	In SH, days between first span after 1st Jul of >5 days with Tmean > 5°C and first span after 1st Jan of >5 days with Tmean < 5°C.	Days	283	364
O.	wsdi	Warm-spell duration	Days with >5 consec. days when Tmax > 90th perc.	Days	7	6
	csdi	Cold-spell duration	Days with >5 consec. days when Tmin < 10th perc.	Days	1	2
	dtr	Diurnal temperature range	Monthly mean difference between Tmax and Tmin	°C	15	10

Table A.2: Precipitation-related climate indices. AP and LL are values from two example stations from the Altiplano (El Alto, La Paz) and the lowlands (El Trompillo, Santa Cruz de la Sierra), averaged from 1960 to 2009. PRCP 5 precipitation.

Cat	ID	Indicator name	Definition	Unit	AP	LL
Abs.	rx1day	Max 1-day prec.	Monthly maximum 1-day PRCP	mm day ⁻¹	31	102
	rx5day	Max 5-day prec.	Monthly maximum consec. 5-day PRCP	mm day ⁻¹	66	154
Thr.	r10	No. days > 10 mm day ⁻¹	Annual count of days when PRCP \geq 10mm	Days	19	40
	r20	No. days > 20 mm day ⁻¹	Annual count of days when PRCP \geq 20mm	Days	4	24
Perc.	r95p	Very wet days	Annual total PRCP when RR > 95th percentile	mm	117	308
	r99p	Extremely wet days	Annual total PRCP when RR > 99th percentile	mm	37	91
Dur.	cdd	Consecutive dry days	Maximum no. of consecutive days with RR < 1mm	Days	59	30
	cwd	Consecutive wet days	Maximum no. of consecutive days with RR \geq 1mm	Days	10	7
Other	sdii	Simple daily intensity index	Annual total PRCP divided by the number of wet days (defined as PRCP \geq 1mm) in the year	mm day ⁻¹	6	16
	preptot	Annual total wet-day PRCP	Annual total PRCP in wet days (RR \geq 1mm)	mm yr ⁻¹	608	1433

Bibliography

- Ahlström, A., B. Smith, J. Lindström, M. Rummukainen, and C. Uvo, 2013: GCM characteristics explain the majority of uncertainty in projected 21st century terrestrial ecosystem carbon balance. *Biogeosciences*, **10** (3), 1517–1528.
- Alexander, L., et al., 2006: Global observed changes in daily climate extremes of temperature and precipitation. *J. geophys. Res.*, **111** (D05109), 22.
- Andreae, M., et al., 2002: Biogeochemical cycling of carbon, water, energy, trace gases, and aerosols in Amazonia: The LBA-EUSTACH experiments. *Journal of Geophysical Research: Atmospheres (1984–2012)*, **107** (D20), LBA–33.
- Arino, O., J. Perez, V. Kalogirou, P. Defourny, and F. Achard, 2010: GlobCover 2009.
- Asner, G. P., D. Nepstad, G. Cardinot, and D. Ray, 2004: Drought stress and carbon uptake in an Amazon forest measured with spaceborne imaging spectroscopy. *Proceedings of the National Academy of Sciences of the United States of America*, **101** (16), 6039–6044.
- Asner, G. P., A. R. Townsend, and B. H. Braswell, 2000: Satellite observation of El Nino effects on Amazon forest phenology and productivity. *Geophysical research letters*, **27** (7), 981–984.
- Atkin, O. K. and M. G. Tjoelker, 2003: Thermal acclimation and the dynamic response of plant respiration to temperature. *Trends in plant science*, **8** (7), 343–351.
- Auger, I. E. and C. E. Lawrence, 1989: Algorithms for the optimal identification of segment neighborhoods. *Bulletin of mathematical biology*, **51** (1), 39–54.
- Baker, I., L. Prihodko, A. Denning, M. Goulden, S. Miller, and H. Da Rocha, 2008: Seasonal drought stress in the Amazon: Reconciling models and observations. *Journal of Geophysical Research: Biogeosciences (2005–2012)*, **113** (G1).
- Baker, T. R., et al., 2004: Increasing biomass in Amazonian forest plots. *Philosophical Transactions of the Royal Society of London. Series B: Biological Sciences*, **359** (1443), 353–365.
- Behrenfeld, M. J., et al., 2001: Biospheric primary production during an ENSO transition. *Science*, **291** (5513), 2594–2597.
- Berry, J. and O. Bjorkman, 1980: Photosynthetic response and adaptation to temperature in higher plants. *Annual Review of Plant Physiology*, **31** (1), 491–543.

- Boulanger, J., et al., 2010: A Europe–South America network for climate change assessment and impact studies. *Climatic change*, **98** (3), 307–329.
- Bourrel, L., L. Phillips, and S. Moreau, 2009: The dynamics of floods in the Bolivian Amazon Basin. *Hydrological Processes*, **23** (22), 3161–3167.
- Bradley, R., M. Vuille, H. Diaz, and W. Vergara, 2006: Threats to water supplies in the tropical Andes. *Science*, **312** (5781), 1755–1756.
- Brienen, R. J., W. Wanek, and P. Hietz, 2011: Stable carbon isotopes in tree rings indicate improved water use efficiency and drought responses of a tropical dry forest tree species. *Trees*, **25** (1), 103–113.
- Brienen, R. J. and P. A. Zuidema, 2005: Relating tree growth to rainfall in Bolivian rain forests: a test for six species using tree ring analysis. *Oecologia*, **146** (1), 1–12.
- Bruno, R. D., H. R. Da Rocha, H. C. De Freitas, M. L. Goulden, and S. D. Miller, 2006: Soil moisture dynamics in an eastern Amazonian tropical forest. *Hydrological Processes*, **20** (12), 2477–2489.
- Cairns, M. A., S. Brown, E. H. Helmer, and G. A. Baumgardner, 1997: Root biomass allocation in the world’s upland forests. *Oecologia*, **111** (1), 1–11.
- Cardona, O. D. and M. L. Carreño, 2011: Updating the Indicators of Disaster Risk and Risk Management for the Americas. *IDRiM Journal*, **1** (1).
- Castanho, A., M. Coe, M. Costa, Y. Malhi, D. Galbraith, and C. Quesada, 2013: Improving simulated Amazon forest biomass and productivity by including spatial variation in biophysical parameters. *Biogeosciences*, **10** (4), 2255–2272.
- Cattiaux, J., H. Douville, A. Ribes, F. Chauvin, and C. Plante, 2013: Towards a better understanding of changes in wintertime cold extremes over Europe: a pilot study with CNRM and IPSL atmospheric models. *Climate Dynamics*, **40**, 2433–2445.
- CBD, 2001: Global Biodiversity Outlook. Secretariat of the Convention on Biological Diversity.
- Chadwick, R., I. Boutle, and G. Martin, 2013: Spatial Patterns of Precipitation Change in CMIP5: Why the Rich Do Not Get Richer in the Tropics. *Journal of Climate*, **26** (11), 3803–3822.
- Chambers, J. Q., et al., 2013: The steady-state mosaic of disturbance and succession across an old-growth Central Amazon forest landscape. *Proceedings of the National Academy of Sciences*, **110** (10), 3949–3954.
- Chen, Y., I. Velicogna, J. S. Famiglietti, and J. T. Randerson, 2013: Satellite observations of terrestrial water storage provide early warning information about drought and fire season severity in the Amazon. *Journal of Geophysical Research: Biogeosciences*.

- Chiang, J. C. and D. J. Vimont, 2004: Analogous Pacific and Atlantic Meridional Modes of Tropical Atmosphere-Ocean Variability*. *Journal of Climate*, **17** (21), 4143–4158.
- Christensen, J., et al., 2007: Regional climate projections. *Climate Change, 2007: The Physical Science Basis. Contribution of Working group I to the Fourth Assessment Report of the Intergovernmental Panel on Climate Change*, University Press, Cambridge, Chapter 11, 847–940.
- Cleveland, W. S. and S. J. Devlin, 1988: Locally weighted regression: an approach to regression analysis by local fitting. *Journal of the American Statistical Association*, **83** (403), 596–610.
- Cochrane, M. A. and C. P. Barber, 2009: Climate change, human land use and future fires in the Amazon. *Global Change Biology*, **15** (3), 601–612.
- Cochrane, T. A., O. Rosales, and T. Killeen, 2007: Agua, gas y agroindustria: gestión sostenible de agua para riego agrícola en Santa Cruz, Bolivia.
- Collins, M., et al., 2010: The impact of global warming on the tropical Pacific Ocean and El Niño. *Nature Geoscience*, **3** (6), 391–397.
- Collins, W., et al., 2011: Development and evaluation of an Earth-system model—HadGEM2. *Geoscientific Model Development Discussions*, **4** (2), 997–1062.
- CONARADE, 2010: Plan de Atención de la Emergencia humanitaria y agropecuaria por sequía para el chaco Boliviano. Tech. rep., Estado Plurinacional de Bolivia, 1–50 pp.
- Cox, P. M., 2001: Description of the TRIFFID dynamic global vegetation model. Tech. rep., Technical Note 24, Hadley Centre, United Kingdom Meteorological Office, Bracknell, UK.
- Cox, P. M., R. Betts, M. Collins, P. Harris, C. Huntingford, and C. Jones, 2004: Amazonian forest dieback under climate-carbon cycle projections for the 21st century. *Theoretical and Applied Climatology*, **78** (1-3), 137–156.
- Cox, P. M., D. Pearson, B. B. Booth, P. Friedlingstein, C. Huntingford, C. D. Jones, and C. M. Luke, 2013: Sensitivity of tropical carbon to climate change constrained by carbon dioxide variability. *Nature*, **494**, 341–344.
- Cressman, G. P., 1959: An operational objective analysis system. *Monthly Weather Review*, **87** (10), 367–374.
- Cuéllar, S., A. Rodríguez, J. Arroyo, S. Espinoza, and D. Larrea, 2012: Mapa de deforestación de las Tierras Bajas y los Yungas de Bolivia 2000-2005-2010. Tech. rep., Fundación Amigos de La Naturaleza.
- da Costa, A. C., et al., 2013: Ecosystem respiration and net primary productivity after 8–10 years of experimental through-fall reduction in an eastern Amazon forest. *Plant Ecology & Diversity*, (ahead-of-print), 1–18.

- Dauber, E., J. Terán, and R. Guzmán, 2000: Estimaciones de biomasa y carbono en bosques naturales de Bolivia. *Superintendencia Forestal, Santa Cruz, Bolivia*.
- de Boer, H. J., E. I. Lammertsma, F. Wagner-Cremer, D. L. Dilcher, M. J. Wassen, and S. C. Dekker, 2011: Climate forcing due to optimization of maximal leaf conductance in subtropical vegetation under rising CO₂. *Proceedings of the National Academy of Sciences*, **108** (10), 4041–4046.
- De Kauwe, M. G., et al., 2013: Forest water use and water use efficiency at elevated CO₂: a model-data intercomparison at two contrasting temperate forest FACE sites. *Global change biology*.
- DeFries, R., J. Townshend, and M. Hansen, 1999: Continuous fields of vegetation characteristics at the global scale at 1-km resolution. *Journal of Geophysical Research: Atmospheres (1984–2012)*, **104** (D14), 16 911–16 923.
- den Hollander, H., 2008: Precipitation influence on savanna vegetation: cover, biomass, leaf area index and C3: C4 ratio. M.S. thesis.
- Dufresne, J.-L., et al., 2013: Climate change projections using the IPSL-CM5 Earth System Model: from CMIP3 to CMIP5. *Climate Dynamics*, 1–43.
- Dunne, J. P., et al., 2012: GFDL’s ESM2 Global Coupled Climate-Carbon Earth System Models. Part I: Physical Formulation and Baseline Simulation Characteristics. *Journal of Climate*, **25** (19), 6646–6665.
- Elguindi, N., U. Turuncoglu, and F. Giorgi, 2013: Assessment of CMIP5 global model simulations over the sub-set of CORDEX domains used in the Phase I CREMA. *EGU General Assembly Conference Abstracts*, Vol. 15, 3121.
- Enfield, D. B., A. M. Mestas-Nunez, P. J. Trimble, et al., 2001: The Atlantic multi-decadal oscillation and its relation to rainfall and river flows in the continental U. S. *Geophysical Research Letters*, **28** (10), 2077–2080.
- Espinoza Villar, J. C., et al., 2009: Spatio-temporal rainfall variability in the Amazon basin countries (Brazil, Peru, Bolivia, Colombia, and Ecuador). *International Journal of Climatology*, **29** (11), 1574–1594.
- Espirito-Santo, F., M. Keller, B. Braswell, B. Nelson, S. Frolking, and G. Vicente, 2010: Storm intensity and old-growth forest disturbances in the Amazon region. *Geophysical Research Letters*, **37** (11).
- FAN, 2003: Estudios de retención de Carbono e investigaciones ambientales para conservación ecológica en los bloques de San Alberto y San Antonio. Tech. rep.
- FAN, 2005: Project Design Document Noel Kempff Climate Action Project (NK-CAP). Tech. rep., Fundación Amigos de la Naturaleza, 1–181 pp.
- FAN, 2010: The Indigenous REDD Program in the Bolivian Amazon. 1–2 pp.
- FAO, 2012: Harmonized world soil database (version 1.2). *FAO, Rome, Italy and IIASA, Laxenburg, Austria*.

- Farquhar, G., S. v. von Caemmerer, and J. Berry, 1980: A biochemical model of photosynthetic CO₂ assimilation in leaves of C₃ species. *Planta*, **149** (1), 78–90.
- Field, C. B., et al., 2012: Managing the risks of extreme events and disasters to advance climate change adaptation. *A Special Report of Working Groups I and II of the Intergovernmental Panel on Climate Change* Cambridge University Press, Cambridge, UK, and New York, NY, USA.
- Fleischer, K., et al., 2013: Evaluating the N-cycle module of LPJ-GUESS at the site-scale. *EGU General Assembly Conference Abstracts*, Vol. 15, 8034.
- Friedlingstein, P., M. Meinshausen, V. K. Arora, C. D. Jones, A. Anav, S. K. Lid-dicoat, and R. Knutti, 2013: Uncertainties in CMIP5 climate projections due to carbon cycle feedbacks. *Journal of Climate*, (2013).
- Friend, A. D., 2010: Terrestrial plant production and climate change. *Journal of experimental botany*, **61** (5), 1293–1309.
- Furrer, R., D. Nychka, and S. Sain, 2012: *fields: Tools for spatial data*. URL <http://cran.r-project.org/package=fields>, r package version 6.6.3.
- Furtado, J. C., E. Di Lorenzo, N. Schneider, and N. A. Bond, 2011: North Pacific decadal variability and climate change in the IPCC AR4 models. *Journal of Climate*, **24** (12), 3049–3067.
- Galbraith, D., P. E. Levy, S. Sitch, C. Huntingford, P. Cox, M. Williams, and P. Meir, 2010: Multiple mechanisms of Amazonian forest biomass losses in three dynamic global vegetation models under climate change. *New Phytologist*, **187** (3), 647–665.
- Garreaud, R., 2000: Cold air incursions over subtropical South America: Mean structure and dynamics. *Monthly Weather Review*, **128** (7), 2544–2559.
- Garreaud, R., M. Vuille, R. Compagnucci, and J. Marengo, 2009: Present-day South American climate. *Palaeogeography, Palaeoclimatology, Palaeoecology*, **281** (3), 180–195.
- Gaston, K. J., 2000: Global patterns in biodiversity. *Nature*, **405** (6783), 220–227.
- Gerten, D., S. Schaphoff, and W. Lucht, 2007: Potential future changes in water limitations of the terrestrial biosphere. *Climatic Change*, **80** (3-4), 277–299.
- Giorgetta, M. A., et al., 2013: Climate and carbon cycle changes from 1850 to 2100 in MPI-ESM simulations for the Coupled Model Intercomparison Project phase 5. *Journal of Advances in Modeling Earth Systems*.
- Girardin, C. A. J., et al., 2010: Net primary productivity allocation and cycling of carbon along a tropical forest elevational transect in the Peruvian Andes. *Global Change Biology*, **16** (12), 3176–3192.
- Goll, D., V. Brovkin, B. Parida, C. Reick, J. Kattge, P. Reich, P. v. Bodegom, and Ü. Niinemets, 2012: Nutrient limitation reduces land carbon uptake in simulations with a model of combined carbon, nitrogen and phosphorus cycling. *Biogeosciences Discussions*, **9** (3), 3173–3232.

- Gumpenberger, M., K. Vohland, U. Heyder, B. Poulter, K. Macey, A. Rammig, A. Popp, and W. Cramer, 2010: Predicting pan-tropical climate change induced forest stock gains and losses—implications for REDD. *Environmental Research Letters*, **5** (1), 014 013.
- Haxeltine, A. and I. C. Prentice, 1996: BIOME3: An equilibrium terrestrial biosphere model based on ecophysiological constraints, resource availability, and competition among plant functional types. *Global Biogeochemical Cycles*, **10** (4), 693–709.
- Hecht, S. B., 2005: Soybeans, development and conservation on the Amazon frontier. *Development and Change*, **36** (2), 375–404.
- Hickler, T., B. Smith, I. C. Prentice, K. Mjöfors, P. Miller, A. Arneth, and M. T. Sykes, 2008: CO₂ fertilization in temperate FACE experiments not representative of boreal and tropical forests. *Global Change Biology*, **14** (7), 1531–1542.
- Holmgren, M., M. Hirota, E. H. van Nes, and M. Scheffer, 2013: Effects of interannual climate variability on tropical tree cover. *Nature Climate Change*.
- Huang, S., S. J. Titus, and D. P. Wiens, 1992: Comparison of nonlinear height-diameter functions for major Alberta tree species. *Canadian Journal of Forest Research*, **22** (9), 1297–1304.
- Huffman, G. J., R. F. Adler, D. T. Bolvin, E. J. Nelkin, F. Hossain, and M. Gebre-michael, 2010: The TRMM multi-satellite precipitation analysis (TMPA). *Satellite rainfall applications for surface hydrology*, 3–22.
- Huntingford, C., et al., 2008: Towards quantifying uncertainty in predictions of Amazon ‘dieback’. *Philosophical Transactions of the Royal Society B: Biological Sciences*, **363** (1498), 1857–1864.
- Huntingford, C., et al., 2013: Simulated resilience of tropical rainforests to CO₂-induced climate change. *Nature Geoscience*.
- Ibisch, P. and N. Mérida, 2003: Biodiversidad: La riqueza de Bolivia. Estado de conocimiento y conservación. Editorial FAN. Santa Cruz de la Sierra, Bolivia.
- Ibisch, P. L., 2005: Biodiversity Conservation in Bolivia: History, Trends and Challenges. *Environmental Issues in Latin America and the Caribbean*, Springer, 55–71.
- Ibisch, P. L., N. Araujo, and C. Nowicki, 2007: *Visión de conservación de la biodiversidad del Corredor Amboró-Madidi*. Editorial FAN.
- IPCC, 2007: Synthesis Report: Contribution of Working Groups I, II and III to the Fourth Assessment Report of the Intergovernmental Panel on Climate Change Core Writing Team. *IPCC, Geneva, Switzerland (2007)*. *Web of Science*.
- IPCC, 2013: *Climate Change 2013 - The Physical Science Basis: Working group I contribution to the fifth assessment report of the IPCC*. Cambridge University Press.

- Jarvis, A., H. Reuter, A. Nelson, and E. Guevara, 2008: Hole-filled SRTM for the globe Version 4. Available from the CGIAR-SXI SRTM 90m database: <http://srtm.csi.cgiar.org>.
- Jarvis, A., J. L. Touval, M. C. Schmitz, L. Sotomayor, and G. G. Hyman, 2010: Assessment of threats to ecosystems in South America. *Journal for Nature Conservation*, **18** (3), 180–188.
- Joetzjer, E., H. Douville, C. Delire, and P. Ciais, 2013: Present-day and future Amazonian precipitation in global climate models: CMIP5 versus CMIP3. *Climate Dynamics*, 1–16.
- Josse, C., et al., 2007: Ecological systems of the Amazon Basin of Peru and Bolivia. Arlington, Virginia, USA., NatureServe, Arlington, Virginia, USA.
- Jupp, T., P. Cox, A. Rammig, K. Thonicke, W. Lucht, and W. Cramer, 2010: Development of probability density functions for future South American rainfall. *New Phytologist*, **187** (3), 682–693.
- Kalnay, E., et al., 1996: The NCEP/NCAR 40-year reanalysis project. *Bulletin of the American meteorological Society*, **77** (3), 437–471.
- Killeen, T. J., V. Calderon, L. Soria, B. Quezada, M. K. Steininger, G. Harper, L. A. Solórzano, and C. J. Tucker, 2007: Thirty years of land-cover change in Bolivia. *AMBIO: A journal of the Human Environment*, **36** (7), 600–606.
- Killeen, T. J., et al., 2006: The Chiquitano dry forest, the transition between humid and dry forest in eastern lowland Bolivia. *Neotropical savannas and seasonally dry forests: plant diversity, biogeography, and conservation*, **69**, 213–233.
- Knutti, R. and J. Sedláček, 2012: Robustness and uncertainties in the new CMIP5 climate model projections. *Nature Climate Change*.
- Knyazikhin, Y., et al., 1999: MODIS leaf area index (LAI) and fraction of photosynthetically active radiation absorbed by vegetation (FPAR) product (MOD15) algorithm theoretical basis document. *Theoretical Basis Document, NASA Goddard Space Flight Center, Greenbelt, MD*, **20771**.
- Köppen, W., 1931: Grundriss der Klimakunde Vol. 12., (Walter de Gruyter: Berlin).
- Körner, C., 2006: Plant CO₂ responses: an issue of definition, time and resource supply. *New phytologist*, **172** (3), 393–411.
- Körner, C., et al., 2005: Carbon flux and growth in mature deciduous forest trees exposed to elevated CO₂. *Science*, **309** (5739), 1360–1362.
- Krinner, G., et al., 2005: A dynamic global vegetation model for studies of the coupled atmosphere-biosphere system. *Global Biogeochemical Cycles*, **19** (1).
- Lagergren, F., A. M. Jönsson, K. Blennow, and B. Smith, 2012: Implementing storm damage in a dynamic vegetation model for regional applications in Sweden. *Ecological Modelling*, **247**, 71–82.

- Larrea, D., R. López, M. Quintanilla, and A. Vargas, 2010: Gap analysis of two savanna-type ecoregions: a two-scale floristic approach applied to the Llanos de Moxos and Beni Cerrado, Bolivia. *Biodiversity and Conservation*, **19** (6), 1769–1783.
- Lenters, J. and K. Cook, 1997: On the origin of the Bolivian high and related circulation features of the South American climate. *Journal of the Atmospheric Sciences*, **54** (5), 656–678.
- Lewis, S. L., P. M. Brando, O. L. Phillips, G. M. van der Heijden, and D. Nepstad, 2011: The 2010 amazon drought. *Science*, **331** (6017), 554–554.
- Li, W., R. Fu, and R. Dickinson, 2006: Rainfall and its seasonality over the Amazon in the 21st century as assessed by the coupled models for the IPCC AR4. *Journal of Geophysical Research*, **111** (D2), D02111.
- Lloyd, J. and J. Taylor, 1994: On the temperature dependence of soil respiration. *Functional ecology*, 315–323.
- Ma, J., S.-P. Xie, and Y. Kosaka, 2012: Mechanisms for Tropical Tropospheric Circulation Change in Response to Global Warming*. *Journal of Climate*, **25** (8), 2979–2994.
- Malhi, Y., J. T. Roberts, R. A. Betts, T. J. Killeen, W. Li, and C. A. Nobre, 2008: Climate change, deforestation, and the fate of the Amazon. *science*, **319** (5860), 169–172.
- Mann, H. B., 1945: Nonparametric tests against trend. *Econometrica: Journal of the Econometric Society*, 245–259.
- Mantua, N. J., S. R. Hare, Y. Zhang, J. M. Wallace, and R. C. Francis, 1997: A Pacific interdecadal climate oscillation with impacts on salmon production. *Bulletin of the American Meteorological Society*, **78** (6), 1069–1079.
- Marengo, J., 2004: Interdecadal variability and trends of rainfall across the Amazon basin. *Theoretical and applied climatology*, **78** (1), 79–96.
- Marengo, J., R. Jones, L. Alves, and M. Valverde, 2009: Future change of temperature and precipitation extremes in South America as derived from the PRECIS regional climate modeling system. *international Journal of Climatology*, **29** (15), 2241–2255.
- Marengo, J., W. Soares, C. Saulo, and M. Nicolini, 2004: Climatology of the low-level jet east of the Andes as derived from the NCEP-NCAR reanalyses: Characteristics and temporal variability. *Journal of climate*, **17** (12), 2261–2280.
- Marengo, J., et al., 2010: Future change of climate in South America in the late twenty-first century: intercomparison of scenarios from three regional climate models. *Climate dynamics*, **35** (6), 1073–1097.
- Marengo, J., et al., 2012: Recent developments on the South American monsoon system. *International Journal of Climatology*, **32** (1), 1–21.

- Markesteyn, L., L. Poorter, F. Bongers, H. Paz, and L. Sack, 2011: Hydraulics and life history of tropical dry forest tree species: coordination of species' drought and shade tolerance. *New Phytologist*, **191** (2), 480–495.
- Mastrandrea, M., et al., 2010: Guidance note for lead authors of the IPCC fifth assessment report on consistent treatment of uncertainties. *Intergovernmental Panel on Climate Change, Geneva*, **5**.
- McClain, M. E. and R. J. Naiman, 2008: Andean influences on the biogeochemistry and ecology of the Amazon River. *BioScience*, **58** (4), 325–338.
- Medlyn, B., et al., 2002: Temperature response of parameters of a biochemically based model of photosynthesis. II. A review of experimental data. *Plant, Cell & Environment*, **25** (9), 1167–1179.
- Melack, J. M. and L. L. Hess, 2011: Remote sensing of the distribution and extent of wetlands in the Amazon basin. *Amazonian Floodplain Forests*, Springer, 43–59.
- Melillo, J. M., A. D. McGuire, D. W. Kicklighter, B. Moore, C. J. Vorosmarty, and A. L. Schloss, 1993: Global climate change and terrestrial net primary production. *Nature*, **363** (6426), 234–240.
- Meyfroidt, P., E. F. Lambin, K.-H. Erb, and T. W. Hertel, 2013: Globalization of land use: distant drivers of land change and geographic displacement of land use. *Current Opinion in Environmental Sustainability*.
- Miguez-Macho, G. and Y. Fan, 2012: The role of groundwater in the Amazon water cycle: 1. Influence on seasonal streamflow, flooding and wetlands. *Journal of Geophysical Research: Atmospheres (1984–2012)*, **117** (D15).
- Monteith, J., 1995: Accommodation between transpiring vegetation and the convective boundary layer. *Journal of Hydrology*, **166** (3), 251–263.
- Monteith, J. and M. Unsworth, 2007: *Principles of environmental physics*. Access Online via Elsevier.
- Morales, J., C. M. Carneiro, and O. Serrano, 2001: *Estado de la Información Forestal en Bolivia*, Vol. 2. 302 pp.
- Moser, G., C. Leuschner, D. Hertel, S. Graefe, N. Soethe, and S. Iost, 2011: Elevation effects on the carbon budget of tropical mountain forests (S Ecuador): the role of the belowground compartment. *Global Change Biology*, **17** (6), 2211–2226.
- Moss, R., et al., 2010: The next generation of scenarios for climate change research and assessment. *Nature*, **463** (7282), 747–756.
- Mostacedo, B., Z. Villegas, J. Licona, A. Alarcón, D. Villarroel, M. Peña-Claros, and T. Fredericksen, 2009: Ecología y silvicultura de los principales bosques tropicales de Bolivia. *Santa Cruz, Bolivia. Instituto Boliviano de Investigación Forestal*.
- Müller, R., D. Müller, F. Schierhorn, G. Gerold, and P. Pacheco, 2012: Proximate causes of deforestation in the Bolivian lowlands: an analysis of spatial dynamics. *Regional Environmental Change*, **12** (3), 445–459.

- Müller, R., T. Pistorius, S. Rohde, G. Gerold, and P. Pacheco, 2013: Policy options to reduce deforestation based on a systematic analysis of drivers and agents in lowland Bolivia. *Land Use Policy*, **30** (1), 895–907.
- Nakicenovic, N., et al., 2000: Special report on emissions scenarios: a special report of Working Group III of the Intergovernmental Panel on Climate Change. Tech. rep., Pacific Northwest National Laboratory, Richland, WA (US), Environmental Molecular Sciences Laboratory (US).
- Navarro, G. and W. Ferreira, 2004: Zonas de vegetación potencial de Bolivia: Una base para el análisis de vacíos de conservación. *Revista Boliviana de Ecología y Conservación Ambiental*, **15**, 1–40.
- Negrón-Juárez, R. I., et al., 2010: Widespread Amazon forest tree mortality from a single cross-basin squall line event. *Geophysical Research Letters*, **37** (16), L16 701.
- Nepstad, D. C., I. M. Tohver, D. Ray, P. Moutinho, and G. Cardinot, 2007: Mortality of large trees and lianas following experimental drought in an Amazon forest. *Ecology*, **88** (9), 2259–2269.
- Nepstad, D. C., et al., 1994: The role of deep roots in the hydrological and carbon cycles of Amazonian forests and pastures.
- Nock, C. A., P. J. Baker, W. Wanek, A. Leis, M. Grabner, S. Bunyavejchewin, and P. Hietz, 2011: Long-term increases in intrinsic water-use efficiency do not lead to increased stem growth in a tropical monsoon forest in western Thailand. *Global Change Biology*, **17** (2), 1049–1063.
- Norby, R. J., J. M. Warren, C. M. Iversen, B. E. Medlyn, and R. E. McMurtrie, 2010: CO₂ enhancement of forest productivity constrained by limited nitrogen availability. *Proceedings of the National Academy of Sciences*, **107** (45), 19 368–19 373.
- Nunez, M., S. Solman, and M. Cabré, 2009: Regional climate change experiments over southern South America. II: Climate change scenarios in the late twenty-first century. *Climate Dynamics*, **32** (7), 1081–1095.
- Oleson, K. W., et al., 2010: Technical description of version 4.0 of the Community Land Model (CLM).
- Oren, R., et al., 2001: Soil fertility limits carbon sequestration by forest ecosystems in a CO₂-enriched atmosphere. *Nature*, **411** (6836), 469–472.
- Oyama, M. D. and C. A. Nobre, 2004: A simple potential vegetation model for coupling with the Simple Biosphere Model (SiB). *Rev. Bras. Meteorol.*, **1** (2), 203–216.
- Pan, Y., et al., 2011: A large and persistent carbon sink in the world's forests. *Science*, **333** (6045), 988–993.
- Pebesma, E. J., 2004: Multivariable geostatistics in S: the gstat package. *Computers & Geosciences*, **30**, 683–691.

- Penman, J., et al., 2003: *Good practice guidance for land use, land-use change and forestry*. Institute for Global Environmental Strategies.
- Phillips, O. L., et al., 2009: Drought sensitivity of the Amazon rainforest. *Science*, **323** (5919), 1344–1347.
- Piani, C., G. Weedon, M. Best, S. Gomes, P. Viterbo, S. Hagemann, and J. Haerter, 2010: Statistical bias correction of global simulated daily precipitation and temperature for the application of hydrological models. *Journal of Hydrology*, **395** (3), 199–215.
- Pinard, M. A., F. E. Putz, and J. C. Licona, 1999: Tree mortality and vine proliferation following a wildfire in a subhumid tropical forest in eastern Bolivia. *Forest Ecology and Management*, **116** (1), 247–252.
- Pinzon, J., M. E. Brown, and C. J. Tucker, 2005: Satellite time series correction of orbital drift artifacts using empirical mode decomposition. *Hilbert-Huang transform: introduction and applications*, (Part II).
- Poulter, B., F. Hattermann, E. Hawkins, S. Zaehle, S. Sitch, N. Restrepo-Coupe, U. Heyder, and W. Cramer, 2010: Robust dynamics of Amazon dieback to climate change with perturbed ecosystem model parameters. *Global Change Biology*, **16** (9), 2476–2495.
- Prentice, I. C., W. Cramer, S. P. Harrison, R. Leemans, R. A. Monserud, and A. M. Solomon, 1992: Special paper: a global biome model based on plant physiology and dominance, soil properties and climate. *Journal of biogeography*, 117–134.
- Prentice, I. C., et al., 2007: Dynamic global vegetation modeling: quantifying terrestrial ecosystem responses to large-scale environmental change. *Terrestrial ecosystems in a changing world*, Springer, 175–192.
- Putz, F., 1983: Liana biomass and leaf area of a "tierra firme" forest in the Rio Negro Basin, Venezuela. *Biotropica*, 185–189.
- Quispe, J. and S. Añez, 2010: Informe Mediciones de Biomasa en Bosques Naturales y Degradados. Tech. rep., 39 pp.
- Quispe, J. P., 2008: Medición de biomasa en áreas de aprovechamiento forestal en la región oeste de Pando. Tech. rep., 40 pp.
- Quispe, J. P., 2011: Informe final de mediciones de biomasa en cuatro regiones en Bolivia. Tech. rep., 32 pp.
- Raddatz, T., et al., 2007: Will the tropical land biosphere dominate the climate-carbon cycle feedback during the twenty-first century? *Climate Dynamics*, **29** (6), 565–574.
- Rammig, A., et al., 2010: Estimating the risk of Amazonian forest dieback. *New Phytologist*, **187** (3), 694–706.

- Reich, P. B., et al., 2006: Nitrogen limitation constrains sustainability of ecosystem response to CO₂. *Nature*, **440** (7086), 922–925.
- Rienecker, M., et al., 2011: MERRA: NASA’s modern-era retrospective analysis for research and applications. *Journal of Climate*, **24** (14), 3624–3648.
- Roche, M.-A. and C. F. Jauregui, 1988: Water resources, salinity and salt yields of the rivers of the Bolivian Amazon. *Journal of Hydrology*, **101** (1), 305–331.
- Rodriguez, A., 2012a: Cartografía multitemporal de quemas e incendios forestales en Bolivia: Detección y validación post-incendio. *Ecología en Bolivia*, **47** (1), 53–71.
- Rodriguez, A., 2012b: Prevención, control y uso del fuego en la Chiquitanía. *Fundación Amigos de la Naturaleza*, 1–12.
- Romero-Saltos, H., L. da SL Sternberg, M. Z. Moreira, and D. C. Nepstad, 2005: Rainfall exclusion in an eastern Amazonian forest alters soil water movement and depth of water uptake. *American Journal of Botany*, **92** (3), 443–455.
- Ronchail, J., 1995: Variabilidad interanual de las precipitaciones en Bolivia. *Bull. Inst. fr. études andines*, **24** (3), 369–378.
- Ronchail, J. and R. Gallaire, 2006: ENSO and rainfall along the Zongo valley (Bolivia) from the Altiplano to the Amazon basin. *International journal of climatology*, **26** (9), 1223–1236.
- Roy, D. P., L. Boschetti, C. O. Justice, and J. Ju, 2008: The collection 5 MODIS burned area product—Global evaluation by comparison with the MODIS active fire product. *Remote Sensing of Environment*, **112** (9), 3690–3707.
- RREE, 2012: Joint mitigation and adaptation mechanism for the comprehensive and sustainable management of forest and the mother earth. The Plurinational State of Bolivia, 1–29 pp.
- Saatchi, S., R. Houghton, R. Dos Santos Alvala, J. Soares, and Y. Yu, 2007: Distribution of aboveground live biomass in the Amazon basin. *Global Change Biology*, **13** (4), 816–837.
- Saatchi, S. S., et al., 2011: Benchmark map of forest carbon stocks in tropical regions across three continents. *Proceedings of the National Academy of Sciences*, **108** (24), 9899–9904.
- Salati, E., A. Dall’Olio, E. Matsui, and J. R. Gat, 1979: Recycling of water in the Amazon basin: an isotopic study. *Water Resources Research*, **15** (5), 1250–1258.
- Salazar, L. F., C. A. Nobre, and M. D. Oyama, 2007: Climate change consequences on the biome distribution in tropical South America. *Geophysical Research Letters*, **34** (9).
- Saleska, S. R., K. Didan, A. R. Huete, and H. R. Da Rocha, 2007: Amazon forests green-up during 2005 drought. *Science*, **318** (5850), 612–612.

- Samanta, A., S. Ganguly, H. Hashimoto, S. Devadiga, E. Vermote, Y. Knyazikhin, R. R. Nemani, and R. B. Myneni, 2010: Amazon forests did not green-up during the 2005 drought. *Geophysical Research Letters*, **37** (5).
- Sampaio, E. and G. Silva, 2005: Biomass equations for Brazilian semiarid caatinga plants. *Acta Botanica Brasílica*, **19** (4), 935–943.
- Scheiter, S., L. Langan, and S. I. Higgins, 2013: Next-generation dynamic global vegetation models: learning from community ecology. *New Phytologist*.
- Schöngart, J., W. J. Junk, M. T. F. Piedade, J. M. Ayres, A. Hüttermann, and M. Worbes, 2004: Teleconnection between tree growth in the Amazonian floodplains and the El Niño–Southern Oscillation effect. *Global Change Biology*, **10** (5), 683–692.
- Seiler, C., R. W. A. Hutjes, and P. Kabat, 2013a: Climate Variability and Trends in Bolivia. *Journal of Applied Meteorology and Climatology*, **52** (1), 130–146.
- Seiler, C., R. W. A. Hutjes, and P. Kabat, 2013b: Likely Ranges of Climate Change in Bolivia. *Journal of Applied Meteorology and Climatology*, **52** (6), 1303–1317.
- Seiler, C. and A. F. Moene, 2011: Estimating Actual Evapotranspiration from Satellite and Meteorological Data in Central Bolivia. *Earth Interactions*, **15** (12), 1–24.
- Seiler, C., et al., 2014: Modeling forest dynamics along climate gradients in Bolivia. *Journal of Geophysical Research: Biogeosciences*.
- SENAMHI, 2009: Climatología de Bolivia.
- Seth, A., J. Thibeault, M. Garcia, and C. Valdivia, 2010: Making sense of twenty-first-century climate change in the Altiplano: observed trends and CMIP3 projections. *Annals of the association of American geographers*, **100** (4), 835–847.
- Silva, G. A. M. d., A. Drumond, and T. Ambrizzi, 2011: The impact of El Niño on South American summer climate during different phases of the Pacific Decadal Oscillation. *Theoretical and applied climatology*, **106** (3), 307–319.
- Silva, V. B. S. and V. E. Kousky, 2012: *The South American Monsoon System: Climatology and Variability*, chap. 5, 398. InTech.
- Sitch, S., et al., 2003: Evaluation of ecosystem dynamics, plant geography and terrestrial carbon cycling in the LPJ dynamic global vegetation model. *Global Change Biology*, **9** (2), 161–185.
- Smith, B., I. C. Prentice, and M. T. Sykes, 2001: Representation of vegetation dynamics in the modelling of terrestrial ecosystems: comparing two contrasting approaches within European climate space. *Global Ecology and Biogeography*, **10** (6), 621–637.
- Smith, C. A., P. D. Sardeshmukh, et al., 2000: The effect of ENSO on the intraseasonal variance of surface temperatures in winter. *International Journal of Climatology*, **20** (13), 1543–1557.

- Smith, N. G. and J. S. Dukes, 2013: Plant respiration and photosynthesis in global-scale models: incorporating acclimation to temperature and CO₂. *Global change biology*, **19** (1), 45–63.
- Soares, W. and J. Marengo, 2009: Assessments of moisture fluxes east of the Andes in South America in a global warming scenario. *International Journal of Climatology*, **29** (10), 1395–1414.
- Taylor, K., 2001: Summarizing multiple aspects of model performance in a single diagram. *J. Geophys. Res.*, **106** (D7), 7183–7192.
- Tejada, A., 2013: *Minería en las tierras bajas de Bolivia*.
- Thibeault, J., A. Seth, and M. Garcia, 2010: Changing climate in the Bolivian Altiplano: CMIP3 projections for temperature and precipitation extremes. *Journal of Geophysical Research*, **115** (D8), D08103.
- Thompson, D. W. and J. M. Wallace, 2000: Annular modes in the extratropical circulation. Part I: month-to-month variability*. *Journal of Climate*, **13** (5), 1000–1016.
- Toledo, M., 2010: *Neotropical lowland forests along environmental gradients*. Wageningen University.
- Tollefson, J., 2013: Experiment aims to steep rainforest in carbon dioxide. *Nature*, **496** (7446), 405.
- UNDP, 2011: Tras las huellas del cambio climático en Bolivia, estado del arte del conocimiento sobre adaptación al cambio climático agua y seguridad alimentaria. 144.
- UNFCCC, 2005: Decision 5/CMP.1. Modalities and procedures for afforestation and reforestation project activities under the clean development mechanism in the first commitment period of the Kyoto Protocol. Tech. rep., 61 pp.
- UNFCCC, 2010: Decision 4/CP.15. Methodological guidance for activities relating to reducing emissions from deforestation and forest degradation and the role of conservation, sustainable management of forests and enhancement of forest carbon stocks in developing countries. Tech. rep., 43 pp.
- Urioste, M., 2012: Concentration and “foreignisation” of land in Bolivia. *Canadian Journal of Development Studies/Revue canadienne d’études du développement*, **33** (4), 439–457.
- Urrutia, R. and M. Vuille, 2009: Climate change projections for the tropical Andes using a regional climate model: temperature and precipitation simulations for the end of the 21st century. *Journal of Geophysical Research*, **114** (D2), D02108.
- van Etten, R. J. H. . J., 2012: *raster: Geographic analysis and modeling with raster data*. URL <http://cran.r-project.org/package=raster>, r package version 2.0-12.

- Van Zomeren, J. and A. Van Delden, 2007: Vertically integrated moisture flux convergence as a predictor of thunderstorms. *Atmospheric research*, **83** (2), 435–445.
- Vecchi, G. A. and B. J. Soden, 2007: Global warming and the weakening of the tropical circulation. *Journal of Climate*, **20** (17), 4316–4340.
- Vecchi, G. A., B. J. Soden, A. T. Wittenberg, I. M. Held, A. Leetmaa, and M. J. Harrison, 2006: Weakening of tropical Pacific atmospheric circulation due to anthropogenic forcing. *Nature*, **441** (7089), 73–76.
- Vera, C., G. Silvestri, B. Liebmann, and P. González, 2006: Climate change scenarios for seasonal precipitation in South America from IPCC-AR4 models. *Geophysical Research Letters*, **33** (13), L13 707.
- Vincent, L., et al., 2005: Observed trends in indices of daily temperature extremes in South America 1960–2000. *Journal of Climate*, **18** (23), 5011–5023.
- Virgilio, N., 2009: Noel Kempff Mercado climate action project: A case study in reducing emissions from deforestation and degradation. *The Nature Conservancy. Washington DC*.
- Voltaire, A., et al., 2012: The CNRM-CM5. 1 global climate model: description and basic evaluation. *Climate Dynamics*, 1–31.
- Volodin, E., N. Dianskii, and A. Gusev, 2010: Simulating present-day climate with the INMCM4. 0 coupled model of the atmospheric and oceanic general circulations. *Izvestiya, Atmospheric and Oceanic Physics*, **46** (4), 414–431.
- Vuille, M., 1999: Atmospheric circulation over the Bolivian Altiplano during dry and wet periods and extreme phases of the Southern Oscillation. *International Journal of Climatology*, **19** (14), 1579–1600.
- Vuille, M., R. S. Bradley, M. Werner, and F. Keimig, 2003: 20th century climate change in the tropical Andes: observations and model results. *Climatic Change*, **59** (1), 75–99.
- Walkley, A. and I. Black, 1934: An examination of the Degtjareff method for determining soil organic matter, and a proposed modification of the chromic acid titration method. *Soil science*, **37** (1), 29–38.
- Wang, X. L., 2003: Comments on “Detection of undocumented changepoints: A revision of the two-phase regression model”. *tc*, **2**, 2.
- Wang, X. L., 2008: Accounting for autocorrelation in detecting mean shifts in climate data series using the penalized maximal t or F test. *Journal of applied meteorology and climatology*, **47** (9), 2423–2444.
- Wang, X. L., H. Chen, Y. Wu, Y. Feng, and Q. Pu, 2010: New techniques for the detection and adjustment of shifts in daily precipitation data series. *Journal of Applied Meteorology and Climatology*, **49** (12), 2416–2436.

- Watanabe, S., et al., 2011: MIROC-ESM 2010: model description and basic results of CMIP5-20c3m experiments. *Geoscientific Model Development*, **4**, 845–872.
- Wild, M., 2008: Short-wave and long-wave surface radiation budgets in GCMs: a review based on the IPCC-AR4/CMIP3 models. *Tellus A*, **60** (5), 932–945.
- Woodward, F. and M. Lomas, 2004: Simulating vegetation processes along the Kalahari transect. *Global Change Biology*, **10** (3), 383–392.
- Woodward, F. I., 1987: *Climate and plant distribution*. Cambridge University Press.
- WorldBank, 2010: Adaptation to Climate Change: Vulnerability Assessment and Economic Aspects. Tech. rep., World Bank, 92 pp.
- Xu, L., A. Samanta, M. H. Costa, S. Ganguly, R. R. Nemani, and R. B. Myneni, 2011: Widespread decline in greenness of Amazonian vegetation due to the 2010 drought. *Geophysical Research Letters*, **38** (7).
- Zaehle, S. and A. Friend, 2010: Carbon and nitrogen cycle dynamics in the O-CN land surface model: 1. Model description, site-scale evaluation, and sensitivity to parameter estimates. *Global Biogeochemical Cycles*, **24** (1).
- Zhang, Y., J. M. Wallace, and D. S. Battisti, 1997: ENSO-like interdecadal variability: 1900–93. *Journal of Climate*, **10** (5), 1004–1020.
- Zhou, J. and K. Lau, 1998: Does a monsoon climate exist over South America? *Journal of Climate*, **11** (5), 1020–1040.
- Ziehn, T., J. Kattge, W. Knorr, and M. Scholze, 2011: Improving the predictability of global CO₂ assimilation rates under climate change. *Geophysical Research Letters*, **38** (10).

Summary

This thesis studies the sensitivity of vegetation dynamics to climate variability and change in Bolivia. The complexity of the problem was approached by integrating information from climate observations, climate projections, biomass measurements, remote sensing data, and a dynamic vegetation model. The first part of the thesis (Chapter 2 and 3) assesses the historic and possible future climates of Bolivia, providing input for the second part (Chapter 4 and 5) that explores vegetation dynamics for recent and possible future climates from a modeling perspective.

Meteorological observations revealed a significant increase in close-to-surface air temperatures at a rate of about 0.1°C per decade, with stronger increases in the Andes and in the dry season (Chapter 2). Rainfall totals increased from 1965 to 1984 (12% in DJF and 18% in JJA) and decreased afterward (-4% in DJF and -10% in JJA), following roughly the pattern of the Pacific Decadal Oscillation (PDO). Total amounts of rainfall, as well as the number of extreme events, were higher during the positive phase of PDO and during El Niño (EN) and La Niña in the lowlands. During austral summer (DJF), EN led to drier conditions in the Andes with more variable precipitation. Trends of climate extremes generally corresponded to trends of climate means. The assessment of climate observations provided us with the necessary reference required for our evaluation of climate models (GCMs) in Chapter 3, as well as with the forcing data used for the dynamic vegetation model LPJ-GUESS in Chapter 4 and 5. Also, having detected historic trends allowed us to simulate the sensitivity of LPJ-GUESS to increasing temperatures and decreasing rainfall in Chapter 4.

After analyzing historic climate patterns in Chapter 2, we proceeded with the evaluation of 35 different GCMs and 5 emission scenarios in Chapter 3. GCMs revealed an overall cold, wet and positive short wave (SW) radiation bias and showed no substantial improvement from the CMIP3 to the CMIP5 ensemble for the Bolivian case. Models projected an increase in temperature (2.5 to 5.9°C) and SW radiation (1 to 5%) for the end of the 21st century, with seasonal and regional differences. In the lowlands, changes in annual rainfall remained uncertain for CMIP3, while CMIP5 GCMs were more inclined to project decreases (-9%), not only with respect to Bolivia, but also regarding the entire Amazon basin. Both ensembles agreed on less rainfall (-19%) during drier months (JJA, SON), with significant changes in interannual rainfall variability, but disagreed on changes during wetter months (JFM). In the Andes, CMIP3 GCMs tended to less (-9%), while CMIP5 to more (+20%) rainfall during parts of the wet season. Knowledge on biases and projections allowed us to make informed choices on the forcing data used in our climate change impact assessment presented in Chapter 5.

We then continued with the adaptation of the dynamic vegetation model LPJ-GUESS to simulate present day potential vegetation (Chapter 4) as a baseline for our climate change impact assessment presented in Chapter 5. Results were compared to biomass measurements from 21 new, and 798 plots from previous field campaigns, as well as to remote sensing data. Using regional parameter values for allometric relations, specific leaf area, wood density and non-fire disturbance interval, a realistic transition from the evergreen Amazon in northern Bolivia to the deciduous dry forests of the south was simulated. This transition coincided with threshold values for precipitation (1400 mm yr^{-1}) and water deficit (-830 mm yr^{-1}), beyond which leaf abscission became a competitive advantage. The model reproduced reasonable values for seasonal leaf abscission, vegetation carbon, and area of burnt forest. Simulated Gross Primary Productivity (GPP) and remotely sensed vegetation greenness (NDVI) both showed that dry forests were more sensitive to rainfall anomalies than wet forests. Simulated GPP was positively correlated to El Niño - Southern Oscillation (ENSO) in the Amazon, and negatively correlated to the consecutive dry day index. Decreasing rainfall trends were simulated to decrease GPP in the Amazon. The regional application and evaluation of LPJ-GUESS under present-day climate is the basis for our climate change impact assessment presented in Chapter 4. We conclude that LPJ-GUESS is sufficiently flexible to make it a suitable modeling framework for regional studies on vegetation dynamics. The success of such a regional application depends on the incorporation of regional parameter values.

Using the same model configuration, the impacts of climate change were then assessed for two contrasting, but equally likely projections in Chapter 5. The impacts of climate change differed strongly between runs based on the wet projection from CNRM-CM5, and the dry projection from IPSL-CM5A-LR, and were heavily affected by the potential fertilizing effect of rising $[\text{CO}_2]$. Vegetation carbon (c_v) increased under the wet projections from CNRM-CM5 when the potential CO_2 -fertilizing effect was included. Turning this effect off caused c_v to remain more or less constant. Forcing LPJ-GUESS with the dry projection (IPSL-CM5A-LR), and keeping the potential CO_2 -fertilization off, substantially reduced c_v in both forests. Only in the wet forest could most of this vegetation loss be avoided by the potential CO_2 -fertilization effect. Vegetation carbon protected by two carbon offset projects changed correspondingly, ranging from 99% more to 41% less c_v . The loss of c_v was primarily driven by a reduction in GPP, and secondarily by enhanced emissions from fires. In the wet forest, less precipitation and higher temperatures equally reduced c_v , while in the dry forest, the impact of precipitation was dominating. The temperature-related reduction of c_v was mainly due to a decrease in photosynthesis, and only to lesser extent because of more autotrophic respiration and less stomatal conductance as a response to an increasing atmospheric demand. Tropical dry forests were simulated to virtually disappear, regardless of the potential fertilizing effect of rising $[\text{CO}_2]$, suggesting a higher risk for forest loss along the drier southern fringe of the Amazon. Our results demonstrate that a climate change induced forest dieback is indeed possible in the Bolivian case. The biggest absolute changes are simulated to occur in the transition zone between

wet and dry tropical forest, while the forests along the Andean slopes were simulated to be less affected. A partial loss of carbon stocks protected by two Bolivian REDD projects is also possible. Results are subjects to uncertainties discussed in Chapter 5, and are highly dependent on the directional change of future annual rainfall.

The possibility of a forest dieback poses a serious threat to biodiversity, as well as rural livelihoods in Bolivia. Adaption measures for Bolivian forests should prioritize actions related to preventing deforestation, fire management, reducing grazing, and improved water resource management (Chapter 6). Progress in climate change impact assessments for the Amazon will greatly depend on our ability to reduce uncertainties of future rainfall projections, possibly through physical reasoning rather than pure ensemble statistics. Otherwise, large uncertainties will remain for climate change impact assessments in the Amazon, despite extensive impact model improvements.

Resumen

Esta tesis investiga la sensibilidad de la dinámica de la vegetación a la variabilidad y cambio climático en Bolivia. La complejidad del problema fue abordada integrando información de observaciones climáticas, proyecciones climáticas, mediciones de biomasa, teledetección y modelación dinámica de la vegetación. La primera parte de la tesis (Capítulo 2 y 3) analiza el clima histórico y los posibles escenarios climáticos futuros en Bolivia, proporcionando insumos para la segunda parte (Capítulo 4 y 5), en la cual se explora, desde una perspectiva de modelación, la dinámica de la vegetación para el clima reciente y futuro.

Las observaciones meteorológicas muestran un incremento significativo de las temperaturas cerca de la superficie de aproximadamente $0,1\text{ }^{\circ}\text{C}$ por década para todo el país, con el incremento más alto en la zona de los Andes y en la época seca (Capítulo 2). La precipitación se incrementó entre 1965 y 1984 (12% en dic/ene/feb y 18% en jun/jul/ago) y luego disminuyó (-4% en dic/ene/feb y -10% en jun/jul/ago), aproximándose al patrón de la Oscilación Decenal del Pacífico (PDO, por sus siglas en inglés). En las tierras bajas, las cantidades totales de precipitación así como el número de eventos extremos, fueron mayores durante la PDO (+), El Niño y La Niña. En los Andes El Niño causó condiciones más secas durante el verano Austral (dic/ene/feb), con precipitaciones más variables. Las tendencias de extremos climáticos generalmente corresponden a las tendencias de los promedios climáticos. El análisis de los datos climáticos observados sirvió como base de datos para evaluar los modelos climáticos de circulación global (GCM) en el Capítulo 3, así como los datos usados en un modelo de la dinámica de la vegetación (LPJ-GUESS) en el Capítulo 4 y 5. Además, la identificación de tendencias históricas permitió simular la sensibilidad del modelo LPJ-GUESS ante incrementos de temperatura y disminución de la precipitación en el Capítulo 4.

Después de analizar el patrón del clima histórico en el Capítulo 2, seguimos con la evaluación de 35 modelos GCM y 5 escenarios de emisiones diferentes en el Capítulo 3. En el caso de Bolivia, los GCM revelaron, en general, un sesgo estadístico de condiciones frías, húmedas y una tendencia positiva de la radiación de onda corta, y no mostraron una mejora considerable entre el ensamble de modelos del CMIP3 y el CMIP5. Los modelos pronostican un incremento de la temperatura (entre $2,5$ y $5,9^{\circ}\text{C}$) y de la radiación de onda corta (entre 1 y 5%) con diferencias estacionales y regionales. En las tierras bajas de Bolivia y también en toda la cuenca amazónica, los cambios de las sumas anuales de la precipitación son inciertos en los modelos CMIP3, mientras que en los modelos CMIP5 la precipitación indica una disminución de hasta -9%. Ambos

modelos coincidieron en menos precipitación (-19%) durante los meses más secos (junio hasta noviembre), con cambios significativos en la variabilidad interanual de la precipitación, pero en los meses húmedos (enero, febrero, marzo) los resultados no son congruentes. En los Andes los modelos CMIP3 tienden a mostrar una disminución de la precipitación (-9%), mientras que los modelos CMIP5 muestran un incremento de 20% durante parte de la estación húmeda. Los resultados de la evaluación del sesgo estadístico y de las proyecciones climáticas nos permitieron seleccionar los datos óptimos para realizar la investigación de los impactos del cambio climático en el Capítulo 5.

En el Capítulo 4 continuamos con la adaptación del modelo dinámico de vegetación LPJ-GUESS para simular la vegetación actual potencial, como línea base para la investigación de los impactos del cambio climático presentada en el Capítulo 5. Los resultados fueron comparados con las mediciones de biomasa de 21 nuevas parcelas y 798 parcelas instaladas previamente, así como datos de sensores remotos. Se ha logrado modelar una transición realista entre el bosque amazónico siempre verde y el bosque seco deciduo, utilizando parámetros regionales de las relaciones alométricas, el área foliar específica, la densidad de madera y los intervalos de perturbación. Esta transición coincidió con los valores límites de la precipitación (1400 mm/a) y déficit de agua (-830 mm/a), más allá de los cuales la abscisión foliar se convierte en una ventaja competitiva. El modelo reprodujo valores razonables para la abscisión foliar, el carbono vegetal (c_v) e incendios forestales. La productividad primaria bruta (GPP) modelada y el índice normalizado de área foliar (NDVI) levantado por teledetección mostraron que los bosques secos son más sensibles a anomalías de precipitación que los bosques húmedos. Existe una correlación positiva entre GPP y el evento ENSO en la Amazonia y una correlación negativa con días secos consecutivos. Se ha simulado un decremento de GPP debido a la disminución de la precipitación en la Amazonia. La aplicación y evaluación regional del modelo LPJ-GUESS con el clima actual es la base para la investigación de los impactos del cambio climático presentada en el Capítulo 5. Concluimos que el modelo LPJ-GUESS es lo suficientemente flexible para ser un marco de modelamiento adecuado para estudios regionales de la dinámica de la vegetación. La aplicación exitosa al nivel regional, por su parte, dependerá de la inclusión de parámetros locales.

En el Capítulo 5 los impactos del cambio climático fueron investigados para dos diferentes proyecciones, aplicando la misma configuración del modelo. Los resultados difieren fuertemente entre las corridas con base a la proyección de condiciones húmedas del modelo GCM CNRM-CM5 y la proyección de condiciones secas del modelo GCM IPSL-CM5A-LR, con efectos intensos por el potencial efecto de fertilización por el aumento de dióxido de carbono (CO_2). El c_v se incrementó en las proyecciones con el GCM CNRM-CM5 para condiciones húmedas, cuando se incluyó el efecto de fertilización del CO_2 , mientras la exclusión de este efecto en la configuración del modelo resultó en valores de c_v más o menos constantes. Correr el modelo LPJ-GUESS con el GCM IPSL-CM5A-LR para condiciones secas y sin el efecto de fertilización por el CO_2 redujo significativamente el c_v para los dos tipos de bosque. Solamente en

los bosques húmedos el efecto potencial de fertilización por CO_2 pudo evitar la pérdida de vegetación. El c_v protegido por dos proyectos de compensación de carbono cambió respectivamente, variando entre un incremento de 99% y un decremento de 41%. La pérdida de c_v se debió principalmente a una reducción de GPP, y en segundo lugar por un aumento de las emisiones por incendios forestales. Igualmente, el c_v de bosques húmedos se redujo por temperaturas incrementadas y un decremento de la precipitación, mientras que en bosques secos el impacto de la precipitación fue más dominante. La reducción de c_v por efectos de la temperatura se debe principalmente a una disminución de la fotosíntesis y en menor medida al aumento de la respiración autotrófica y menos conducción por los estomas como respuesta al incremento de la demanda atmosférica. Se simuló la desaparición de los bosques secos tropicales, independientemente del efecto potencial de la fertilización por el CO_2 . Los resultados sugieren un riesgo más alto en el sur de la Amazonia por la pérdida de bosques en la zona seca. Los impactos más fuertes están simulados para la zona transicional entre el bosque seco tropical y el bosque húmedo tropical, mientras que los bosques en los valles andinos se verían menos afectados. Es posible que los depósitos de carbono protegidos por dos proyectos REDD en Bolivia, se vean reducidos. Estos resultados están sujetos a incertidumbres discutidas en el Capítulo 5, y mayormente dependen de los cambios de la precipitación anual en el futuro.

La posibilidad de la muerte regresiva del bosque (forest dieback) es una amenaza seria para la biodiversidad y los medios de vida rurales. Por eso, las medidas de adaptación en Bolivia deberían priorizar actividades para controlar la deforestación, el manejo del fuego, pastoreo y manejo de recursos hídricos. Los avances en las investigaciones del impacto del cambio climático en la Amazonia dependen en gran medida de nuestra habilidad para reducir las incertidumbres de las proyecciones de precipitación futura, más por razonamientos físicos que meramente por cálculos estadísticos. De otra manera, las altas incertidumbres se mantendrán en los análisis de impactos del cambio climático en la Amazonia, a pesar de las amplias mejoras de los modelos.

Samenvatting

Dit proefschrift onderzoekt de gevoeligheid van de vegetatiedynamiek voor klimaatvariabiliteit en –verandering in Bolivia. De complexiteit van het probleem noodzaakte tot een integratie van informatie met betrekking tot klimaatwaarnemingen, klimaatprojecties door modellen, vegetatiewaarnemingen in het veld en met behulp van satellieten en het modelleren van vegetatiedynamiek. In het eerste deel van dit proefschrift (hoofdstuk twee en drie) analyseert het historische en het mogelijk toekomstige klimaat van Bolivia. Dit dient als invoer voor het tweede deel (hoofdstuk vier en vijf) dat de vegetatiedynamiek verkent voor zowel het recente als het toekomstige klimaat vanuit een modelperspectief.

Meteorologische waarnemingen laten een significante toename zien van de 2m - temperatuur van ongeveer 0.1°C per decade, met nog grotere waarden in de Andes en in het droge seizoen (hoofdstuk 2). Neerslag totalen namen tussen 1965 en 1984 toe (12% in DJF en 18% in JJA) en daarna weer af (-4% in DJF en -10% in JJA) ruwweg in fase met de Pacifisch Decadale Oscillatie (PDO). Zowel de totale neerslag, als het aantal extremen waren hoger tijdens de positieve fase van de PDO (PDO+) en tijdens El Niño situaties, en juist tijdens La Niña situaties in de laaglanden. Tijdens de zuidelijk zomer (DJF) leidden El Niño situaties juist tot minder en meer variabele neerslag in de Andes. De veranderingen in extremen volgen over het algemeen de veranderingen in de gemiddelden. De klimaatwaarnemingen vormden de noodzakelijke referentie voor de evaluatie van de klimaatmodellen (GCMs) in hoofdstuk drie en als invoer voor het dynamische vegetatie model LPJ-GUESS in hoofdstuk vier en vijf. In hoofdstuk vier hebben we met de vastgestelde historische trends ook de gevoeligheid van LPJ-GUESS voor toenemende temperatuur en afnemende neerslag gesimuleerd.

Na de patronen in het historische klimaat geanalyseerd te hebben in hoofdstuk twee, worden in hoofdstuk drie 35 GCMs en 5 emissiescenario's geanalyseerd. Over het algemeen simuleren de GCMs voor Bolivia een te koud en te nat klimaat met een teveel kortgolvlige straling; hierin is van de CMIP3 naar de CMIP5 ensembles geen significante verbetering opgetreden. Voor de toekomst projecteerden de klimaatmodellen een toename in temperatuur (2.5 tot 5.9°C) en kortgolvlige straling (1 tot 5%) enigszins afhankelijk van seizoen en regio. Voor het laagland waren de neerslagveranderingen op jaarbasis onzeker in het CMIP3 ensemble, terwijl de CMIP5 modellen sterker neigden naar een afname (-9%), niet alleen in Bolivia maar in de gehele Amazone. Beide ensembles projecteerden een neerslagafname (-19%) in de droge maanden (JJA, SON) gepaard aan significante veranderingen in variabiliteit tussen jaren, maar waren het niet eens ten aanzien van neerslagveranderingen in het natte seizoen (JFM).

In de Andes neigt het CMIP3 ensemble naar 9% minder en het CMIP5 ensemble naar 20% meer neerslag in het natte seizoen. De opgedane kennis van modelafwijkingen en de verschillende projecties stelden ons in staat een bewuste keuze te maken tav de te kiezen forceringsdata voor de klimaat-effectenstudie van hoofdstuk vijf.

Vervolgens hebben we in hoofdstuk vier het dynamisch vegetatie model LPJ-GUESS dusdanig aangepast dat het de huidige potentiële vegetatie kon simuleren als base line voor de klimaat-effectenstudie van hoofdstuk vijf. De simulaties werden vergeleken met biomassa waarnemingen van 21 nieuwe en 798 bestaande veldopnames en met satelliet waarnemingen. Met gebruik van regionaal vastgestelde waarden voor allometrische relaties, specifiek bladoppervlak, houtdichtheid en verstoringsfrequenties kon een realistische gradiënt gesimuleerd worden van het altijdgroene Amazone bos in het noorden van Bolivia naar het bladverliezende droge bos in het zuiden. Deze overgang viel samen met grenswaarden in de neerslag (1400 mm/jaar) en vochttekort (830 mm/jaar), waar voorbij bladverlies een concurrentievoordeel werd. Het model reproduceerde redelijk waarden voor bladval, koolstofopslag in vegetatie en ook voor de frequentie van opgetreden bosbranden. Gesimuleerde bruto primaire productie (GPP) en satelliet waargenomen bladhoeveelheden (NDVI) lieten beiden zien dat het droge bos gevoeliger reageert op neerslagafwijkingen dan het regenwoud. Gesimuleerde GPP was positief gecorreleerd met de El Niño – Zuidelijke Oscillatie (ENSO) in de Amazone en negatief met de opeenvolgende regendagen index. Afnemende neerslag trends leidden tot een gesimuleerde GPP afname in de Amazone. Deze regionale implementatie en validatie van LPJ-GUESS voor het huidige klimaat vormt de basis voor onze klimaat-effectenstudie in hoofdstuk 4. Wij concluderen dat LPJ-GUESS voldoende flexibel is om het geschikt te maken als raamwerk voor regionale studies van vegetatie dynamiek. Het succes daarvan hangt wel af van het gebruik van regionaal bepaalde parameter waarden.

Met deze modelopzet werd het effect van klimaatverandering op de vegetatie bepaald voor twee contrasterende, maar even waarschijnlijke klimaatprojecties. Die effecten verschilden sterk tussen de simulatie geforceerd door de natte projectie van het CNRM-CM5 klimaatmodel en die van de droge projectie van het IPSL-CM5A-LR model en waren sterk afhankelijk van het bemestingseffect van toekomstige hoge kooldioxideconcentraties in de atmosfeer. De hoeveelheid (koolstof in) de vegetatie nam toe bij de natte CNRM-CM5 projecties en ingeschakelde CO₂-bemesting, maar bleef gelijk wanneer dit proces werd uitgeschakeld. Forceerden we LPJ-GUESS met de droge IPSL-CM5A-LR projectie en uitgeschakelde CO₂-bemesting, dan nam de hoeveelheid vegetatie in beide bostypen flink af. Het ingeschakelde CO₂-bemestingseffect kon alleen in het natte bos een vegetatieafname voorkomen. Ook in twee beschermde bosgebieden (tbv koolstof compensatie projecten) nam de hoeveelheid vegetatie sterk af door klimaatverandering (41-99% minder). De afname van koolstof in de vegetatie werd primair gedreven door een afname in GPP maar vervolgens versterkt door toegenomen brandgevoeligheid. In het natte bos waren zowel neerslagvermindering als ook temperatuuroptuename in gelijke mate verantwoordelijk voor de vegetatieafname, terwijl in het droge bos de neerslagafname hierin domineerde. De temperatuur

gedreven afname van koolstof in de vegetatie werd vooral veroorzaakt door een afname van de fotosynthese en in mindere mate door een toegenomen autotrofe respiratie en tegenomen stomataire weerstand in reactie op een oplopende atmosferische vochtvraag. Het droge bos verdween vrijwel geheel in de simulaties, ongeacht of het CO₂-bemestingseffect was ingeschakeld of niet, wat een hoog risico suggereert voor bosverlies langs de droge zuidelijke grens van de Amazone. Onze resultaten laten zien dat een klimaat geïnduceerde bossterfte inderdaad tot de mogelijkheden behoort in Bolivia. De grootste veranderingen simuleerde het model voor de overgangszone van nat naar droog tropisch bos, terwijl de bossen op de flanken van de Andes minder gevoelig leken te zijn. Ook bestaat er gerede kans op een gedeeltelijk verlies van koolstofvoorraden in de twee Boliviaanse REDD projecten. De resultaten hangen af van de onzekerheden die in hoofdstuk vijf verder besproken worden, maar vooral van het teken van de neerslagverandering.

De potentiële bossterfte vormt een serieuze bedreiging voor biodiversiteit en het levensonderhoud in ruraal Bolivia. Adaptatiebeleid voor Boliviaanse bossen zou voorrang moeten geven aan maatregelen gericht op het voorkomen van ontbossing, bosbrandbeheer, terugdringen van veeteelt en verbetering van waterbeheer (hoofdstuk zes). Progressie in klimaateffectenstudies voor de Amazone hangt sterk af van ons vermogen de onzekerheden in de toekomstige neerslagprojecties terug te brengen, wellicht meer door fysisch redeneren dan door verbeterde ensemble statistiek. Anders blijven de onzekerheden voor klimaateffectenstudies bestaan ondanks aanmerkelijke verbetering van de effectenmodellen.

Acknowledgments

I am grateful to my promoter Pavel Kabat, who has given me the opportunity to convert my work at FAN into a PhD-thesis. Pavel, thank you very much for your support, and for the inspiring meetings throughout all stages of this research. I thank my co-promoters Ronald Hutjes and Bart Kruijt from whom I have obtained most of my skills during this time. I appreciate your dedication to the details, and that you were always accessible. Ronald, thank you for baring with me the entire time, for your detailed reviews, and countless meetings. Bart, thank you for welcoming me to the AMAZALERT project. I would like to thank for the support from all other co-authors, namely Thomas Hickler, Vivek Arora, Joe Melton, Jaime Quispe and Sandro Añez. Thomas (LOEWE BiK-F), thank you for sharing your insights on dynamic vegetation modeling, and for your computational support. In this context I would also like to thank your colleague Matt Forrest for his crucial help and feedback. I thank Vivek Arora (CCCma) for having welcomed me to his research group in Canada, which turned out to become a crucial step for my career. Thanks to Joe Melton (CCCma) for sharing his experiences with LPJ-GUESS, and for the detailed review of our manuscript.

Jaime Quispe and Sandro Añez (FAN) were not only co-authors, but also organized and conducted biomass measurements in the field. Thank you for baring all operational and physical challenges, and for having returned safely. Field data collection was only possible thanks to the tremendous efforts from over 60 community members from Baures, Churcos, El Espino, Postrevalle, Santa Ana de Velasco and Tierras Nuevas. I am grateful to my Bolivian colleagues at FAN, where I first started working in 2004. FAN provided me with the unique opportunity to work with a highly skilled team for nature conservation in Bolivia. In particular I would like to thank for the support from Natalia Caldron, Verónica Ibarregaray, and Jörg Seifert-Granzin. I am very grateful for family Venegas and Culeman for welcoming and hosting me during several years in Bolivia. Also, I would like to thank all office mates at Wageningen for having made this time such a wonderful experience.

None of this would have been possible without the tremendous support from my parents Hanna and Christoph Seiler, as well as my brothers Nikolaus and Bastian. Thank you for being such a wonderful family. Finally, I would like to thank my wife Diana Córdoba for sharing not only this time, but her life with me. Our wedding in the Netherlands and in Colombia were two out of many beautiful moments we shared during this research.

Curriculum Vitae

Christian Seiler was born on the 28th of May 1980 in Celle, Germany. After finishing secondary school in 2000, he spent one year with voluntary social work and traveling in Brazil. He then studied International Forest Ecosystem Management (BSc) in Eberswalde, Germany (2001-2004), with an internship related to reforestation in Costa Rica, and a final semester abroad at the Gabriel René Moreno Autonomous University in Santa Cruz de la Sierra, Bolivia. After his graduation he started to work as a consultant for the Fundación Amigos de la Naturaleza (FAN), a non-governmental organization for nature conservation in Bolivia. This work was related to the Noel Kempff forest carbon offset project, and included mainly land use change detection and modeling. In 2006 he returned to Europe to study Earth System Science (MSc) at the University of Wageningen. His last semester he spent as a visiting researcher at the International Center for Tropical Agriculture (CIAT) in Colombia, where he wrote his MSc-thesis on remotely sensed actual evapotranspiration. He then returned to Bolivia and continued working for FAN on the development of regional climate change scenarios. After one year, he continued his research as a PhD student in Wageningen, with continuous travels between Bolivia and the Netherlands. In 2012 he spent one semester as a visiting researcher at the Canadian Centre for Climate Modelling and Analysis (CCCma) in Victoria. Christian now lives in Canada, where he works as a post-doc at the Pacific Climate Impacts Consortium (PCIC) on the analysis of extratropical cyclones simulated by general circulation models.

Publications

Seiler, C., R.W.A. Hutjes, B. Kruijt, T. Hickler, The Sensitivity of Wet and Dry Tropical Forests to Climate Change in Bolivia, *submitted*, 2014.

Seiler, C., R.W.A. Hutjes, B. Kruijt, J. Quispe, S. Añez, V. K. Arora, J.R. Melton, T. Hickler, and P. Kabat, Modeling forest dynamics along climate gradients in Bolivia, *Journal of Geophysical Research - Biogeosciences*, 119, 2014.

Seiler, C., R.W.A. Hutjes, and P. Kabat, Likely Ranges of Climate Change in Bolivia, *Journal of Applied Meteorology and Climatology*, 52 (6), 1303–1317, 2013.

Seiler, C., R.W.A. Hutjes, and P. Kabat, Climate Variability and Trends in Bolivia, *Journal of Applied Meteorology and Climatology*, 52 (1), 130–146, 2013.

Seiler, C., Moene, A.F., Estimating Actual Evapotranspiration from Satellite and Meteorological Data in Central Bolivia. *Earth Interactions*, 15, 1–24, 2011.



Netherlands Research School for the
Socio-Economic and Natural Sciences of the Environment

C E R T I F I C A T E

The Netherlands Research School for the
Socio-Economic and Natural Sciences of the Environment
(SENSE), declares that

Christian Seiler

born on 28 May 1980 in Celle, Germany

has successfully fulfilled all requirements of the
Educational Programme of SENSE.

Wageningen, 19 May 2014

the Chairman of the SENSE board

Prof. dr. Huub Rijnaarts

the SENSE Director of Education

Dr.-Ad van Dommelen

The SENSE Research School has been accredited by the Royal Netherlands Academy of Arts and Sciences (KNAW)



K O N I N K L I J K E N E D E R L A N D S E
A K A D E M I E V A N W E T E N S C H A P P E N



The SENSE Research School declares that **Mr. Christian Seiler** has successfully fulfilled all requirements of the Educational PhD Programme of SENSE with a work load of 40 ECTS, including the following activities:

SENSE PhD Courses

- o Environmental Research in Context
- o Research Context Activity: Participating in elaborating two research proposals in relation to the PhD research, and writing an accessible press release on PhD research outcomes

Other Courses

- o Fluid Mechanics
- o Atmosphere-Vegetation-Soil Interactions

External Training at a foreign research institute

- o Dynamic vegetation modelling under the supervision of Dr. Vivek Arora, Canadian Centre for Climate Modelling and Analysis (CCCma), Canada
- o Dynamic vegetation modelling under the supervision of Prof. Thomas Hickler, Biodiversity and Climate Research Centre, Germany

Oral Presentations

- o Climate Variability and Trends in Bolivia, WIMEK/SENSE Symposium "Water & Energy Cycles at Multiple Scales", 1 March 2012, Wageningen
- o Modelling Vegetation Dynamics in Bolivia, Meeting at the Canadian Centre for Climate Modelling and Analysis, 3 September 2012, Victoria, Canada
- o Measuring Carbon Stocks in Bolivia, AMAZALERT mid-term project meeting, 11-15 March 2013, Wageningen

SENSE Coordinator PhD Education

Dr. ing. Monique Gulickx

Funding

The research described in this thesis was financially supported by the Fundación Amigos de la Naturaleza (FAN) through the Departmental Pilot Program of Adaptation to Climate Change (PDACC). Additional financial support was provided by the Wageningen Institute for Environment and Climate Research (WIMEK), as well as the project Raising the Alert about Critical Feedbacks between Climate and Land Use Change in Amazonia (AMAZALERT, project number: 282664). AMAZALERT is jointly funded by the European 7th Framework Programme and national organizations.

Financial support from Wageningen University for printing this thesis is gratefully acknowledged.